Gravitational backreaction on a cosmic string: Formalism

David F. Chernoff,[1] Éanna É. Flanagan,[1] and Barry Wardell[1,2]
[1]Department of Astronomy, Cornell University, Ithaca, New York 14853, USA
[2]School of Mathematics and Statistics, University College Dublin, Belfield, Dublin 4 D04 V1W8, Ireland

(Received 30 August 2018; published 17 April 2019)

We develop a method for computing the linearized gravitational backreaction for Nambu-Goto strings using a fully covariant formalism. We work with equations of motion expressed in terms of a higher dimensional analog of the geodesic equation subject to self-generated forcing terms. The approach allows arbitrary spacetime and world sheet gauge choices for the background and perturbation. The perturbed spacetime metric may be expressed as an integral over a distributional stress-energy tensor supported on the string world sheet. By formally integrating out the distribution, this quantity may be reexpressed in terms of an integral over the retarded image of the string. In doing so, one must pay particular attention to contributions that arise from the field point and from nonsmooth regions of the string. Then, the gradient of the perturbed metric decomposes into a sum of boundary and bulk terms. The decomposition depends upon the world sheet coordinates used to describe the string, but the total is independent of those considerations. We illustrate the method with numerical calculations of the self-force at every point on the world sheet for loops with kinks, cusps and self-intersections using a variety of different coordinate choices. For field points on smooth parts of the world sheet the self-force is finite. As the field point approaches a kink or cusp the self-force diverges, but is integrable in the sense that the displacement of the world sheet remains finite. As a consistency check, we verify that the period-averaged flux of energy-momentum at infinity matches the direct work the self-force performs on the string. The methodology can be applied to address many fundamental questions for string loop evolution.

DOI: 10.1103/PhysRevD.99.084036

I. INTRODUCTION

A. Cosmological superstrings

Cosmic superstrings [1] are the strings of string theory stretched to macroscopic length scales by the Universe's early phase of exponential, inflationary growth [2–4]. The strings produced near the close of that epoch have formed a complicated evolving network of various string elements during the subsequent, more leisurely epochs of expansion [5–7]. Long, horizon-crossing strings stretch; short curved pieces accelerate and attempt to straighten; and, occasionally, individual segments intercommute (collide, break and reattach) chopping out loops and forming new, connected string pathways. Analytic and numerical calculations demonstrate that these processes rapidly drive the network and the loops to self-similar evolution with macroscopic statistical properties largely determined by the string tension [8–12]. The energy densities in long strings, in loops, and in gravitational radiation divided by the critical energy density are all independent of time. The distribution of loops of a given size relative to the horizon scale is also fixed.

An understanding of this evolution is informed by previous studies of one-dimensional defects in the context of symmetry breaking in grand unified theories (GUTs [13]; for a general review see [14]). One important difference for superstrings is the expected value of the string tension. In GUT theories the string tension $G\mu/c^2 \sim \Lambda_{\rm GUT}^2/M_p^2 \sim 10^{-6}$ is fixed by the GUT energy scale $\Lambda_{\rm GUT}$. Observations of the microwave sky have ruled out GUT strings as the source of cosmological perturbations [15–17] and led to upper bounds on the string tension. Currently, broadly model-independent limits from lensing [18–25], CMB studies [15–17,26–35] and gravitational wave background and bursts [36–49] give $G\mu/c^2 \lesssim 10^{-7}$. More stringent but somewhat more model-dependent limits from pulsar timing [50–54] have regularly appeared. Currently, the strongest inferred limit is $G\mu/c^2 \lesssim 10^{-11}$ [55,56].

Low tension strings are natural in string theory and have little difficulty in this regard. In the most well-studied compactifications, standard model physics is located at the bottom of a warped throat where all energy scales are exponentially diminished compared to the string scale. Superstrings have tensions that are reduced by exactly this effect and can correspond to energies as small as TeV (see [1,57] for reviews).

The magnitude of $G\mu/c^2$ influences many properties of the strings and loops that make up the network. A loop with characteristic size ℓ and energy $\propto \mu\ell$ will completely dissipate by gravitational wave emission in times $t \sim \ell/(\Gamma G\mu/c)$ where $\Gamma \sim 50$ is a loop-dependent pure number

[36,58–64]. If $G\mu/c^2 \ll 10^{-6}$ then superstring loops evaporate by gravitational wave emission much less rapidly than GUT string loops. The characteristic size of loops that evaporate gravitationally in t_H, the age of the Universe, is $\ell_g = t_H \Gamma G\mu/c$. These turn out to dominate the distribution of loop sizes found in the Universe today.

Current simulations report that about 10%–20% of the string network that is chopped out ends up in the form of large loops, with sizes within a few orders of magnitude of the horizon scale at birth [11,12]. The rest form very small loops with size scale relative to the horizon set by a power of $G\mu/c^2$ [65–70]. These rapidly evaporate. Today, the string network's energy density is dominated by the large loops formed at an early epoch. If $G\mu/c^2 < 7 \times 10^{-9}$ it is before matter-radiation equality. Today's size distribution increases as $\ell \to \ell_g$ from above (the Universe was denser at earlier times and formed more smaller loops); the distribution is cut off by the evaporation process at $\ell < \ell_g$.

Long gravitational lifetimes have another important effect: the center of mass velocity of the old loops is small and they cluster like cold dark matter [71]. This opens the way to experimental tests of string theory that are based upon direct detection of gravitational wave emission and observation of string microlensing of background stellar sources [72].

B. Gravitational backreaction in the string network

The most numerous loops are close to the characteristic size ℓ_g, set by gravitational backreaction. An understanding of string gravitational backreaction is crucial for making forecasts of experimental studies and planning future observational campaigns. The emission of gravitational radiation and the associated dissipative forces shrink the size of the loop (energy loss) and impart a recoil (momentum and angular momentum loss). These may change the character of the loop oscillation over long timescales. The radiative emission processes have been well studied assuming that the loop is a long-lived periodic oscillator [36,58–64,73,74]. The secular effects of gravitational backreaction on the loop oscillation are relatively unexplored. Two important aspects are the propensity of loops to self-intersection and the evolution of discontinuous features on the loops.

Self-intersections are important because they can lead to the rapid demise of the long-lived loops which are of greatest observational interest. The reason is simple: isolated, dissipationless loops are exactly periodic. If a loop can self-intersect it will do so over and over again eventually leading to intercommutation and breakage. This process shatters the loop into many small looplets [64] moving apart at relativistic speeds, each of which will evaporate in only a fraction of the time required by the original loop. Self-intersections have the potential to radically depress the number of old loops of size ℓ_g that would otherwise exist throughout the Universe. The loop distribution will be cut off at scale $> \ell_g$; the number density at that cutoff will be substantially smaller. Furthermore, the intercommutation process evicts the shattered progeny from being bound to the galaxy. Backreaction can significantly alter experimental forecasts.

Another important aspect of gravitational backreaction is the presence of kinks and cusps on loops. Typically when a new loop is formed from a smooth segment of string the orbit of the new loop will contain an infinitesimal element of string that moves at the speed of light for an infinitesimal time, repeating once per period. This is a cusp, a well-characterized, periodic strong source of gravitational wave emission. Cusp emission is the principle target of gravitational wave searches from string loops because it is strong, beamed and has a well-understood signal form [36–49]. The author of Ref. [70] has argued that a scaling network may be inefficient at forming loops with cusps for the following reason. Scaling requires chopping out a significant fraction of the long strings' length each time the Universe doubles in size. The chopping removes loops and inevitably adds kinks (derivative discontinuities) to the remaining long string segments. Smooth long strings accumulate kinks and grow dense with small scale structure as the Universe ages. New loops inherit the small scale structure. The first time that the loop begins to form a cusplike structure the kinky string reconnects, effectively excising the part of the loop responsible for the cusp. Such a loop is left with nothing but kinks. Kinks may also be detected by gravitational wave searches but are not as strong or as unidirectional. Recent cosmological network simulations support this theoretical prediction [11,12]. In particular, they show that loops with kinks are formed preferentially and there are few cusps.[1]

This general evolutionary outline prompts a number of questions related to how gravitational backreaction influences the evolution of derivative discontinuities on loops and long strings. Qualitatively, we understand that gravitational backreaction will smooth kink discontinuities (lessening the size of the jump in the tangent vector from one side to the other) and theoretically allow new cusps to form. There is a competition between the rate at which the discontinuity diminishes and the rate at which the loop shrinks. One question is whether the loop fully evaporates before the cusp reforms. Another question is whether a reformed cusp has the same scale as the loop itself or an intrinsically smaller scale. These can be answered by calculating the dynamical evolution of a string loop with backreaction for many orbits.

Another aspect that requires a full treatment of backreaction is how a loop with many kinks evolves (since the

[1]It must be noted that it is not clear whether the string substructure in even the biggest simulations has entered a scaling regime or is still in the process of evolving.

scaling solution suggests the ubiquity of kinks). If the total rate of gravitational wave emission scales linearly with the number of kinks [75] then the loop's lifetime is shortened. However, the backreaction of many closely spaced radiating kinks may qualitatively affect the evolution predicted on the basis of a single kink. It is therefore of interest to understand how backreaction operates when there is a high density of kinks on long strings and loops.

C. Theory and simulation

In this paper we develop a complete formalism for computing the gravitational backreaction on cosmic string loops, and we demonstrate the method by computing the gravitational self-force for several specific cosmic string configurations. Some similar studies were previously done in Refs. [76,77], but these were limited in scope and did not include many of the details considered here.

Quashnock and Spergel (QS) [76] derived linearized equations of motion for a string interacting with its own gravitational field (in this context, linearized means first order in $G\mu/c^2$ expanded about flat spacetime). They worked with particular coordinates and gauge choices that were chosen to simplify many aspects of the calculation. The weak field approximation breaks down at kinks, cusps and self-intersections, but these freely moving line singularities were treated in a perturbative sense.

QS computed the self-force at a field point as sourced by elements of the retarded, distant string image. They concluded that only finite divergence-free backreaction forces existed for field points with smooth sources, and that the contribution to the backreaction forces tended to zero as the source point approached the field point. This situation stands in contrast to the analogous point particle case studied by Dirac [78], in which self-interaction leads to a renormalized mass. Carter and Battye [79] and Buonanno and Damour [80] showed that while a general string has a local divergent part to its perturbed metric, the Nambu-Goto string is special and the total force density due to all the local divergent pieces exactly vanishes. The remaining force is given by long-range interactions.

Kinks and cusps are examples where smoothness in the vicinity of the field point fails to hold. QS did not explicitly discuss the limiting behavior near a kink but did argue on general grounds that the backreaction force per source coordinate interval at a cusp would be infinite, but integrable. They also solved numerically for the evolution of the loop represented both as a continuous function and as a set of kinks (straight line segments with small tangent vector discontinuities) by integrating the backreaction over a full period. The simulations showed that cusps survive backreaction but are deformed and delayed. Longer integrations suggested that the amplitude of the cusp and the associated asymmetric rocket effects were suppressed by backreaction. Finally, QS also showed that small (compared to the size of the loop) kinks decay more rapidly than the string as a whole. The magnitude of the discontinuity at a kink (change in tangent vectors) lessens but the discontinuity itself is not smoothed out by dissipation.

It is some measure of the complexity of the problem that most work since the QS investigation has dealt with specific issues and has not attempted such an ambitious numerical treatment. Anderson [81] analytically calculated the gravitational backreaction forces for the Allen-Casper-Ottewill (ACO) loop [61], a rotating loop configuration with a pair of kinks (one tangent vector is continuous and the other is discontinuous). The coordinates and gauge conditions used were equivalent to those of [76]. Anderson demonstrated explicitly that all the components of 4-vector acceleration diverged near the kink. The calculated forces were, however, integrable so that the equations of motion in the weak field limit were integrable too.[2]

In this paper we do not evolve the string configuration (that will be done in a follow-up) but study in detail the method of calculation of the first-order self-force. Certain intermediate quantities in our calculations exhibit divergences. The occurrence of these calculational divergences is tied to three interrelated factors: the choice of world sheet gauge (e.g., conformal or other), the specification of residual gauge freedom in the choice of world sheet coordinates (e.g., null or non-null coordinates), and the existence of discontinuous sources anywhere on the loop's retarded image (the intersection of the world sheet with the past light cone of the field point). However, the total integrated self-force at any point on a smooth region of the world sheet is always finite due to cancellations of divergences, and it is independent of these choices. This finiteness is consistent with the lack of renormalization of the string tension discussed in [82] and with the general conclusions of smoothness of [76].

While the self-force is finite in smooth regions of the world sheet, it diverges in the limit when the field point approaches cusps or kinks on the world sheet. However, when one solves the linearized equation of motion for the perturbation to the world sheet, the linearized displacement of the world sheet is finite. Going beyond this treatment will involve critically examining the linearized approximation and the distributional representation of features such as kinks and cusps. The question of whether physical divergences occur in a fully self-consistent evolution is beyond the scope of this paper. Nevertheless, the methodology we develop in this paper should allow addressing certain aspects of the question in the future. Our methodology will allow us to refine the gauge during the course of a self-consistent evolution (continuing to use linearization with distributional models) to separate invariant physical divergences from calculational divergences. In the case of the cusp, for example, we would need to step carefully

[2]The author of [81] did not evaluate forces at the kink itself where the metric is ill determined.

through a single period of oscillation to handle the occurrence of the divergence at a single spacetime point.

As a result of the work in this paper there is evidence that any such singularity is weak in the "physical" sense. In particular, period-averaged changes are given by simple quadratures over the world sheet. Orbit averaging does not require instant-by-instant evolution but presumes that the metric and string are only mildly perturbed in some average sense. We find that over an oscillation both the kink and cusp lead to finite displacements of the world sheet and finite small changes in energy, momentum and angular momentum. All period-averaged physical divergences are small and bounded in the sense of being proportional to $G\mu$. This is quite mild compared to the character of the singular behavior of point masses in general relativity, for example.

Recently, Wachter and Olum [83,84] have studied the evolution of loops composed of linear pieces (both right and left moving modes are given by a set of fixed tangent vectors which generate kinks). Using the methodology of [76] they found the metric perturbations and the loop's acceleration and analytically evaluated the backreaction for a planar rectangular loop [59]. They deduced the energy loss, changes to the left and right moving modes and the kink smoothing (diminishing the tangent vector jumps). Small angle kinks (acute angles) disappeared more quickly than large angle kinks (of order $\pi/4$). This observation is complementary to that of [76] which reported that small sized kinks (with a small length compared to the loop size) disappeared more quickly than large sized kinks (with length a fraction of the full loop size). The authors of Refs. [83,84] compared the loop evaporation time to the kink smoothing time and found that the loop angle was a key parameter. For small angles, kinks disappeared rapidly. For large angles, the loop evaporated first. Finally, the analysis of the piecewise loops showed that the straight line segments begin to curve after a short period for all except loops with special symmetry.

D. Lagrangian methodology

Carter pioneered the treatment of perturbations in an arbitrarily curved spacetime background with relativistic string, membrane or other brane models where p, the spatial dimension of the brane, is less than n, the spatial dimension of spacetime ([85–87]; see [88] for a review). The action in such models is

$$\mathcal{I} = \int \mathcal{L} d\bar{\Sigma} \tag{1.1}$$

$$d\bar{\Sigma} = |\gamma|^{1/2} d^{p+1}\zeta \tag{1.2}$$

where $d\bar{\Sigma}$ is the surface measure element induced on the timelike world sheet by the background metric, γ is the determinant of the induced metric and ζ stands for the $(p+1)$ internal coordinates. We may assume a constant scalar Lagrangian $\mathcal{L} = -m^{p+1}$ where m is a characteristic mass scale and $\hbar = c = 1$. For $p < n$ the brane and the Lagrangian are distributional in spacetime. The brane is concentrated on lower dimensional world sheets in the higher dimensional spacetime. The case $p = 1$ and $n = 3$ is an effective low-energy description of minimally coupled F- and D-strings with two-dimensional world sheets.

In this work we apply the formalism to compute the metric perturbation generated by a cosmic string. Two important considerations guide our efforts. First, the distributional nature of the strings motivates a Lagrangian approach. Second, we work as much as possible in terms of tensorial quantities of the background spacetime and avoiding the use of specific systems of intrinsic coordinates for the brane submanifolds. We develop a fully covariant formalism and apply it in a variety of circumstances.

E. Conventions used in this paper

Throughout this paper we follow the conventions of Ref. [89]. We use a "mostly positive" metric signature, $(-,+,+,+)$ for the spacetime metric and $(-,+)$ for the world sheet metric; the connection coefficients are defined by $\Gamma^{\lambda}_{\mu\nu} = \frac{1}{2} g^{\lambda\sigma}(g_{\sigma\mu,\nu} + g_{\sigma\nu,\mu} - g_{\mu\nu,\sigma})$; the Riemann tensor is $R^{\alpha}{}_{\lambda\mu\nu} = \Gamma^{\alpha}_{\lambda\nu,\mu} - \Gamma^{\alpha}_{\lambda\mu,\nu} + \Gamma^{\alpha}_{\sigma\mu}\Gamma^{\sigma}_{\lambda\nu} - \Gamma^{\alpha}_{\sigma\nu}\Gamma^{\sigma}_{\lambda\mu}$; the Ricci tensor and scalar are $R_{\alpha\beta} = R^{\mu}{}_{\alpha\mu\beta}$ and $R = R_{\alpha}{}^{\alpha}$; and the Einstein equations are $G_{\alpha\beta} = R_{\alpha\beta} - \frac{1}{2} g_{\alpha\beta} R = 8\pi T_{\alpha\beta}$. We use standard geometrized units, with $c = G = 1$, latin indices for world sheet components and greek indices for four-dimensional spacetime components.

II. COVARIANT EQUATIONS OF MOTION FOR A NAMBU-GOTO COSMIC STRING LOOP

We begin by considering a Nambu-Goto cosmic string tracing out a two-dimensional world sheet in spacetime. We identify a point on the string by a pair of world sheet coordinates $\{\zeta^1, \zeta^2\}$ and denote the spacetime coordinate of that point by $z^{\alpha}(\zeta^a)$.

Given the full spacetime metric, $g_{\alpha\beta}$, the induced metric on the world sheet is defined by

$$\gamma_{ab} = g_{\alpha\beta}\partial_a z^{\alpha}\partial_b z^{\beta}. \tag{2.1}$$

The world-sheet-tangent projection tensor is defined as

$$P^{\alpha\beta} = \gamma^{ab}\partial_a z^{\alpha}\partial_b z^{\beta} \tag{2.2}$$

where $\gamma^{ab}\gamma_{bc} = \delta^a_c$. The corresponding world-sheet-orthogonal projection tensor is

$$\perp^{\alpha\beta} = g^{\alpha\beta} - P^{\alpha\beta}. \tag{2.3}$$

For tensor fields with support confined to the world sheet, the tangentially projected covariant derivative is

$$\bar{\nabla}_\alpha = P_\alpha{}^\mu \nabla_\mu. \tag{2.4}$$

Finally, defining the extrinsic curvature (or second fundamental tensor) and its trace,

$$K_{\alpha\beta}{}^\gamma \equiv P_{\mu\beta}\bar{\nabla}_\alpha P^{\mu\gamma}, \qquad K^\gamma \equiv g^{\alpha\beta}K_{\alpha\beta}{}^\gamma, \tag{2.5}$$

Battye and Carter [90] showed that the equation of motion of the string may be written in the compact form

$$K^\rho = 0. \tag{2.6}$$

This can be expanded explicitly as

$$K^\gamma = \frac{1}{\sqrt{-\gamma}}\partial_a(\sqrt{-\gamma}\gamma^{ab}\partial_b z^\gamma) + P^{\alpha\beta}\Gamma^\gamma_{\alpha\beta}, \tag{2.7}$$

where $\gamma = \det(\gamma_{ab})$ and $\Gamma^\gamma_{\alpha\beta}$ is evaluated at the spacetime coordinate of the world sheet point $z^\mu(\zeta^a)$.

III. GRAVITATIONAL PERTURBATIONS OF COSMIC STRING LOOPS

We now wish to specialize to the case where the string tension is small and the problem may be treated perturbatively in $G\mu/c^2$. Then, the string can be considered to be moving in a perturbed spacetime with metric

$$g_{\alpha\beta} = \overset{\circ}{g}_{\alpha\beta} + h_{\alpha\beta},$$

where the background, unperturbed metric is $\overset{\circ}{g}_{\alpha\beta}$ and the perturbation $h_{\alpha\beta}$ is sourced by the string's own stress energy. We can likewise parametrize the world sheet in terms of a background piece plus a perturbation,

$$z^\alpha = z^\alpha_{(0)} + z^\alpha_{(1)}, \tag{3.1}$$

and will work to first order[3] in both the metric perturbation, $h_{\alpha\beta}$, and in the world sheet perturbation, $z^\alpha_{(1)}$.

A. Zeroth-order equation of motion

For the case where backreaction is ignored, we may treat the string as moving in a fixed background spacetime with equation of motion

$$\frac{1}{\sqrt{-\gamma}}\partial_a(\sqrt{-\gamma}\gamma^{ab}\partial_b z^\gamma_{(0)}) + P^{\alpha\beta}\Gamma^\gamma_{\alpha\beta} = 0. \tag{3.2}$$

If the background is Minkowski spacetime, the second term vanishes and the equation of motion is just the standard two-dimensional scalar wave equation for each component of the world sheet coordinate vector.

Further simplification can be obtained by considering the gauge freedom in defining the world sheet coordinates. A common class of choices invokes the conformal gauge condition, whereby the world sheet metric is required to be conformally flat:

$$\gamma_{ab} = \phi\eta_{ab}, \tag{3.3}$$

where η_{ab} is a two-dimensional Minkowski metric and $\phi > 0$ is a conformal factor. A consequence of this choice is that the world sheet derivatives, $\partial_{\zeta^1} z^\mu$ and $\partial_{\zeta^2} z^\mu$, must satisfy certain orthogonality conditions (the details of which depend on the particular choice of world sheet coordinates) and that the equation of motion is given by

$$\phi^{-1}\eta^{ab}\partial_a\partial_b z^\gamma_{(0)} = 0. \tag{3.4}$$

This is just the $1+1$D flat space scalar wave equation for each spacetime component of the string world sheet vector $z^\alpha_{(0)}$. The solutions to this equation are periodic in both ζ^1 and ζ^2 in the sense that for a loop of length L we have $z^\alpha(\zeta^1,\zeta^2) = z^\alpha(\zeta^1 + L/2, \zeta^2 + L/2)$.

Weak solutions of Eqs. (3.2) and (3.4) allow derivative discontinuities, so generic solutions are not smooth. The tangent sphere representation provides a description of the derivatives of the two components of a solution [14]. Perfectly smooth string loop solutions have two continuous paths on the tangent sphere. However, there may be long-lived kinks (corresponding to gaps in the tangent sphere) that propagate around the string along null world sheet directions, and cusps (corresponding to intersections in the tangent sphere) that only exist instantaneously. There may also be self-intersections, where the string crosses over on itself.

B. First-order equation of motion for the string world sheet

We now return to the general case (no specialization of gauge or metric) to write down the perturbed equation of motion. Demanding that the perturbed trace of the extrinsic curvature vanish as in Eq. (2.6) and assuming that the zeroth-order equation of motion is satisfied gives [87,90]

$$\perp^\rho{}_\chi \bar{\nabla}_\mu\bar{\nabla}^\mu z^\chi_{(1)} - 2\bar{\nabla}_\mu z^\alpha_{(1)} K^\mu{}_\alpha{}^\rho + \perp^{\beta\rho}P^{\mu\nu}R_{\mu\varepsilon\nu\beta}z^\varepsilon_{(1)} = K^{\alpha\beta\rho}h_{\alpha\beta} - \perp^\rho{}_\beta P^{\lambda\tau}\left(\nabla_\lambda h^\beta{}_\tau - \frac{1}{2}\nabla^\beta h_{\lambda\tau}\right). \tag{3.5}$$

[3]For notational simplicity, from here on we will always make explicit the dependence on the perturbed quantities $h_{\alpha\beta}$ and $z^\alpha_{(1)}$, but we will implicitly define everything else in terms of background quantities. So, for example, we will have $\gamma_{ab} = \overset{\circ}{g}_{\alpha\beta}\partial_a z^\alpha_{(0)}\partial_b z^\beta_{(0)}$ and likewise for all of the other quantities defined in Sec. II.

The homogeneous version of this equation is a higher dimensional analog of the geodesic deviation equation.

Identifying the term on the right-hand side as a self-force, it is convenient to split this force into separate contributions, one involving the metric perturbation and the other involving its derivative,

$$F^\rho = F_1^\rho + F_2^\rho, \tag{3.6a}$$

$$F_1^\rho \equiv -\perp^\rho{}_\lambda P^{\mu\nu}\left(\nabla_\mu h_\nu{}^\lambda - \frac{1}{2}\nabla^\lambda h_{\mu\nu}\right), \tag{3.6b}$$

$$F_2^\rho \equiv K^{\mu\nu\rho} h_{\mu\nu}. \tag{3.6c}$$

Using the definition (2.5) of $K^{\mu\nu\rho}$ we can write F_2^ρ in terms of $H_{ab} \equiv h_{\mu\nu}\partial_a z^\mu \partial_b z^\nu$ (the projection of $h_{\mu\nu}$ along the world sheet),

$$\begin{aligned} F_2^\rho &= (\gamma^{ac}\gamma^{bd}\partial_c z^\sigma \partial_d z^\lambda \nabla_\lambda P_\sigma{}^\rho) H_{ab} \\ &= \perp^\rho{}_\sigma \gamma^{ac}\gamma^{bd}(\partial_c\partial_d z^\sigma + \Gamma^\sigma_{\lambda\tau}\partial_c z^\lambda \partial_d z^\tau) H_{ab}. \end{aligned} \tag{3.7}$$

We can also write the first term as

$$F_1^\rho = -\frac{1}{\sqrt{-\gamma}} \perp^\rho{}_\lambda \mathcal{F}^\lambda_{\rm conf}, \tag{3.8}$$

where[4]

$$\mathcal{F}^\rho_{\rm conf} \equiv \sqrt{-\gamma} P^{\mu\nu}\left(\nabla_\mu h_\nu{}^\rho - \frac{1}{2}\nabla^\rho h_{\mu\nu}\right) \tag{3.9}$$

is the quantity that appears on the right-hand side of the conformal gauge equation of motion (3.14) below. Battye and Carter [90] showed that for a general choice of gauge it is crucial to both project orthogonal to the world sheet and to include the additional term involving $K^{\mu\nu\rho}$ in order to get the correct gravitational self-force.[5] In a subsequent work [91] they showed that, despite the presence of divergences in the metric perturbation, the gravitational self-force (3.6) is finite for strings in four spacetime dimensions with smooth world sheets.

[4]We use a caligraphic font for $\mathcal{F}^\mu_{\rm conf}$ since it is not a gauge-specialized version of the general self-force F^μ, because the left-hand side of Eq. (3.14) is not obtained from the left-hand side of (3.5) by a gauge specialization.

[5]In fact, a sequence of papers provided derivations of the fundamental equations of motion with increasing degrees of rigor. Following on from Ref. [90], Battye and Carter [87] performed a more careful analysis using a second-order Lagrangian variational treatment to derive the first-order equations of motion for the displacement vector of the world sheet and for the metric perturbations. When restricted to the linearized back-reaction regime, their final results [given in Eqs. (30), (31) and (33) of [87] with terms involving K_ρ identically zero for linearized backreaction] are consistent with their earlier results and with the expressions above.

The very general form for the equations of motion given by Eq. (3.5) allows an arbitrary choice of gauge for the background, both for the spacetime coordinates and for the world sheet coordinates. It also allows separate arbitrary gauge transformations for the perturbations and is invariant under two different types of linearized gauge transformations:

(i) Linearized coordinate transformations in spacetime, which induce changes in the world sheet and metric perturbations, $z^\alpha_{(1)} \to z^\alpha_{(1)} + \xi^\alpha$, $h_{\alpha\beta} \to h_{\alpha\beta} - 2\nabla_{(\alpha}\xi_{\beta)}$.

(ii) Linearized coordinate transformations on the world sheet, which induce the changes

$$z^\alpha_{(1)} \to z^\alpha_{(1)} + \partial_a z^\alpha \xi^a. \tag{3.10}$$

This gauge freedom shows that only the component of $z^\alpha_{(1)}$ that is perpendicular to the world sheet contains physical information.

C. Choices of gauge

1. Gauge choice to zeroth order

We now once again specialize to Minkowski spacetime in Lorentzian coordinates at zeroth order. Then, the third term on the left-hand side of Eq. (3.5) vanishes identically. The first term simplifies to

$$\perp^\rho{}_\chi \frac{1}{\sqrt{-\gamma}}\partial_a(\sqrt{-\gamma}\gamma^{ab}\partial_b z^\chi_{(1)}), \tag{3.11}$$

and the second term is

$$-2\partial_a z^{(1)}_\alpha \gamma^{ab} z^\sigma_{(0),bd} z^\alpha_{(0),c}\gamma^{cd}\perp_\sigma{}^\rho. \tag{3.12}$$

The first two terms simplify further if we use the conformal gauge [Eq. (3.3)] to zeroth order, in which case the left-hand side becomes

$$\perp^\rho{}_\chi \frac{1}{\sqrt{-\gamma}}\eta^{ab}\partial_a\partial_b z^\chi_{(1)}. \tag{3.13}$$

2. Gauge choice to first order

At first order we adopt Lorenz gauge[6] for the spacetime coordinates. For the world sheet coordinates there are several natural choices. We focus here on the conformal gauge as it is computationally the most convenient, and direct the reader to Appendix A 4 for a discussion of other possible choices.

The choice of conformal gauge at first order amounts to choosing the world sheet coordinates so that the conformal

[6]This gauge condition is often referred to as Lorentz gauge but is actually due to Lorenz [92].

flatness condition (3.3) holds to first order as well as zeroth order. Anderson [81] showed that in this gauge the equation of motion, Eq. (3.5), takes the simple form

$$\eta^{ab}\partial_a\partial_b z^{\chi}_{(1)} = -\mathcal{F}^{\chi}_{\rm conf}. \tag{3.14}$$

When our sign convention for the metric is taken into account, this form is consistent with that used by Buonanno and Damour [82].

Comparing with the covariant equation, Eq. (3.5), we see a number of differences due to the gauge specialization:

(i) The right-hand side of Eq. (3.14) corresponds to the second term on the right-hand side of Eq. (3.5), but with the projection tensor dropped.
(ii) The left-hand side of Eq. (3.14) corresponds to the first term on the left-hand side of Eq. (3.5), but again with the projection tensor dropped.
(iii) The remaining two terms in Eq. (3.5) involving couplings to the extrinsic curvature tensor have been dropped—they cancel against the effect of dropping the projection tensors in this gauge. (We have already dropped the term involving the Riemann tensor since we are working in flat spacetime.)

A simple proof of this can be obtained by starting with the general coordinate expression (2.7) for K^ρ before considering perturbations, and applying the conformal gauge condition (3.3). We have

$$K^\rho = \frac{1}{\sqrt{-\gamma}}\eta^{ab}\partial_a\partial_b z^\rho + \gamma^{ab}z^\lambda_{,a}z^\mu_{,b}\Gamma^\rho_{\lambda\mu} \tag{3.15}$$

without approximation (z^ρ, γ_{ab}, $g_{\alpha\beta}$, $\Gamma^\rho_{\lambda\mu}$ exact). Now consider evaluating this expression with the metric $g_{\alpha\beta} \to \eta_{\alpha\beta} + h_{\alpha\beta}$ and world sheet $z^\alpha \to z^\alpha_{(0)} + z^\alpha_{(1)}$. The zeroth-order term vanishes by assumption. The variation of the first term in Eq. (3.15) comes from replacing z^ρ with $z^\rho_{(0)} + z^\rho_{(1)}$, since the zeroth-order quantity $\eta^{ab}\partial_a\partial_b z^\rho_{(0)}$ vanishes. Therefore this term yields the left-hand side of Eq. (3.14). Similarly, the variation of the second term in Eq. (3.15) comes from the variation in $\Gamma^\rho_{\lambda\mu}$, since this quantity vanishes in the background by assumption (we are working in Lorentzian coordinates in Minkowski spacetime). Using expression (2.2) for the projection tensor we see that the variation of this term yields the right-hand side of Eq. (3.14).

For the specific choice of gauge in this section $\mathcal{F}^\rho_{\rm conf}$ naturally appears in the balance laws for energy and momentum relating the flux of radiation at infinity to the local dissipation forces (see Appendix C).

D. First-order metric perturbation

The stress tensor for a Nambu-Goto cosmic string is given by [14]

$$T^{\alpha\beta}(x) = -G\mu\iint P^{\alpha\beta}\delta_4(x,z)\sqrt{-\gamma}d\zeta^{1'}d\zeta^{2'} \tag{3.16}$$

where $\delta_4(x,z) = \frac{\delta_4(x-z)}{\sqrt{-g}}$ is the four-dimensional invariant Dirac delta distribution and z, $P^{\alpha\beta}$ and γ are all functions of $\zeta^{a'}$. A coupling of the string to gravity leads to deviations of the spacetime from the background. For sufficiently small string tensions, $G\mu/c^2 \ll 1$, this deviation may be treated perturbatively by expanding the metric about the background spacetime,

$$g_{\alpha\beta} = \mathring{g}_{\alpha\beta} + h_{\alpha\beta}. \tag{3.17}$$

The perturbation satisfies the linearized Einstein equation, which in Lorenz gauge is just the wave equation,

$$\Box\bar{h}_{\alpha\beta} + 2R_\alpha{}^\gamma{}_\beta{}^\delta h_{\gamma\delta} = -16\pi T_{\alpha\beta} \tag{3.18}$$

where $\bar{h}_{\alpha\beta} \equiv h_{\alpha\beta} - \frac{1}{2}\mathring{g}_{\alpha\beta}\mathring{g}^{\gamma\delta}h_{\gamma\delta}$ is the trace-reversed metric perturbation. We can invert this equation using the retarded Green function, which satisfies the wave equation,

$$\Box G_{\alpha\beta}{}^{\alpha'\beta'} + 2R_\alpha{}^\gamma{}_\beta{}^\delta G_{\gamma\delta}{}^{\alpha'\beta'} = -g_\alpha{}^{\alpha'}g_\beta{}^{\beta'}\delta^4(x,x'). \tag{3.19}$$

In a four-dimensional Minkowski background ($\mathring{g}_{\alpha\beta} = \eta_{\alpha\beta}$) the solution is

$$G^{\rm ret}_{\alpha\beta}{}^{\alpha'\beta'}(x,x') = \frac{1}{4\pi}\Theta_-(x,x')\delta^{\alpha'}_{(\alpha}\delta^{\beta'}_{\beta)}\delta[\sigma(x,x')]. \tag{3.20}$$

Here, $\sigma(x,x')$ is the Synge world function, defined to be one-half of the square of the geodesic distance between x and x', so that the Dirac delta function is nonzero only when x and x' are null separated. In Minkowski spacetime, we have the closed form

$$\sigma(x,x') = \frac{1}{2}\eta_{\alpha\beta}(x^\alpha - x^{\alpha'})(x^\beta - x^{\beta'}). \tag{3.21}$$

The metric perturbation is then given by convolving the Green function with the source,

$$\begin{aligned}\bar{h}_{\alpha\beta}(x) &= 16\pi\int G^{\rm ret}_{\alpha\beta}{}^{\alpha'\beta'}(x,x')T_{\alpha'\beta'}(x')\sqrt{-g(x')}d^4x' \\ &= -4G\mu\iint P_{\alpha\beta}\delta[\sigma(x,z)]\sqrt{-\gamma}d\zeta^{1'}d\zeta^{2'},\end{aligned} \tag{3.22}$$

where $P_{\alpha\beta}$, z^α and γ are all functions of $\zeta^{1'}$ and $\zeta^{2'}$.

In practical calculations it is convenient to perform one of the integrals immediately using the identity

$$\delta[\sigma(x,z(\zeta^1,\zeta^2))] = \frac{\delta[\zeta^1 - \zeta^1_{\rm ret}(x,\zeta^2)]}{|r_1|} \tag{3.23}$$

where $r_1 \equiv \partial_{\zeta^{1'}}\sigma = (\partial_{\zeta^{1'}} z^{\alpha'})(\partial_{\alpha'}\sigma)$ and $\zeta^1_{\rm ret}(x,\zeta^2)$ parametrizes the retarded image, defined by

$$\sigma[x, z(\zeta^1_{\rm ret}, \zeta^2)] = 0. \tag{3.24}$$

This gives

$$\bar{h}_{\alpha\beta}(x) = -4G\mu \oint \left[\frac{\sqrt{-\gamma}P_{\alpha\beta}}{|r_1|}\right]_{\zeta^{1'}_{\rm ret}} d\zeta^{2'}, \tag{3.25}$$

where the quantity in square brackets is evaluated at $\zeta^{1'} = \zeta^{1'}_{\rm ret}(\zeta^{2'})$. The one-dimensional integration traces exactly one period of the loop's retarded image and there is no boundary; it is a closed loop. Equivalently, the nontrace-reversed metric perturbation is given by

$$h_{\alpha\beta}(x) = -4G\mu \oint \left[\frac{\sqrt{-\gamma}}{|r_1|}\Sigma_{\alpha\beta}P\right]_{\zeta^{1'}_{\rm ret}} d\zeta^{2'}, \tag{3.26}$$

where $\Sigma_{\alpha\beta} \equiv P_{\alpha\beta} - \frac{1}{2}\eta_{\alpha\beta}P$ with $P \equiv P^{\gamma}{}_{\gamma}$. Note that the integral does not converge when x is a point on the world sheet; this is because the integrand diverges whenever $r_1 = 0$, which occurs when source and field points coincide, i.e., $x = z$.

Derivatives of the first-order metric perturbation may be computed in a similar manner to $h_{\alpha\beta}$ itself, with the caveat that care must be taken in nonsmooth regions of the string. These nonsmooth regions occur at kinks and cusps, and also in the vicinity of the field point, x, if it is on the world sheet.

Ignoring the issue of smoothness for now, and differentiating Eq. (3.22) with respect to the field point, x, we get

$$\begin{aligned}
\partial_\gamma \bar{h}_{\alpha\beta}(x) &= -4G\mu \iint P_{\alpha\beta}\partial_\gamma(\delta[\sigma(x,z)])\sqrt{-\gamma}d\zeta^{1'}d\zeta^{2'} \\
&= -4G\mu \iint P_{\alpha\beta}\partial_\gamma\sigma\delta'[\sigma(x,z)]\sqrt{-\gamma}d\zeta^{1'}d\zeta^{2'} \\
&= -4G\mu \iint P_{\alpha\beta}\frac{\partial_\gamma\sigma}{\partial_{\zeta^{1'}}\sigma}\partial_{\zeta^{1'}}(\delta[\sigma(x,z)])\sqrt{-\gamma}d\zeta^{1'}d\zeta^{2'} \\
&= -4G\mu \iint \frac{P_{\alpha\beta}\Omega_\gamma}{r_1}\partial_{\zeta^{1'}}(\delta[\sigma(x,z)])\sqrt{-\gamma}d\zeta^{1'}d\zeta^{2'},
\end{aligned} \tag{3.27}$$

where $\Omega^\alpha \equiv x^\alpha - x^{\alpha'}$ is the coordinate distance between x and x'. On a smooth world sheet, this may be integrated by parts to give

$$\begin{aligned}
\partial_\gamma \bar{h}_{\alpha\beta}(x) &= 4G\mu \iint \partial_{\zeta^{1'}}\left[\frac{\sqrt{-\gamma}P_{\alpha\beta}\Omega_\gamma}{r_1}\right]\delta[\sigma(x,z)]d\zeta^{1'}d\zeta^{2'} \\
&= 4G\mu \oint \left[\frac{1}{|r_1|}\partial_{\zeta^{1'}}\left(\frac{\sqrt{-\gamma}P_{\alpha\beta}\Omega_\gamma}{r_1}\right)\right]_{\zeta^{1'}_{\rm ret}} d\zeta^{2'}.
\end{aligned} \tag{3.28}$$

Note that there are no boundary terms introduced in the integration by parts as the integration is over a closed loop. Additionally, note that we can also arrive at the same equation by differentiating Eq. (3.25) and accounting for the fact that the dependence on x appears both through r_1 and through $\zeta^{1'}_{\rm ret}$, along with the relation $\partial_\gamma\zeta^{1'}_{\rm ret} = -\Omega_\gamma/r_1$ (see Sec. 10 of [93]). Again, we may write this in the nontrace-reversed form,

$$\partial_\gamma h_{\alpha\beta}(x) = 4G\mu \oint \left[\frac{1}{|r_1|}\partial_{\zeta^{1'}}\left(\frac{\sqrt{-\gamma}\Sigma_{\alpha\beta}\Omega_\gamma}{r_1}\right)\right]_{\zeta^{1'}_{\rm ret}} d\zeta^{2'}. \tag{3.29}$$

E. First-order self-force

With the results from the previous section at hand, it is straightforward to obtain an integral expression for the first-order gravitational self-force. Substituting Eqs. (3.26) and (3.29) into (3.6) we obtain

$$\begin{aligned}
F^\mu_1(z) = &-4G\mu \perp^{\mu\gamma} P^{\alpha\beta} \\
&\times \oint \left[\frac{1}{|r_1|}\partial_{\zeta^{1'}}\left(\frac{\sqrt{-\gamma}(\Sigma_{\beta\gamma}\Omega_\alpha - \frac{1}{2}\Sigma_{\alpha\beta}\Omega_\gamma)}{r_1}\right)\right]_{\zeta^{1'}_{\rm ret}} d\zeta^{2'},
\end{aligned} \tag{3.30}$$

$$F^\mu_2(z) = -4G\mu K^{\beta\alpha\mu} \oint \left[\frac{\sqrt{-\gamma}\Sigma_{\alpha\beta}}{|r_1|}\right]_{\zeta^{1'}_{\rm ret}} d\zeta^{2'}. \tag{3.31}$$

Here, it is understood that the $\perp^{\mu\gamma}$, $P^{\alpha\beta}$ and $K^{\beta\alpha\mu}$ appearing outside the integral are to be evaluated at z, whereas the $P^{\alpha\beta}$ and γ appearing inside the integral are to be evaluated at the retarded point z'.

One may expect a difficulty to arise from the fact that $\bar{h}_{\alpha\beta}$ diverges logarithmically (and $\partial_\gamma\bar{h}_{\alpha\beta}$ is even more divergent) when the source and field points coincide. This would appear to be a major obstacle for computing the self-force since the integral expressions for $\bar{h}_{\alpha\beta}$ and $\partial_\gamma\bar{h}_{\alpha\beta}$ will not converge when the field point, x, is on the world sheet. Fortunately, it turns out that for field points on smooth parts of the world sheet, some miraculous cancellations in the particular combination appearing in the equation of motion [and hence the self-force, Eq. (3.6)] lead to many of the divergent terms canceling. The result is that one obtains a convergent integral and a finite self-force. This was shown to hold in [82] for the conformal gauge and in [91] for an arbitrary gauge. However, both cases implicitly assumed a

smooth string world sheet. It turns out that the conclusions continue to hold for a nonsmooth world sheet provided the field point is on a smooth part of the world sheet. As a field point approaches a nonsmooth point on the world sheet the total self-force diverges.

Despite this latter divergence, there is one further important consideration, namely the physical significance of the self-force itself. It is possible that a divergence in the self-force is a spurious artifact arising from, for example, an unfortunate choice of gauge or from a distributional treatment of nonsmooth world sheet features. Indeed, Anderson [81] computed explicit closed form expressions for the self-force in the case of the ACO string. His expressions diverge logarithmically and as negative powers in the vicinity of the kink. However, this divergence is integrable and he was able to solve the equations of motion to compute finite deviations in both the position and velocity of the string.[7] Similar conclusions have also been drawn in other work [76,83,84].

In this work, we empirically find results that are consistent with these previous conclusions; although the equation of motion has a divergent self-force term it turns out to give a finite change to the world sheet. Any physical measurement must be consistent with the inferred finite displacement. With a distributional description of kinks and cusps as adopted here finite displacements can lead to singular changes in derivative quantities such as tangent vectors on the world sheet.[8] Optimistically, we can expect the finiteness of world sheet displacements to carry through to more general scenarios, and we hope that the divergences in the force are always integrable. A proof of this fact can likely be obtained from a local expansion of the type given in Sec. IV D below, adapted to allow for a kink or cusp within the "local" region. Since there are considerable subtle details in this calculation, we will leave its exploration for future work.

[7]More precisely, the derivative along the direction orthogonal to the kink's propagation direction was divergent at the kink; however Anderson was able to obtain a gauge transformation which eliminated this divergence and so it can be attributed to nonphysical coordinate effects.

[8]Divergent behavior of this sort (changes of order $G\mu/c^2$ in the tangent vector direction over a single period of oscillation) has recently been reported by Blanco-Pillado, Olum and Wachter (see Acknowledgements). In our treatment here we emphasize that we ignore the possibility of additional contributions coming from the kink itself. It is difficult to validate this assumption within a distributional approach. It is likely that a matched asymptotic approach along the lines of Ref. [94] for point particles would be required to provide a definitive answer to the question of whether the distributional treatment omits any important physical effects. We anticipate that such a treatment would also regularize singular tangent vector derivatives so that all physical measurements are finite, not merely consistent with the inferred finite world sheet displacement.

IV. EVALUATING THE GRADIENT OF THE RETARDED METRIC PERTURBATION

In the previous section, we obtained integral expressions for the metric perturbation, its derivative, and the gravitational self-force. The latter two are valid provided the retarded image of the world sheet is smooth. In reality, we do not have the luxury of a smooth world sheet for at least two reasons:

(1) We are interested in studying strings with kinks and cusps, and the world sheet is nonsmooth at the location of any kink or cusp;
(2) We are interested in computing the self-force, which requires us to evaluate the metric perturbation and its derivative in the limit $x \to z$. In that case, if one considers the retarded image of a point directly on the string, $x = z$, one finds that it is not in general smooth at the field point, $\zeta^{2'} = \zeta^{2'}(x)$.

These can lead to important distributional type contributions to the integrand in the expression for the self-force which are easily missed. In the following subsections, we extend Eqs. (3.29) and (3.30) above to allow for these nonsmooth features. We begin with a general covariant derivation of the integral to explain how coordinate-dependent divergences arise, and we follow up with an explicit treatment of both issues mentioned above.

A. Covariant evaluation of the world sheet integral

The expression for the gradient of the metric perturbation at a point x^α is of the form (dropping spacetime tensor indices)

$$I = \int_{\mathcal{W}} \omega_{ab}\delta'(\sigma). \tag{4.1}$$

Here $\mathcal{W}$ is the world sheet defined by $x^\alpha = z^\alpha(\zeta^a)$, ω_{ab} is some given smooth two-form on the world sheet, and the function σ is as defined in Eq. (3.21). In this subsection we will derive some identities for integrals of the form (4.1) for arbitrary ω_{ab} and arbitrary smooth σ, and in the next subsection we will specialize to the specific form (3.21) of σ for our application here.

As a warm-up, let us first consider a simpler version of the integral (4.1), namely

$$J = \int_{\mathcal{W}} \omega_{ab}\delta(\sigma). \tag{4.2}$$

Let $\mathcal{C}$ be the curve given by $\sigma = 0$. We would like to derive an expression for J of the form

$$J = \int_{\mathcal{C}} \theta_a \tag{4.3}$$

where θ_a is a one-form on the world sheet. The result for θ_a is

$$\theta_a = \frac{D_a h}{\omega^{bc} D_b \sigma D_c h}. \tag{4.4}$$

Here D_a can be taken to be either a covariant or a partial derivative on the world sheet, and ω^{ab} is the inverse of ω_{ab}. Finally h can be taken to be any smooth function on the world sheet which has the property that $dh \wedge d\sigma \neq 0$.

Note that the expression (4.4) for the one-form, when pulled back onto the curve $\mathcal{C}$, is independent of the choice of h. To see this, suppose we replace h with a function H of h and σ,

$$h \to H(h, \sigma). \tag{4.5}$$

Under this transformation

$$D_a h \to H_{,h} D_a h + H_{,\sigma} D_a \sigma. \tag{4.6}$$

When this expression is inserted into the one-form (4.4), the contribution from the second term to the denominator vanishes because of antisymmetrization, and the contribution to the numerator vanishes when the one-form is pulled back to $\mathcal{C}$, since $\sigma = 0$ on $\mathcal{C}$. The factors of $H_{,h}$ cancel between the numerator and the denominator, and so we see that the pullback of θ_a to $\mathcal{C}$ is invariant under the transformation. Thus it is independent of the choice of h.

We now turn to the derivation of the formula (4.4). We specialize to coordinates $\zeta^{\bar{0}} = \sigma$, $\zeta^{\bar{1}} = h$. The integral (4.2) becomes

$$J = \int d\sigma \int dh\, \omega_{\sigma h}(\sigma, h)\delta(\sigma) \tag{4.7}$$

where $\omega_{\sigma h} = \omega_{\bar{0}\,\bar{1}}$. Evaluating the integral using the delta function gives

$$J = \int dh\, \omega_{\sigma h}(0, h). \tag{4.8}$$

We now rewrite this in a form which is valid in arbitrary coordinate systems. The factor $\int dh$ can be written as the integral over $\mathcal{C}$ of the one-form $D_a h$. The factor $\omega_{\sigma h}$ can be written as

$$\omega_{\sigma h} = \frac{1}{\omega^{\sigma h}}. \tag{4.9}$$

Using the tensor transformation law we have

$$\omega^{\sigma h} = \omega^{\bar{0}\bar{1}} = \omega^{ab} \frac{\partial \zeta^{\bar{0}}}{\partial \zeta^a} \frac{\partial \zeta^{\bar{1}}}{\partial \zeta^b} = \omega^{ab} \frac{\partial \sigma}{\partial \zeta^a} \frac{\partial h}{\partial \zeta^b}. \tag{4.10}$$

Combining Eqs. (4.8)–(4.10) now yields the result given by Eqs. (4.3) and (4.4).

Turn next to the corresponding analysis for the integral (4.1). Suppose that instead of integrating over the entire world sheet, we integrate over a region $\Delta\mathcal{W}$ of it. The intersection of the boundary $\partial\Delta\mathcal{W}$ of this region with the curve $\mathcal{C}$ will consist of a set of discrete points $\mathcal{P}_i$. The formula for the integral is

$$I = \int_{\Delta\mathcal{W}} \omega_{ab}\delta'(\sigma) = I_{\text{boundary}} + I_{\text{bulk}} \tag{4.11}$$

where the contribution from the boundary is

$$I_{\text{boundary}} = \sum_i \pm \frac{1}{\varphi} \frac{k^a D_a h}{k^b D_b \sigma}. \tag{4.12}$$

Here k^a is the tangent to the boundary $\delta\Delta\mathcal{W}$ and

$$\varphi = \omega^{ab} D_a \sigma D_b h. \tag{4.13}$$

The contribution from the bulk is

$$I_{\text{bulk}} = \int_{\mathcal{C}} \theta_a \tag{4.14}$$

where the one-form θ_a is

$$\theta_a = \frac{1}{\varphi^3} (\omega^{bc} D_b \varphi D_c h) D_a h. \tag{4.15}$$

Under a change of the function h of the form (4.5), the one-form θ_a is no longer invariant. Instead, it transforms by an exact form[9]

$$\theta_a \to \theta_a + D_a \lambda, \tag{4.16}$$

where $\lambda = H_{,\sigma}/(\varphi H_{,h})$. The change in the boundary integral is

$$\sum_i \pm \frac{H_{,\sigma}}{\varphi H_{,h}}, \tag{4.17}$$

which cancels against the change (4.16) in the one-form. Thus we make the important observation that the integral (4.11) is independent of choice of h, but the split into boundary and integral terms is not.

We now turn to the derivation of the formula (4.11). As before we initially specialize to coordinates $(\zeta^{\bar{0}}, \zeta^{\bar{1}}) = (\sigma, h)$. Inserting the identity

$$\omega_{\sigma h}\delta'(\sigma) d\sigma \wedge dh = d[\omega_{\sigma h}\delta(\sigma) dh] - \delta(\sigma) d\omega_{\sigma h} \wedge dh \tag{4.18}$$

into the integral (4.11) and using Stokes's theorem gives a result of the form of the right-hand side of (4.11), with

$$I_{\text{boundary}} = \int_{\partial\Delta\mathcal{W}} \omega_{\sigma h}\delta(\sigma) dh \tag{4.19}$$

[9]This formula is valid when pulled back to the curve $\mathcal{C}$.

and

$$I_{\rm bulk} = -\int_{\Delta\mathcal{W}} \delta(\sigma)\omega_{\sigma h,\sigma} d\sigma dh. \tag{4.20}$$

We evaluate the first term by taking the parameter along the boundary $\delta\Delta\mathcal{W}$ to be σ and using $dh = d\sigma(dh/d\sigma)$. This gives

$$I_{\rm boundary} = \sum_i \omega_{\sigma h}\frac{dh}{d\sigma}. \tag{4.21}$$

Using Eqs. (4.10) and (4.13) this reduces to the formula (4.12).

For the bulk contribution, from the formula (4.20) and using arguments similar to those given for the integral J, we find

$$\theta_a = -\partial_\sigma(1/\varphi)D_a h = \frac{\varphi_{,\sigma}}{\varphi^2}D_a h, \tag{4.22}$$

where we have used $\varphi = 1/\omega_{\sigma h}$. We evaluate the σ derivative using

$$\varphi_{,\sigma} = \frac{\partial\varphi}{\partial\zeta^{\bar 0}} = \frac{\partial\varphi}{\partial\zeta^a}\frac{\partial\zeta^a}{\partial\zeta^{\bar 0}}. \tag{4.23}$$

We express the Jacobian matrix in terms of its inverse using

$$\frac{\partial\zeta^a}{\partial\zeta^{\bar a}} = \frac{2}{[\omega^{cd}\omega_{\bar c\,\bar d}\frac{\partial\zeta^{\bar c}}{\partial\zeta^c}\frac{\partial\zeta^{\bar d}}{\partial\zeta^d}]}\omega^{ab}\omega_{\bar a\,\bar b}\frac{\partial\zeta^{\bar b}}{\partial\zeta^b}. \tag{4.24}$$

This formula is specific to two dimensions and is valid for any choice of two-form. Specializing to $\bar a = \bar 0$ gives

$$\frac{\partial\zeta^a}{\partial\zeta^{\bar 0}} = \frac{\omega^{ab}D_b h}{\omega^{cd}D_c\sigma D_d h}. \tag{4.25}$$

Inserting this into (4.23) and then into (4.22) finally gives the result (4.15).

Finally, although the results derived in this subsection are covariant, they do depend on a choice of arbitrary function h on the world sheet. While the complete final result (4.11) does not depend on h, the integrand (4.15) of the bulk integral, as well as the splitting into bulk and boundary terms, does depend on h. Elsewhere in this paper, we choose to identify h with one of the world sheet coordinates, which explains the coordinate dependence of the integrand and of the splitting.

B. World sheets with kinks

We may now consider how our 1D integral expressions (3.26) and (3.29) for the retarded metric perturbation and its gradient must be modified to allow for the presence of a kink. A cosmic string with a kink may be treated as piecewise smooth, with discontinuities in certain tangent vectors whenever a kink is crossed. To obtain an expression allowing for these discontinuities we assume that the retarded image on the world sheet is nonsmooth at $\zeta^2 = k$, where k may depend on the field point x.[10] Then, one way to achieve the desired result is to break up the integration in Eq. (3.25) at the discontinuity,

$$\bar h_{\alpha\beta}(x) = -4G\mu\int_{k^+}^{k^-+L}\left[\frac{\sqrt{-\gamma}P_{\alpha\beta}}{|r_1|}\right]_{\zeta^{1'}_{\rm ret}} d\zeta^{2'}, \tag{4.26}$$

where k^+ (k^-) is a point just to the right (left) of the kink. Now, when we differentiate this expression we have to take account of the possible dependence of the end points on x. If the discontinuity in the string is at a fixed value of ζ^2 (i.e., in the case of a kink propagating along the ζ^1 direction), then k does not depend on x and the boundary terms vanish. If, instead, the discontinuity is at a fixed value of ζ^1 (i.e., in the case of a kink propagating along the ζ^2 direction), then k does depend on x. Then, using $\partial_\gamma\zeta^2(\zeta^1_{\rm ret}) = -\Omega_\gamma/r_2$, where $r_2 \equiv \partial_{\zeta^{2'}}\sigma = (\partial_{\zeta^2}z^{\alpha'})(\partial_{\alpha'}\sigma)$, we get

$$\partial_\gamma\bar h_{\alpha\beta}(x) = 4G\mu\left\{\int_{k^+}^{k^-+L}\left[\frac{1}{|r_1|}\partial_{\zeta^{1'}}\left(\frac{\sqrt{-\gamma}P_{\alpha\beta}\Omega_\gamma}{r_1}\right)\right]_{\zeta^{1'}_{\rm ret}} d\zeta^{2'} + \left[\frac{\sqrt{-\gamma}P_{\alpha\beta}\Omega_\gamma}{|r_1|r_2}\right]_{k^-} - \left[\frac{\sqrt{-\gamma}P_{\alpha\beta}\Omega_\gamma}{|r_1|r_2}\right]_{k^+}\right\}. \tag{4.27}$$

It is easy to check that one can arrive at the same expression by appropriately including the boundary terms from the integration by parts described in Sec. IV A above. The presence (or lack thereof) of boundary terms is then manifestly dependent on the particular choice of world sheet coordinates. Importantly, this apparent world sheet coordinate dependence only appears in the split between boundary and bulk terms; the sum of the two does *not* have any world sheet coordinate dependence.

In the case of a smooth string, the two boundary terms are identical and cancel, so we recover the same formula as we had before. In the presence of a kink, however, the boundary terms in the two limits k^+ and k^- yield different values and so we pick up an overall contribution from the kink in addition to the integral over the smooth portion of the string. A similar contribution arises when we utilize multiple coordinate systems to cover the string worldsheet: we account for the boundary terms (4.21) that arise when the coordinates change by evaluating the dependence of the end points on x in a similar manner to our treatment of kinks.

[10] Although there are world sheet coordinates where one of the coordinates is a constant along a kink, we will not restrict ourselves to only that case here. We permit the kink to have a general path in terms of the worldsheet coordinates, fix ζ^1 by the null condition with respect to the field point and observe that the kink location given in terms of ζ^2 generally varies with the field point.

C. World sheets with cusps

We have already seen that care must be taken in computing the self-force for cosmic strings with kinks. Since cusps also introduce nonsmoothness in the world sheet, one may expect similar care to be required for cuspy strings. However, there is one crucial difference between a string with kinks and one with cusps: cusps typically occur at a single *point* on a world sheet while kinks occur along a one-dimensional curve. The result is that, in the case of kinks, all points on the string "see" a kink at some point in their retarded image, and hence the integrand in Eq. (3.29) will always be supplemented by a boundary term somewhere. Conversely, there is only a one-dimensional set of points on the string which "see" a cusp in their retarded image; everywhere else the integrand does not encounter a discontinuity.

This suggests that strings with cusps may not need the same careful treatment as those with kinks. This appears to be the case in our test case in Sec. VI below, where we probe the region around the one-dimensional cusp-seeing curve and find no evidence of unusual behavior. This is, of course, merely empirical evidence, and it should be followed with a more formal treatment; it is likely that the local expansions developed in Sec. IV D will prove useful in such an analysis.

D. Contribution from the field point

The final place where we must take care is in the case where the field point itself is on the string. Then, just as in the case of a kink, the retarded image may have a discontinuity at the field point. While it may be possible in such cases to use a similar treatment to what we have done for kinks, there is subtlety in taking the limit of the field point to the world sheet which makes such a treatment difficult. Instead we choose a more robust approach, by using a local expansion of the integrand for field points nearby[11] the string and then analytically taking the limit of the field point to the world sheet.

The purpose of the following subsections is to develop the pieces required for such an expansion. In doing so we make some assumptions:

(1) We will study the contribution to the self-force integral nearby where the force is to be computed and will ultimately shrink the size of this region down to zero;
(2) We will assume that the world sheet is smooth in this region. This is true everywhere except when the field point exactly lies on a kink or cusp; points arbitrarily close to a kink or cusp will, however, be perfectly acceptable.
(3) We will assume that the induced metric does not diverge (or vanish) on the string. This will be true everywhere except where a field point lies exactly on a cusp.
(4) We will assume a conformal gauge for the background world sheet, in particular Eq. (3.3) and the orthogonality relations for $\partial_{\zeta^1} z^\mu$ and $\partial_{\zeta^2} z^\mu$ which follow from it. This step is not a strict requirement of the approach, but it does significantly simplify the tensor algebra in the calculation.

Before we proceed with the derivation of the local expansion, we point out one interesting feature, namely that the divergence in the self-force that arises on kinks and cusps comes purely from the short-distance portion of the self-field, i.e., the contribution to the integral from nearby points. It is therefore likely that a more careful treatment of what happens to the self-force exactly on a kink or cusp may be obtained from a local expansion of the kind given here. We leave the exploration of this issue for future work.

1. Setup of the local expansion

We wish to compute the contribution to the self-force for points near the field point. To do so, we will construct a local expansion of the self-force integrand about a point on the world sheet which is assumed to be nearby the field point, x^α, and to lie on its retarded image, $z^\alpha[\zeta^1_{\rm ret}(x,\zeta^2),\zeta^2]$. We denote this expansion point by $\bar{z}^\alpha \equiv z^\alpha[\bar{\zeta}^1,\bar{\zeta}^2]$ with $\bar{\zeta}^1 \equiv \zeta^1_{\rm ret}(x,\bar{\zeta}^2)$ for a particular choice of $\bar{\zeta}^2$. The conformal factor at this point is $\bar{\phi} \equiv \phi(\bar{\zeta}^1,\bar{\zeta}^2)$ and we assume the expansion has a radius of convergence that includes part of the image. We can then simplify the evaluation of the local integration over that part of the image utilizing the approximate expansion.

We will now seek an expansion of the self-force integrand (3.30) (note that there is no contribution to F_2^μ from the field point since it does not involve derivatives of $h_{\alpha\beta}$) in $\Delta\zeta^2 \equiv \zeta^2 - \bar{\zeta}^2$.[12] The first stage in our calculation is to find an expansion of the retarded coordinate $\zeta^1_{\rm ret}(x,\zeta^2)$ about $\bar{\zeta}^1 = \zeta^1_{\rm ret}(x,\bar{\zeta}^2)$. We denote the difference between these two quantities $\Delta\zeta^1$ and will seek an expansion of it in powers of $\Delta\zeta^2$. In doing so, we will need to be careful about what our particular choice of world sheet coordinate is. We will also need to separately consider the cases where $\Delta\zeta^2$ is

[11] Here, we use the term "nearby" loosely as such a notion is obviously dependent on the choice of world sheets, and in particular on the choice of coordinate which is used as the variable of integration. Not surprisingly, we will find that the conclusions we draw will depend on the choice of world sheet coordinates. Nevertheless, just as in Sec. IV A, this apparent coordinate dependence is merely an artifact of how we choose to split up the self-force into contributions from various integrals and boundary terms. In reality, the total self-force obtained by combining all of these contributions is independent of the choice of world sheet coordinates.

[12] Notationally, the integration in (3.29) is over the dummy variable $\zeta^{2'}$ but we suppress these primes for clarity.

positive or negative, as in some instances the expansion has a different form in the two cases.

2. Expansion of the light-cone condition: Space-time coordinates

In this section we focus on a pair of spacelike and timelike type coordinates which we will denote by ζ (for space) and τ (for time), i.e., $(\zeta^1, \zeta^2) = (\tau, \zeta)$. The important defining features of these coordinates are the conformal gauge orthogonality relations

$$g_{\alpha\beta}\partial_\tau z^\alpha \partial_\tau z^\beta = -\phi, \tag{4.28}$$

$$g_{\alpha\beta}\partial_\tau z^\alpha \partial_\zeta z^\beta = 0, \tag{4.29}$$

$$g_{\alpha\beta}\partial_\zeta z^\alpha \partial_\zeta z^\beta = \phi. \tag{4.30}$$

We can also obtain similar relations involving higher derivatives (with respect to τ and/or ζ) of z^α by differentiating these fundamental relations. We additionally have the conformal gauge equation of motion, Eq. (3.4), which in $\tau - \zeta$ coordinates gives us a relation between second τ and second ζ derivatives of z^α:

$$\partial_{\tau\tau} z^\alpha = \partial_{\zeta\zeta} z^\alpha. \tag{4.31}$$

We will use these identities throughout the following calculation to simplify the results we obtain.

We will start from the fact that the (retarded) source point $z^{\alpha'}$ and the field point z^α are null separated, $\sigma(z^\alpha, z^{\alpha'}) = 0$. Expanding this about $\bar\sigma \equiv \sigma(z^\alpha, \bar z^\alpha)$ we obtain a power series in $\Delta\tau$ and $\Delta\zeta$,

$$\begin{aligned}\sigma = {}& \bar\sigma + \bar\sigma_{,\tau}\Delta\tau + \bar\sigma_{,\zeta}\Delta\zeta \\ & + \frac{1}{2}(\bar\sigma_{,\tau\tau}\Delta\tau^2 + 2\bar\sigma_{,\tau\zeta}\Delta\tau\Delta\zeta + \bar\sigma_{,\zeta\zeta}\Delta\zeta^2) \\ & + \frac{1}{6}(\bar\sigma_{,\tau\tau\tau}\Delta\tau^3 + 3\bar\sigma_{,\tau\tau\zeta}\Delta\tau^2\Delta\zeta + 3\bar\sigma_{,\tau\zeta\zeta}\Delta\tau\Delta\zeta^2 \\ & + \bar\sigma_{,\zeta\zeta\zeta}\Delta\zeta^3) + \cdots.\end{aligned} \tag{4.32}$$

Using $\partial_a = (\partial_a z^\alpha)\nabla_\alpha$ (acting upon the second argument of $\bar\sigma$) along with the identities above and the fact that $\nabla_\alpha\nabla_\beta\sigma = g_{\alpha\beta}$ for Minkowski spacetime, it is straightforward to rewrite the coefficients in terms of world sheet derivatives of $\bar z^\alpha$ and $\bar\phi$:

$$\bar\sigma_{,\tau\tau} = \bar z^\alpha_{,\zeta\zeta}\bar\sigma_\alpha - \phi, \tag{4.33}$$

$$\bar\sigma_{,\tau\zeta} = \bar z^\alpha_{,\tau\zeta}\bar\sigma_\alpha, \tag{4.34}$$

$$\bar\sigma_{,\zeta\zeta} = \bar z^\alpha_{,\zeta\zeta}\bar\sigma_\alpha + \phi, \tag{4.35}$$

$$\bar\sigma_{,\tau\tau\tau} = \bar z^\alpha_{,\tau\zeta\zeta}\bar\sigma_\alpha - \frac{3}{2}\phi_{,\tau}, \tag{4.36}$$

$$\bar\sigma_{,\tau\tau\zeta} = \bar z^\alpha_{,\zeta\zeta\zeta}\bar\sigma_\alpha - \frac{1}{2}\phi_{,\zeta}, \tag{4.37}$$

$$\bar\sigma_{,\tau\zeta\zeta} = \bar z^\alpha_{,\tau\zeta\zeta}\bar\sigma_\alpha + \frac{1}{2}\phi_{,\tau}, \tag{4.38}$$

$$\bar\sigma_{,\zeta\zeta\zeta} = \bar z^\alpha_{,\zeta\zeta\zeta}\bar\sigma_\alpha + \frac{3}{2}\phi_{,\zeta}, \tag{4.39}$$

and likewise for higher-order terms (for the current calculation of the contribution to the self-force from the field point it is only necessary to go to the cubic order given here).

3. Expansion of the retarded time

In order to obtain the desired expansion of $\Delta\tau(\Delta\zeta)$, we now make the ansatz that $\Delta\tau$ has an expansion in integer powers of an order counting parameter $\epsilon \sim \Delta\zeta$ and that $\bar\sigma = \mathcal{O}(\epsilon^2)$. Substituting our ansatz into Eq. (4.32) and solving order by order in ϵ then yields the desired expansion of $\Delta\tau$ in terms of ϵ,

$$\Delta\tau = \frac{1}{\phi}\left[\bar\sigma_{,\tau} - \sqrt{\bar\sigma_{,\tau}^2 + \phi(2\Delta\zeta\bar\sigma_{,\zeta} + 2\bar\sigma + \phi\Delta\zeta^2)}\right] + \mathcal{O}(\epsilon^2). \tag{4.40}$$

The expressions for the higher-order coefficients are somewhat cumbersome, but are fortunately not required for the current calculation.

4. Expansion of quantities appearing in the integrand for the self-force

We now expand each of the quantities appearing in the integrand of F_1^μ [Eq. (3.30)]:

$$\Sigma_{\mu\nu} = \Sigma^{(0,0)}_{\mu\nu} + \Sigma^{(1,0)}_{\mu\nu}\Delta\tau + \Sigma^{(0,1)}_{\mu\nu}\Delta\zeta + \cdots, \tag{4.41}$$

where

$$\Sigma^{(0,0)}_{\mu\nu} = \partial_\zeta z_\mu \partial_\zeta z_\nu - \partial_\tau z_\mu \partial_\tau z_\nu - \phi g_{\mu\nu}, \tag{4.42}$$

$$\begin{aligned}\Sigma^{(1,0)}_{\mu\nu} = {}& \partial_\tau\partial_\zeta z_\mu \partial_\zeta z_\nu + \partial_\zeta z_\mu \partial_\tau\partial_\zeta z_\nu - \partial_\tau z_\mu \partial_\zeta\partial_\zeta z_\nu \\ & - \partial_\zeta\partial_\zeta z_\mu \partial_\tau z_\nu - \partial_\tau\phi g_{\mu\nu},\end{aligned} \tag{4.43}$$

$$\begin{aligned}\Sigma^{(0,1)}_{\mu\nu} = {}& \partial_\zeta\partial_\zeta z_\mu \partial_\zeta z_\nu + \partial_\zeta z_\mu \partial_\zeta\partial_\zeta z_\nu - \partial_\tau z_\mu \partial_\tau\partial_\zeta z_\nu \\ & - \partial_\tau\partial_\zeta z_\mu \partial_\tau z_\nu - \partial_\zeta\phi g_{\mu\nu}.\end{aligned} \tag{4.44}$$

We also have

$$\begin{aligned}r = {}& \bar\sigma_{,\tau} + \bar\sigma_{,\tau\tau}\Delta\tau + \bar\sigma_{,\tau\zeta}\Delta\zeta \\ & + \frac{1}{2}(\bar\sigma_{,\tau\tau\tau}\Delta\tau^2 + 2\bar\sigma_{,\tau\tau\zeta}\Delta\tau\Delta\zeta + \bar\sigma_{,\tau\zeta\zeta}\Delta\zeta^2) + \cdots,\end{aligned} \tag{4.45}$$

and

$$\Omega_\mu = \bar{\Omega}_\mu - z_{\mu,\tau}\Delta\tau - z_{\mu,\zeta}\Delta\zeta - \frac{1}{2}z_{\mu,\tau\tau}\Delta\tau^2 - z_{\mu,\tau\zeta}\Delta\tau\Delta\zeta - \frac{1}{2}z_{\mu,\zeta\zeta}\Delta\zeta^2 + \cdots. \quad (4.46)$$

Note that there are three potentially small parameters in these expansions: $\Delta\tau$; $\Delta\zeta$; and the distance of the field point from the string, which we will denote Δx. In the above, the dependence on $\Delta\tau$ and $\Delta\zeta$ appears explicitly; the dependence on Δx appears through $\bar{\Omega}_\mu \sim \Delta x$ and $\bar{\sigma}_\alpha \sim \Delta x$.

To make further progress, we will assume that all three are of the same order, $\Delta\tau \sim \epsilon$, $\Delta\zeta \sim \epsilon$ and $\Delta x \sim \epsilon$. Now, substituting the expansions into the integral equation for the derivative of the metric perturbation, Eq. (3.29) and expanding out in powers of ϵ, we find that the integrand has a contribution at order ϵ^{-2} and at order ϵ^{-1}, plus higher-order terms. More explicitly, the $\mathcal{O}(\epsilon^{-2})$ piece is given by

$$\partial_\gamma h_{\alpha\beta} \approx -4\int \frac{[\bar{\sigma}_{,\tau\tau}]\Sigma^{(0,0)}_{\alpha\beta}\bar{\Omega}_\gamma - [\bar{\sigma}_{,\tau\tau}]\Sigma^{(0,0)}_{\alpha\beta}z_{\gamma,\zeta}\Delta\zeta + \Sigma^{(0,0)}_{\alpha\beta}z_{\gamma,\tau}\bar{\sigma}_{,\tau}}{(\bar{\sigma}_{,\tau} + [\bar{\sigma}_{,\tau\tau}]\Delta\tau)^3}d\zeta + \mathcal{O}(\epsilon^{-1}) \quad (4.47)$$

where square brackets denote a coincidence limit, $[\bar{\sigma}_{,\tau\tau}] \equiv \lim_{\Delta x\to 0}\bar{\sigma}_{,\tau\tau}$. Now, it is immediately apparent that if we instead substitute our expansions into the integral expression for F^μ_1 this leading-order piece identically vanishes since $P^{\mu\nu}\Sigma_{\mu\nu} = 0$.[13] Likewise, since $\Sigma^{(0,1)}_{\mu\nu}z_{\mu,\zeta} = \Sigma^{(1,0)}_{\mu\nu}z_{\mu,\tau}$, many other terms either identically vanish or simplify significantly. Then, the only remaining piece of the $\mathcal{O}(\epsilon^{-1})$ contribution to the derivative of the metric perturbation which does not vanish upon substitution into the self-force is given by

$$-\int \frac{4}{(\bar{\sigma}_{,\tau} + [\bar{\sigma}_{,\tau\tau}]\Delta\tau)^3}([\bar{\sigma}_{,\tau\tau}]\Sigma^{(0,1)}_{\alpha\beta}\bar{\Omega}_\gamma\Delta\zeta - \Sigma^{(1,0)}_{\alpha\beta}\bar{\Omega}_\gamma\bar{\sigma}_{,\tau} + \Sigma^{(1,0)}_{\alpha\beta}z_{\gamma,\zeta}\bar{\sigma}_{,\tau}\Delta\zeta + \Sigma^{(0,1)}_{\alpha\beta}z_{\gamma,\tau}\bar{\sigma}_{,\tau}\Delta\zeta - [\bar{\sigma}_{,\tau\tau}]\Sigma^{(1,0)}_{\alpha\beta}z_{\gamma,\tau}\Delta\zeta^2 + 2\Sigma^{(1,0)}_{\alpha\beta}z_{\gamma,\tau}\bar{\sigma}_{,\tau}\Delta\tau + [\bar{\sigma}_{,\tau\tau}]\Sigma^{(1,0)}_{\alpha\beta}z_{\gamma,\tau}\Delta\tau^2)d\zeta. \quad (4.48)$$

Our final step is to substitute in the expansion of the retarded time, rescale our integration range by ϵ and integrate from $\Delta\zeta/\epsilon = -\infty$ to $+\infty$. The factor of ϵ in the integral weight cancels with the $1/\epsilon$ in the integrand and so the result is ultimately independent of ϵ.

[13]Strictly speaking, this depends on how we extend the definition of $P^{\mu\nu}$ off the world sheet. However, since we are in the end only interested in taking the limit to the world sheet the particular choice of extension is irrelevant and does not change the result.

5. Expansion of the self-force

Performing the integral explicitly in the limit where the field point tends to the world sheet, we finally arrive at a surprisingly simple expression for the field point contribution to the self-force. In $\tau - \zeta$ coordinates, this is given by

$$F^\mu_{\text{field,ST}} = 4\phi^{-2}\perp^\mu{}_\alpha(z^\alpha_{,\zeta}\phi_{,\zeta} + z^\alpha_{,\tau}\phi_{,\tau} - 2z^\alpha_{,\zeta\zeta}\phi). \quad (4.49)$$

One can go through a similar procedure in the null case (see Appendix D for details of the retarded time expansion in null coordinates). Then, if we use ζ^- as our integration variable, the equivalent expression for the field point contribution to the self-force is

$$F^\alpha_{\text{field,N}} = 4\phi^{-2}\perp^\mu{}_\alpha(z^\alpha_{,\zeta^+}\phi_{,\zeta^+} - z^\alpha_{,\zeta^+\zeta^+}\phi). \quad (4.50)$$

Likewise, one can change $+ \to -$ when ζ^+ is used as the integration variable. The expressions (4.49) or (4.50) must be added to the previous results given by Eq. (3.30) to obtain the total contribution to F^α_1.

V. NUMERICAL METHODS AND REGULARIZATION

For this work have developed several different techniques to evaluate the self-force on the string by completely finite, numerical calculations. In the next section, we will compare these calculations to validate the exact methods we have discussed. Before doing so, here we will schematically outline the different approaches. The abbreviations for the methods are given in square brackets.

A. 2D, smoothed kink or cusp [2D]

The most general approach is to do the 2D integration over the world sheet in Eq. (3.22). This circumvents having to eliminate one world sheet coordinate in terms of another (e.g., solving for the retarded time in $\tau - \zeta$ coordinates) and possibly having to patch different coordinate systems (e.g., two different null coordinate systems on either side of the field point). The world sheet integration produces manifestly coordinate invariant results.

Schematically, we replace the singular retarded Green function with a finite approximation. For a source at x_s and field at x_f

$$\mathcal{G}(x_f, x_s) = \Theta(x_s, x_f)\delta(\sigma) \quad (5.1)$$

where $\Theta = 1$ when the time of the source t_s precedes the time of the field point t_f and 0 otherwise. We transform

$$\delta(\sigma) \to \frac{e^{-\sigma^2/(2w_1^2)}}{\sqrt{2\pi}w_1} \quad (5.2)$$

$$\Theta \to \frac{1 - \tanh((t_s - t_f)/w_2)}{2} \quad (5.3)$$

to generate a smooth, finite integrand. The parameters w_1 and w_2 describe the width of the smoothed delta function and the width of the causal function. (We use w_i schematically in this discussion. In Appendix E we introduce unique symbols.)

Source points are over-retarded and appear slightly inside the field point's backwards light cone. Over-retardation [95] is a covariant method for classical renormalization. We modify the Synge function

$$\sigma(x,z) = \frac{1}{2}(x-z)^{\alpha} g_{\alpha\beta}(x-z)^{\beta} + w_3 \tag{5.4}$$

where $w_3 \geq 0$ is the parameter. Over-retardation disallows the source-field point coincidence.

Finally, we round off discontinuous features on the string. For kinks the transition from one derivative value to another is smoothed. For cusps a small patch of the world sheet near the cusp is excised. We introduce a parameter w_4 that yields the discontinuous solution when $w_4 \to 0$. Smoothing must be implemented separately for each loop of interest. In the 2D approach any discontinuity, even if it were not on the field point's exact light cone, must be smoothed because all world sheet points are sampled by the smoothed delta function.

The 2D calculation does not require any special treatment for boundaries, any special choice of coordinates or any special handling of the field point. The discontinuities in the source must be smoothed. We let $\{w_1, w_2, w_3, w_4\} \to 0$ in lockstep together. We have found that the limit is not impacted if we set $w_2 = 0$ (the smoothing of the causal step function) and $w_3 = 0$ (the over-retardation) from the beginning. Using the Gaussian approximation to the delta function and smoothing the discontinuities on the string are sufficient to regulate the calculation.

B. 1D, over-retarded, smoothed kink or cusp [1DOS]

The 1D calculations in which the Green function has been integrated out must handle the case where the field and source points coincide, the string discontinuities and coordinate changes along the retarded loop image.

In the [1DOS] method we use over-retardation and smooth the discontinuities on the string if they are visible on the field point's exact light cone. We integrate Eq. (3.30) over the image if coordinate ζ^2 covers the entire image; we additionally include boundary terms of the type given in Eq. (4.27) if multiple coordinate systems are utilized. Here a boundary term arises not because of a string discontinuity but because of the coordinate change. We let $\{w_3, w_4\} \to 0$.

C. 1D, over-retarded, discontinuous kink or cusp [1DO]

As above we use over-retardation for the [1DO] method, but we do not smooth the kink. We numerically locate the kink and use boundary terms of the type given in Eq. (4.27) to handle both jumps in the string source and coordinate changes. We can evaluate the force for the cusp as long as the cusp is not on the light cone (almost all world sheet points). We let $\{w_3\} \to 0$.

D. 1D, discontinuous kink or cusp [1D]

For the [1D] method we use the analytic results (4.49) for the contribution from the source and field points coinciding, along with boundary terms and of the form given in Eq. (4.27) for jumps in the string source and coordinate changes. As above we can evaluate the force for strings with cusps as long as the cusp is not on the light cone. This is the computationally most efficient method and the one that we are primarily interested in validating for future calculations of loops evolving under the effect of gravitational backreaction. It does not require any regularization parameters w_i.

There are many related questions that we address using these techniques. For example, we compare the self-force calculated utilizing different coordinate systems (this is possible for all the methods, but we concentrate on the [1D] case). We also consider a limiting process in which the [1DO] method is used for a field point off the world sheet, and we verify that the correct behavior is recovered as the field point approaches the world sheet.

VI. NUMERICAL RESULTS

We now apply the derivations of the previous sections to some specific examples, numerically computing the self-force for a range of nontrivial string configurations that feature kinks, cusps and self-intersections. We perform several consistency checks in the process:

(1) For strings with a particularly simple structure we compare against existing calculations in the literature;
(2) For more nontrivial strings we compare different versions of the [1D] integration done with different choices of world sheet coordinates;
(3) We compare against the smoothed approaches [1DOS] and [1DO] for handling kinks and field point contributions. The field point contribution is recovered by evaluating the integral for the force with a small over-retardation of the retarded time and numerically taking the limit as this over-retardation vanishes. The kink contribution is similarly recovered by introducing a small smoothing to the kink and taking the limit of the smoothing parameter going to zero.
(4) We further compare against our other entirely independent [2D] approach, whereby the force is directly determined from a full 2D integration over the world sheet, approximating the Dirac δ distribution in the Green function by a narrow Gaussian.
(5) We verify that the flux of radiation to infinity (as computed using standard frequency domain methods [96]) appropriately balances the local self-force.

There are infinitely many possible cosmic string loops which satisfy (3.4). The examples which have typically been studied in the literature are those with a low number of harmonics. As a demonstration of our prescription for computing the self-force, we will compute the self-force for several of these strings. Our goal is not to be exhaustive, but rather to select a set of test cases that cover all scenarios (kinks, cusps, self-intersections, and strings without too much symmetry). In all cases below, we define the world sheet in terms of two functions $a^\alpha(\zeta^+)$ and $b^\alpha(\zeta^-)$, where $\zeta^+ \equiv \tau + \zeta$ and $\zeta^- \equiv \tau - \zeta$ are null world sheet coordinates. Then, the spacetime position of the string is $z^\mu = (1/2)[a^\mu(\zeta^+) + b^\mu(\zeta^-)]$. Throughout the discussion, we will also refer to the three-vectors **a** and **b**, which are defined to be the spatial projections of $a^\alpha(\zeta^+)$ and $b^\alpha(\zeta^-)$. Finally, we will specialize to the specific case $t = \tau$ within the class of conformal gauges.

A. Allen, Casper and Ottewill self-similar string

ACO [61] identified a particularly simple class of strings for which the average power radiated is easily calculated in closed form. All strings in the class have a pair of kinks, each propagating along lines of constant $\zeta^+_{k_1} = 0$ and $\zeta^+_{k_2} = L/2$, respectively. ACO's motivation was to find the string which radiates most slowly and is thus most long lived. Our motivation for studying the ACO string[14] stems from a different consequence of the simplicity of the ACO solution. Anderson [81] showed that the description of the ACO string world sheet is sufficiently simple that it is possible to determine the self-force analytically.[15] This provides a valuable reference point against which we can check our numerical approach.

The ACO string world sheet is given in Cartesian coordinates by

$$a^\alpha(\zeta^+) = A[\zeta^+/A, 0, 0, |\zeta^+|],$$
$$b^\alpha(\zeta^-) = A[\zeta^-/A, \cos(\zeta^-/A), \sin(\zeta^-/A), 0], \qquad (6.1)$$

where $A \equiv \frac{L}{2\pi}$ and L is the length of the string. For $\zeta^+ < -\frac{L}{2}$ or $\zeta^+ > \frac{L}{2}$ the periodic extension of a^z is used; i.e., a^z is the triangle function centered about the origin and with period L. The ACO string can be visualized as shown in Fig. 1; its evolution is a rigid rotation of this shape about the z-axis.[16]

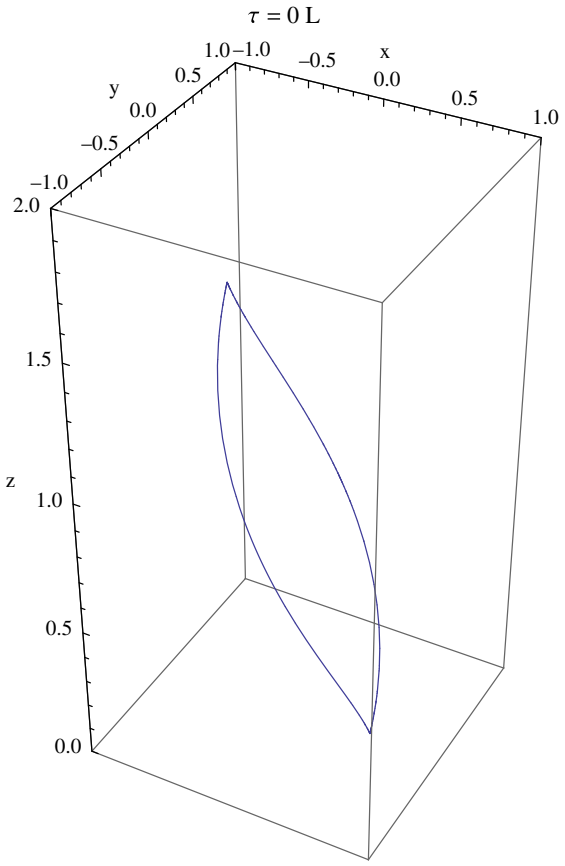

FIG. 1. Snapshot of the ACO string loop configuration in spacetime at time $\tau = 0$. At later times the configuration can be obtained by a rigid rotation about the z-axis.

We characterize the ACO string in terms of its tangent-sphere representation, as shown in Fig. 2.

Adopting the conformal gauge to first order, Anderson [81] was able to compute the self-force [which in the conformal gauge case is defined to be the right-hand side of Eq. (3.14)] by analytically determining the first-order metric perturbation generated by an ACO string. Factoring out the rigid rotation using the matrix

$$M^\alpha{}_\beta = \begin{pmatrix} 1 & 0 & 0 & 0 \\ 0 & \cos(2\pi\zeta^-) & \sin(2\pi\zeta^-) & 0 \\ 0 & -\sin(2\pi\zeta^-) & \cos(2\pi\zeta^-) & 0 \\ 0 & 0 & 0 & 1 \end{pmatrix}, \qquad (6.2)$$

the conformal gauge self-force in a corotating frame is given by $f^\mu = M^\mu{}_\alpha \mathcal{F}^\alpha_{\rm conf}$, where $f^\mu = [f^t(\zeta^+), f^L(\zeta^+), f^N(\zeta^+), \mathrm{sgn}(\zeta^+) f^t(\zeta^+)]$. We can interpret f^N and f^L as the normal and longitudinal components of the force in the x–y plane, respectively. Note that this factorized form is quite convenient as the dependence on ζ^+ is entirely contained within f^μ, while the dependence on ζ^- is entirely in $M^\chi{}_\mu$.

[14]We will study just one case in the class of ACO strings, the one which is simplest and which radiates power most slowly. ACO call this particular string "case (1) with $M = 1$." We will simply refer to it as *the* ACO string.

[15]In fact, in [97] Anderson was able to go one step further and analytically self-consistently evolve the string under the influence of gravitational backreaction.

[16]In [97] Anderson showed that this shape is preserved when backreaction is taken into account, in which case the string evolves (shrinks) self-similarly.

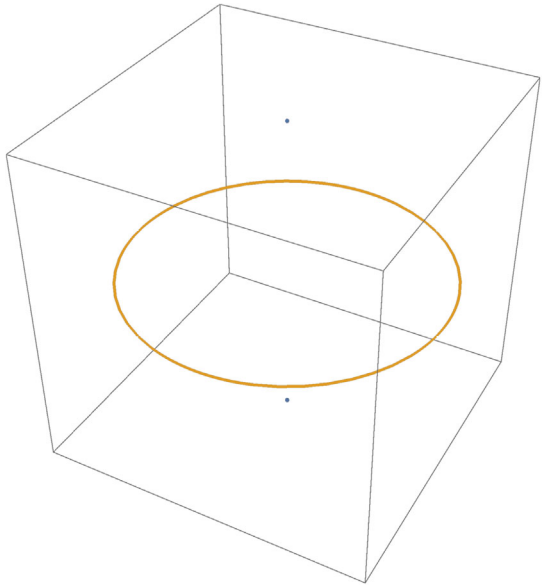

FIG. 2. Tangent sphere representation of the ACO string loop configuration with $\mathbf{a}'(\zeta^+)$ denoted by the two blue dots and $\mathbf{b}'(\zeta^-)$ by the orange circle.

As an important consistency check on our work, we have verified that our numerical approach exactly reproduces the analytic result derived by Anderson. Figure 3 shows the factored components of the force as a function of ζ^+, with Anderson's expressions plotted as solid lines and our numerical values [computed using Eq. (3.30) plus boundary terms of the type given in Eq. (4.27) at the kinks and Eq. (4.49) for the field point contribution] shown as dots.

One interesting feature is the divergence of the force components as a kink is approached. Although one may be concerned about the physical implications of this divergence, for the ACO string it turns out that it is a spurious gauge artifact, and that the string world sheet itself only ever picks up a small perturbation from the self-force. The simplicity of the ACO solution makes it straightforward to see this explicitly: as shown by Anderson [81], the explicit form of the divergence near the kink can be written as

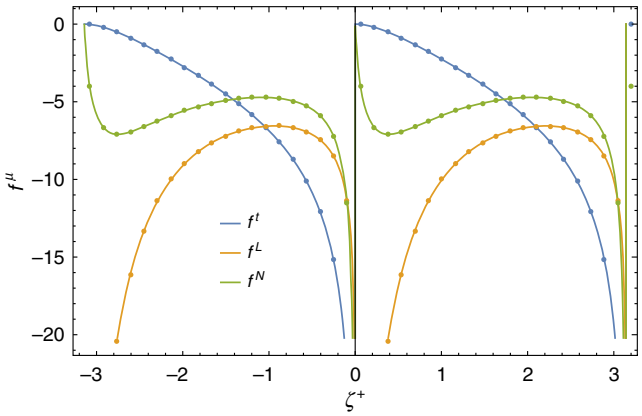

FIG. 3. Corotating self-force for the ACO string.

$$f^t \approx \left\{-32\left(\frac{1}{6}\pi^2\right)^{1/3}\mu/|\zeta^+|^{1/3}, -128\pi^2\mu(\zeta^+)^2\right\},$$
$$f^L \approx 32\pi\mu\ln|\zeta^+|\left\{\frac{1}{3}, 1\right\},$$
$$f^N \approx \left\{-32\left(\frac{1}{6}\pi^2\right)^{1/3}\mu/|\zeta^+|^{1/3}, 128\pi^2\mu\zeta^+\ln|\zeta^+|\right\}, \quad (6.3)$$

depending on whether the limit $\zeta^+ \to 0$ is taken from the left or the right. Anderson goes on to show that integrating up the equation of motion, the physical (nongauge) displacement of the string due to this divergent force is finite.

B. Kibble and Turok strings with cusps and self-intersections

A simple family of string loop solutions of the zeroth-order equations of motion was written down by Kibble and Turok [98,99]. The gravitational radiation of representative examples was calculated by Vachaspati and Vilenkin [36]. We will refer to the family as KT strings. The family is described by the general form

$$a^\alpha(\zeta^+) = A\Big[\zeta^+/A, (1-\alpha)\sin(\zeta^+/A) + \frac{\alpha}{3}\sin(3\zeta^+/A),$$
$$(\alpha-1)\cos(\zeta^+/A) - \frac{\alpha}{3}\cos(3\zeta^+/A),$$
$$-2\sqrt{\alpha(1-\alpha)}\cos(\zeta^+/A)\Big],$$
$$b^\alpha(\zeta^-) = A[\zeta^-/A, \sin(\zeta^-/A),$$
$$-\cos\phi\cos(\zeta^-/A), -\sin\phi\cos(\zeta^-/A)], \quad (6.4)$$

where $0 \le \alpha \le 1$ and $-\pi \le \phi \le \pi$ are two parameters.

We first focus on the case $\alpha = 0$ and $\phi = \pi/6$ ($N = M = 1$ Burden loops [58]). Nine snapshots of the spacetime configuration of the loop are shown in Fig. 4. The loop generally possesses an elliptical shape. It tumbles in space while stretching and contracting. Twice per period it forms a degenerate, linelike shape with a pair of cusps on opposite sides. The tangent sphere representation is particularly simple: there are two continuous great circles that cross at $\tau + n\pi = \zeta + m\pi = 0$ for any integers n and m. Each crossing gives rise to a cusp and to a spacelike line of string overlap in the center of momentum frame. These two effects make the calculation of the self-force particularly challenging.

We first compute the self-force at two points on the string (which we denote case I and case II):

$$(\tau, \zeta) = (32\pi/50, 13\pi/50) \quad \text{Case I} \quad (6.5)$$

$$(\tau, \zeta) \simeq (0.42, \pi/5) \quad \text{Case II.} \quad (6.6)$$

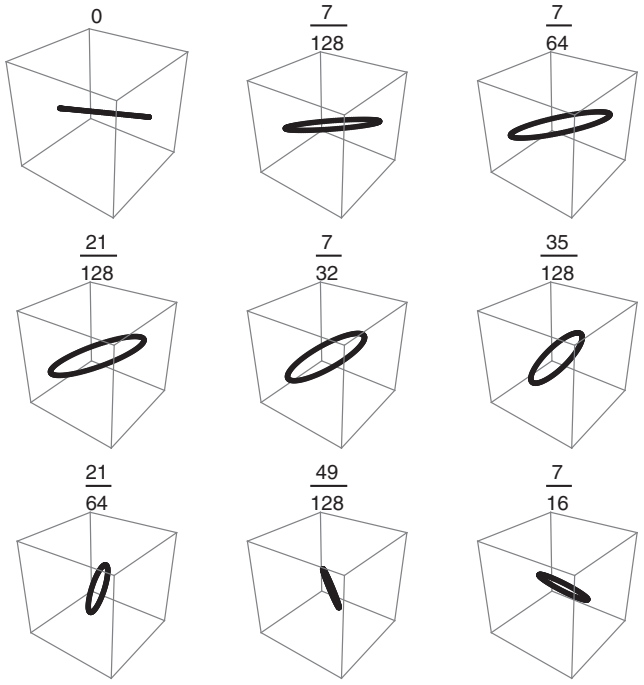

FIG. 4. Snapshots of the KT string loop ($\alpha = 0$ and $\phi = \pi/6$) configuration in spacetime, each labeled by time in units of L. All the boxes have the same size axes, -1 to 1 for $L = 2\pi$, and fixed orientation.

For case I, the field point is such that no cusp is present on the retarded image of the string. Since the left and right moving modes are continuous the loop stress-energy source is completely smooth except at the field point itself.[17] The case I results calculated by the [1D] method described in Sec. IV are given in the first part of Table I. In this case, there are two important contributions to F_1^ρ: the row labeled $\int$ is the integral contribution arising from the 1D integral over the smooth world sheet using Eq. (3.30); and δ is the contribution from the field point obtained using Eq. (4.49). The total is $F_1 = \int + \delta$.

For case II, we have carefully chosen a field point such that the cusp at $(\tau, \zeta) = (0, 0)$ lies on the retarded string image. Numerical results for this case (which were again obtained using the [1D] method) are given in the second part of Table I.

One notable feature of these numerical results is that the field point contribution is comparable in magnitude to the contribution from the integral. As such, this case provides a valuable and stringent test of our derivation of the expression for the field point contribution. By comparing to a different approach which does not rely on these terms we may distinguish between $\int$ and F_1. The [2D] integration method (described in detail in Appendix E) provides just such a comparison. In Table II we tabulate the results of the [2D] integration method and compare against the 1D results for case I in Table I. This comparison unambiguously confirms that the field point contribution is essential. The agreement provides a strong validation of our formalism. Appendix E includes analogous [2D] results for case II. These are in equally good agreement so we omit additional discussion of the comparison.

We now proceed to compute the self-force at *all* points on the world sheet. The results are shown in Figs. 5 and 6. Unlike the ACO case, the extra complexity in the KT solution means that there is no simple factorization of the force into a piece which only depends on ζ^+ and another piece which depends on ζ^-. As such, the self-force for the KT string is presented as a 2D surface plot, showing the force contributions to F^μ ($\log_{10}$ of the absolute value of a contribution, color coded by sign) at all[18] points on the

TABLE I. Self-force at two points on the KT string ($\alpha = 0$ and $\phi = \pi/6$) calculated by the 1D method.

		Contravariant spacetime components			
Case	Force	t	x	y	z
I	$\int$	9.28612	−4.96366	14.7739	−1.68376
	δ	−0.680917	1.09474	1.16578	−4.35077
	F_1	8.6052	−3.86891	15.9397	−6.03453
	F_2	−12.181	4.56246	−25.3768	14.1391
II	$\int$	44.5678	49.5374	22.8974	−1.99924
	δ	1.7937	1.5892	1.1546	−4.30897
	F_1	46.3615	51.1266	24.052	−6.30821
	F_2	−75.6739	−82.35	−39.8936	21.8117

TABLE II. The two contributions to the self-force calculated by the [2D] method in case I of the KT string ($\alpha = 0$ and $\phi = \pi/6$). First column is the name of the component; second column is the force extrapolated to zero grid spacing; three column is the uncertainty in the extrapolation; column 4 is the difference in the force determined by the [2D] and [1D] methods.

Force	Extrapolated Force	Extrapolated error	2D − 1D
F_1^t	8.60882	0.0020	−0.0036
F_1^x	−3.87143	−0.0016	0.0025
F_1^y	15.9437	0.0013	−0.0040
F_1^z	−6.0318	0.0030	−0.0027
F_2^t	−12.181	3.6×10^{-5}	1.0×10^{-5}
F_2^x	4.56246	-1.5×10^{-6}	-9.6×10^{-7}
F_2^y	−25.3768	-1.6×10^{-5}	2.7×10^{-5}
F_2^z	14.1391	-7.5×10^{-6}	1.5×10^{-5}

[17]In a patch of the world sheet that extends $\pm\pi$ about the field point the cusps at $(\tau, \zeta) = (0, 0)$ and $(0, \pi)$ are potentially visible for a causal off-shell Green function.

[18]In all of our plots we show the segment of the world sheet defined by $\tau \in [0, L/2]$, $\zeta \in [-L/2, L/2]$. This covers the entire set of unique points on the world sheet; other values can be obtained by periodically extending in the τ and/or ζ direction.

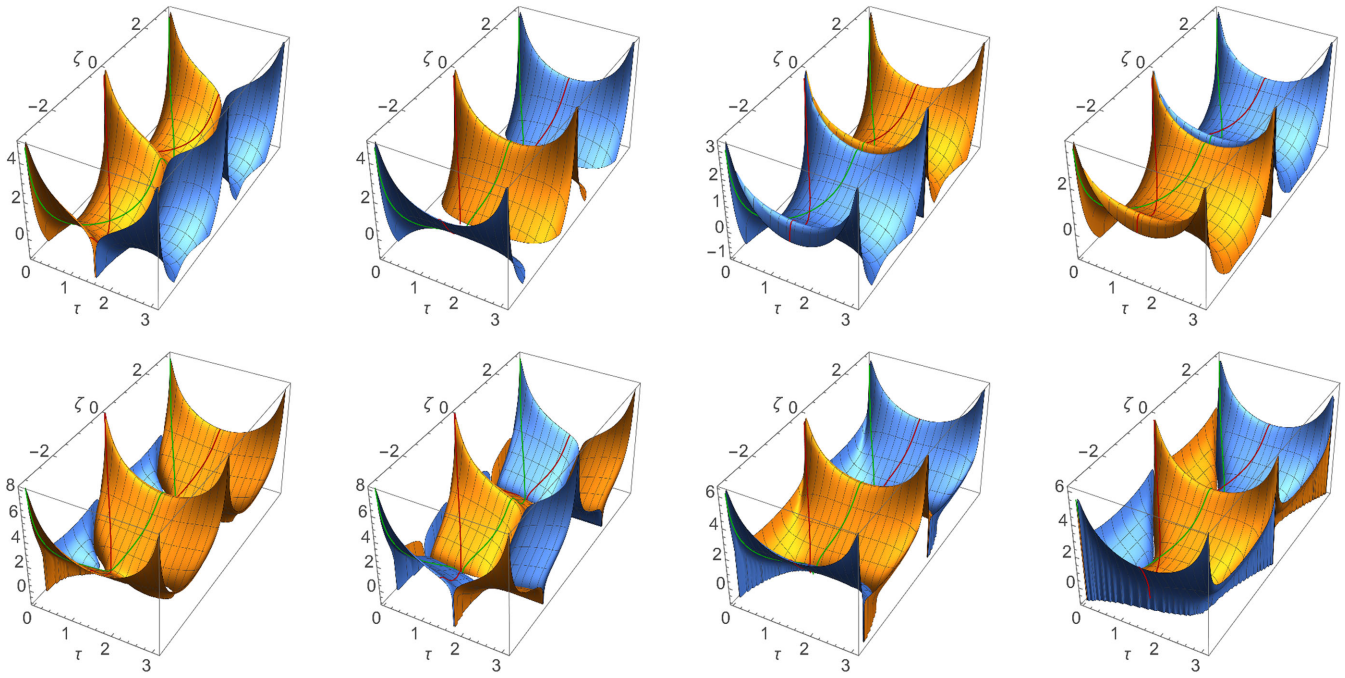

FIG. 5. Contributions to F_1^μ for the KT string ($\alpha = 0$ and $\phi = \pi/6$) when computed using the 1D integration method with integration with respect to ζ. Each subfigure shows the relevant contribution to the force at all points on the string in the region $\tau \in (0, L/2)$, $\zeta \in (-L/2, L/2)$; all other points can be obtained from the standard periodic extension of the string. Each column corresponds to a different component of the force: F_1^t, F_1^x, F_1^y, and F_1^z. The rows correspond to the contributions from (i) the field point and (ii) the integral over ζ (ignoring distributional contributions at the field point). For the purposes of the plots, we have set the string tension, μ, and Newton's constant, G, equal to 1; other values simply introduce an overall scaling. Note that we have used a logarithmic scale and denoted positive (negative) values by coloring the plot orange (blue).

two-dimensional world sheet. The green and red curves trace the advanced images of the cusps on the loop; each point on these curves has the cusp at $(\tau, \zeta) = (0, 0)$ (red) or at $(\tau, \zeta) = (0, L/2)$ (green) on its past light cone. The gross variation of the self-force depends on the product of two factors which have simple physical origins. First, the loop's linelike structure, periodically formed at $\tau = 0$ and $L/2$, creates a ridge spanning all ζ at these particular times. Second, at any given time the points along the string loop which are least contracted and have the largest $\sqrt{-\gamma}$ occur at $\zeta = \pm L/4$. These produce a trough or minimum in the force at $\zeta = \pm L/4$. The product of these two factors yields the egg-crate-like symmetry in the force with the cusps at the corners.

These plots show several interesting features:

(1) The self-force is finite at almost all points on the world sheet, the notable exceptions being the location of the two cusps, where it appears to diverge.
(2) The two contributions to F_1^μ (coming from the integral over the smooth world sheet and from the field point) are comparable in magnitude. It is therefore crucial that both contributions be included.
(3) The contributions from F_1^μ and F_2^μ are both comparable in magnitude and both exhibit the same qualitative behavior in terms of divergence at the cusp and finiteness elsewhere.

Although this case provides a good check of the general methodology it involves special features that can be traced to the self-intersections. In the next section we modify the parameter choice to avoid self-intersections.

C. KT strings with cusps without self-intersections

Next we consider a KT string with parameter values $\alpha = 1/2$ and $\phi = 0$. Snapshots of this loop are shown in Fig. 7. The loop rotates about the z-axis and forms cusps transiently at $(\tau, \zeta) = (0, 0)$ and $(0, L/2)$. There are no self-intersections except infinitesimally close to the cusp itself.

Figures 8 and 9 show the self-force at all points on the world sheet of this KT string. These are analogous to the plots for the self-intersecting KT string shown in Figs. 5 and 6. The peaks clearly show the cusp locations and the diagonal striping is related to the overall sense of rotation of the loop. The spacelike line of overlap and the egg-crate symmetry seen in the previous KT case are now absent.

This nonintersecting case allows for a detailed analysis of the behavior of the total backreaction force in the vicinity of the cusp at $(\tau, \zeta) = (0, 0)$. At times close to cusp formation the tip's position (the string coordinate at fixed $\zeta = 0$) is

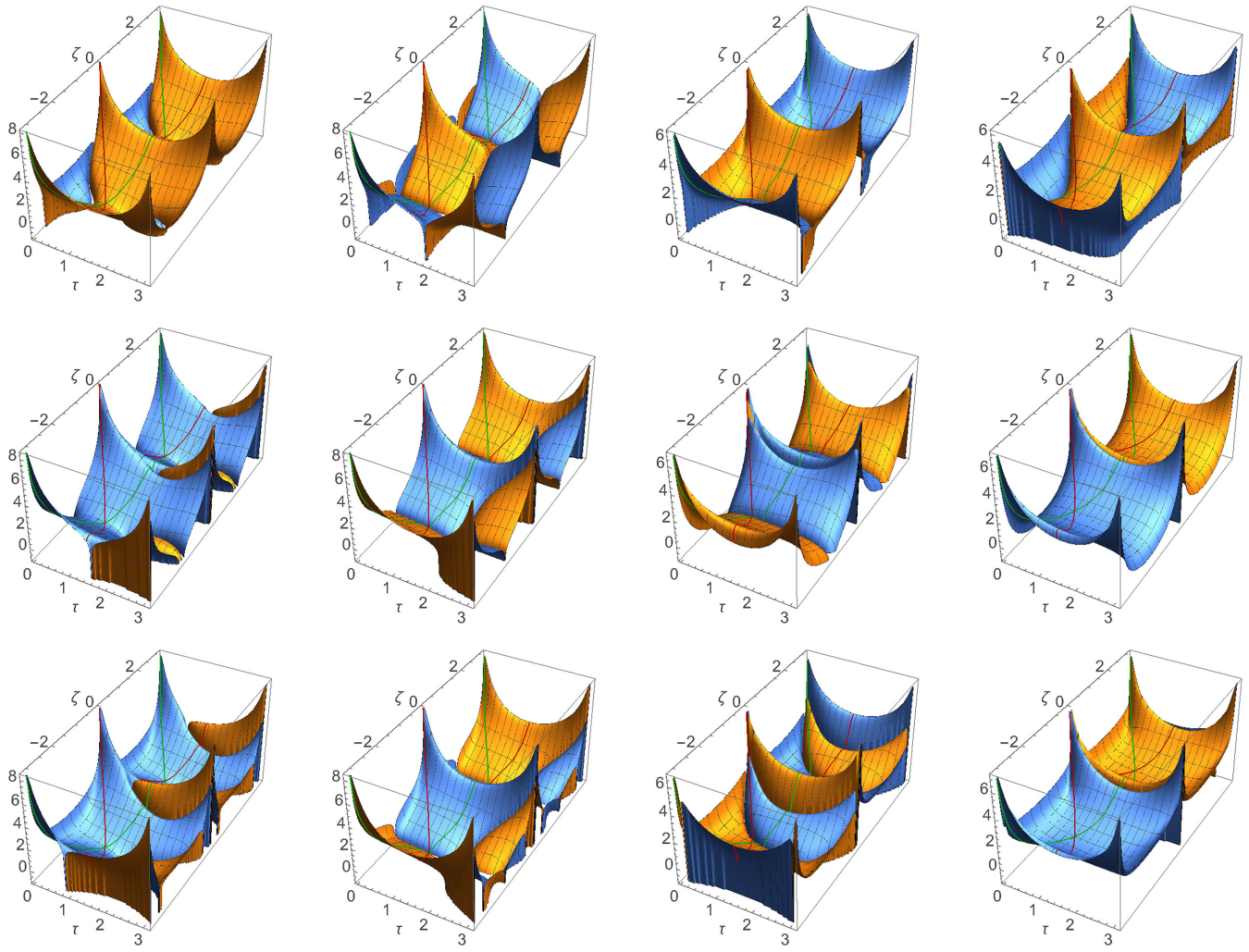

FIG. 6. The two pieces of the self-force, F_1^μ (row 1) and F_2^μ (row 2), and the total self-force F^μ (row 3) for the KT string ($\alpha = 0$ and $\phi = \pi/6$) as a function of position on the string. The F_1^μ part can be obtained by summing the two rows in Fig. 5. For the purposes of the plots, we have set the string tension, μ, and Newton's constant, G, equal to 1; other values simply introduce an overall scaling. Note that we have used a logarithmic scale and denoted positive (negative) values by coloring the plot orange (blue).

$$\mathbf{z}^i \sim \{0, -0.83, -0.5\} + \{1, 0, 0\}\tau + \{0, 1.5, 0.5\}\frac{\tau^2}{2} + \{-3, 0, 0\}\frac{\tau^3}{6} + \{0, -7.5, -0.5\}\frac{\tau^4}{24} + \cdots \tag{6.7}$$

The velocity lies in the x-direction and the acceleration in the y- and z-directions. Conversely, the velocities in the y- and z-directions and the acceleration in the x-direction vanish. On physical grounds we expect the y- and z-accelerations to source transverse gravitational waves and the relativistic motion in the x-direction to lead to strong beaming.

The driving force F^α which enters the string loop's equation of motion, Eq. (3.5), encodes the fully nonlocal, self-interacting gravitational dynamics. If we were to adopt the conformal gauge at first order then $\mathcal{F}^\alpha_{\rm conf}$ would naturally appear as the driving force in the equation of motion. We will not restrict ourselves to that choice for much of the discussion in this section. We will show, however, that many of the features of the full world sheet variation of F_1^α can be understood based on the observed properties of the formally defined quantity $\mathcal{F}^\alpha_{\rm conf}$ (which may be defined in any gauge; only its interpretation as the driving force is restricted to conformal gauge). We will be explicit whenever our statements demand the specification of the conformal gauge.

The large dynamic range evident in Figs. 8 and 9 necessitates looking at small patches to examine special features like the cusp. We begin by displaying $\mathcal{F}^\mu_{\rm conf}$ in Fig. 10. The special coordinate system shows a small patch near the cusp which is located at $\zeta = 0 = \tau$. Results for $\ln|\mathcal{F}^\mu_{\rm conf}|$ are displayed in these figures, color coded according to the sign of the quantity: orange (blue) dots represent positive (negative) values. Each figure combines four plots with axes $\{\mathrm{sgn}(\zeta)\ln|\zeta|, \mathrm{sgn}(\tau)\ln|\tau|\}$, arranged and oriented in the same way as a normal linear plot (plus a

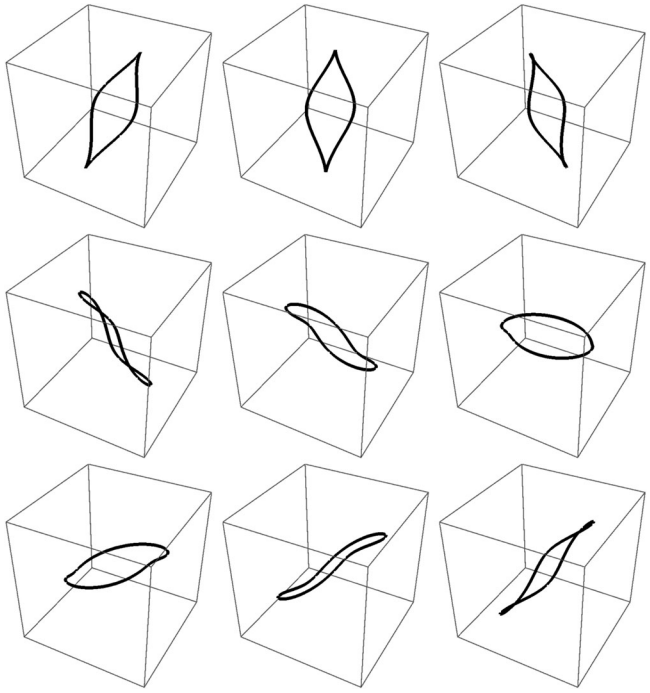

FIG. 7. Snapshots of the KT string loop ($\alpha = 1/2$ and $\phi = 0$) configuration in spacetime, at equally spaced times during the fundamental period (as in Fig. 4). All the boxes have the same size axes, -1 to 1 for $L = 2\pi$, and fixed orientation.

constant shift selected to bring small values close to the center). The lower left-hand quadrant has $\zeta < 0$ and $\tau < 0$. Smaller values of $|\tau|$ and $|\zeta|$ lie near the center for all four quadrants. The gap encompasses all values near the sign change of the independent coordinates.

We find that $\mathcal{F}^t_{\rm conf} < 0$ for the entire area of the patch. The magnitude of $\mathcal{F}^t_{\rm conf}$ is much less than F^t and is less strongly divergent—the two are related by a projection factor and an overall factor of $1/\sqrt{-\gamma}$ [see Eq. (3.6)], both of which diverge as the cusp is approached. Likewise, $\mathcal{F}^x_{\rm conf} < 0$, $\mathcal{F}^y_{\rm conf} > 0$ and $\mathcal{F}^z_{\rm conf} > 0$ have single, well-defined signs throughout most of the area of the corresponding patch.

In the conformal gauge the negative value for $\mathcal{F}^t_{\rm conf}$ implies [see Eq. (C57) in Appendix C] that the string is losing energy and decelerating in the x-direction both before and after the cusp forms. This makes physical sense; the self-force saps the mechanical energy during the period of large acceleration and the relativistic beaming ensures that gravitational waves are emitted primarily in the x-direction, thus creating the largest decelerating force in that direction. A small spatial segment of the string near where the cusp forms behaves in a coherent fashion before and after the moment of cusp formation in terms of the signs of $\mathcal{F}^\alpha_{\rm conf}$ for all components. $\mathcal{F}^\alpha_{\rm conf}$ shows a net positive acceleration in the y- and z-directions throughout most of the area of these figures.

As the figures of $\mathcal{F}^\mu_{\rm conf}$ make clear, the asymptotic behavior near the cusp varies depending upon the direction of approach. A common diagonal feature is the locus in the world sheet where $\sqrt{-\gamma} \geq 0$ is small. Only at the cusp is γ exactly equal to zero, but along the visible fold its values are small.

Regardless of direction, however, the scaling with radial distance from the cusp is clear and unambiguous in each of the components. The smooth integral contribution to $\mathcal{F}^\mu_{\rm conf}$

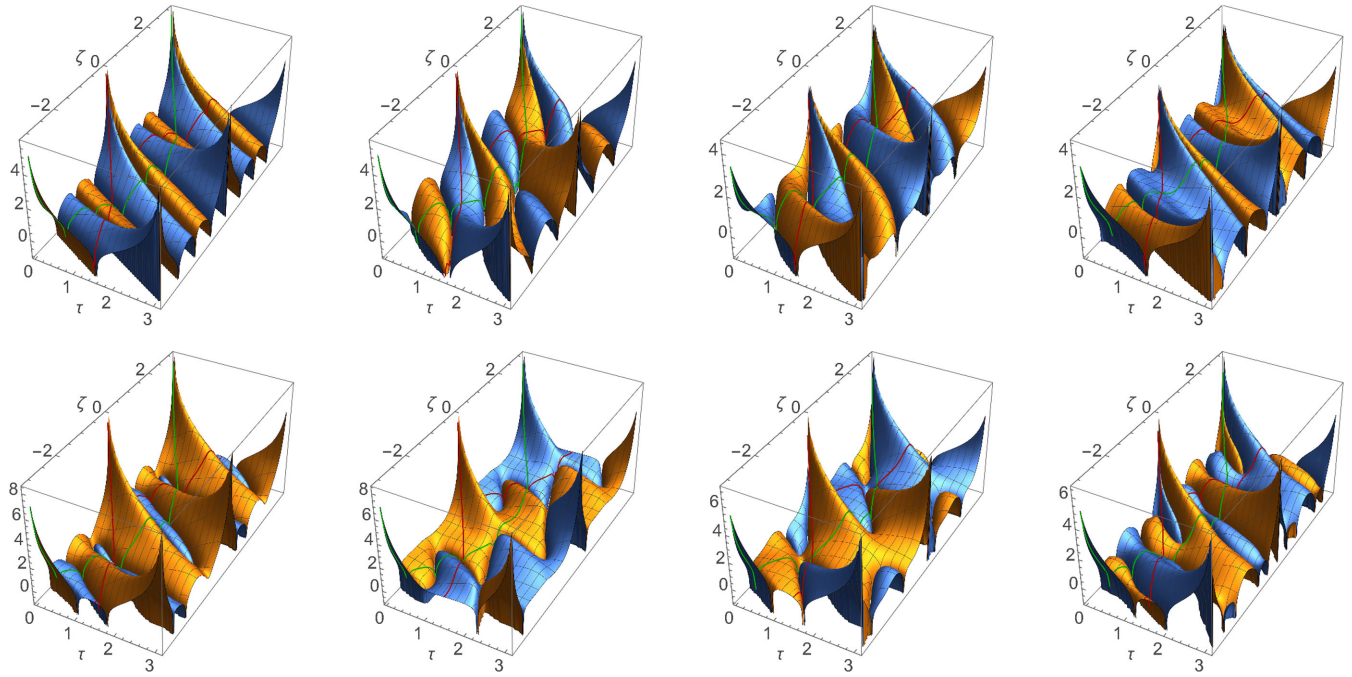

FIG. 8. Contributions to F^μ_1 for the KT string ($\alpha = 1/2$ and $\phi = 0$) as otherwise described in Fig. 5.

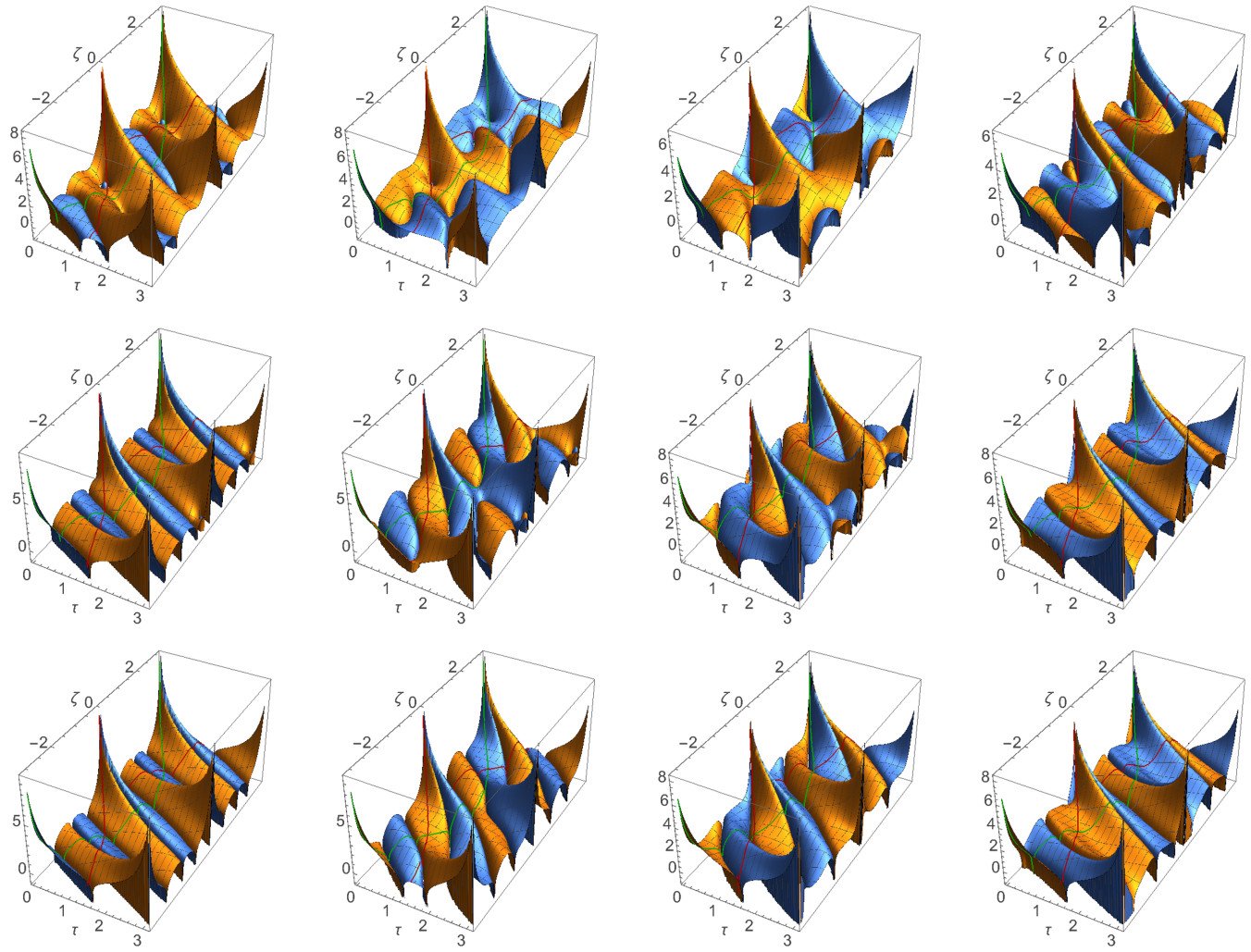

FIG. 9. The two pieces of the self-force, F_1^μ (row 1) and F_2^μ (row 2), and the total self-force F^μ (row 3) for the KT string ($\alpha = 1/2$ and $\phi = 0$) as otherwise described in Fig. 6.

is shown in Fig. 11 for rays approaching the cusp with angle $\theta = 0$ ($\delta\tau = 0$) and $\theta = \pi/2$ ($\delta\zeta = 0$). The red dots are numerical results and the blue lines are fits of the form $\log|F^\mu| = a\log|\log r| + b\log r + c$.[19] The angular variation and scaling of the delta-function term and the smooth integral contribution are illustrated in Fig. 12 and discussed in the caption.

Two-dimensional numerical fits for the integral part of $\mathcal{F}^\mu_{\rm conf}$ are summarized in Appendix F. We find that $\mathcal{F}^t_{\rm conf}$ and $\mathcal{F}^x_{\rm conf}$ scale as the inverse distance from the cusp, and that $\mathcal{F}^y_{\rm conf}$ and $\mathcal{F}^z_{\rm conf}$ are at worst much less singular (consistent with a log divergence). From this we conclude that when one adopts the conformal gauge at first order the self-force near the cusp has a weak, integrable divergence on the world sheet and that any integrated quantities (such as the radiated energy) are finite.

[19]The occurrence of both $\log|\log r|$ and $\log r$ are consistent with recently reported analytic results of Blanco-Pillado, Olum and Wachter (see Acknowledgments).

Given the scalings for $\mathcal{F}^\mu_{\rm conf}$ nearby the cusp, it is straightforward to deduce the corresponding scaling for $F_1^\mu = -\frac{1}{\sqrt{-\gamma}}\perp^\mu{}_\nu \mathcal{F}^\nu_{\rm conf}$. Working with the exact expression for the determinant of the induced metric in this case,

$$\gamma = -\frac{1}{16}[2 - \cos(2\zeta) - \cos(4\zeta + 2\tau)]^2, \tag{6.8}$$

and expanding the relationship between F_1^μ and $\mathcal{F}^\mu_{\rm conf}$ to next from leading order, we find

$$F_1^t \approx F_1^x \approx -\frac{1}{\gamma}\left\{(\mathcal{F}^t_{\rm conf} - \mathcal{F}^x_{\rm conf}) - \frac{1}{2}[(\mathcal{F}^z_{\rm conf} + 3\mathcal{F}^y_{\rm conf})\tau + (\mathcal{F}^z_{\rm conf} + \mathcal{F}^y_{\rm conf})\zeta] + \cdots\right\}, \tag{6.9}$$

$$F_1^y \approx -\frac{1}{2\gamma}(\mathcal{F}^t_{\rm conf} - \mathcal{F}^x_{\rm conf})(\zeta + 3\tau) + \cdots, \tag{6.10}$$

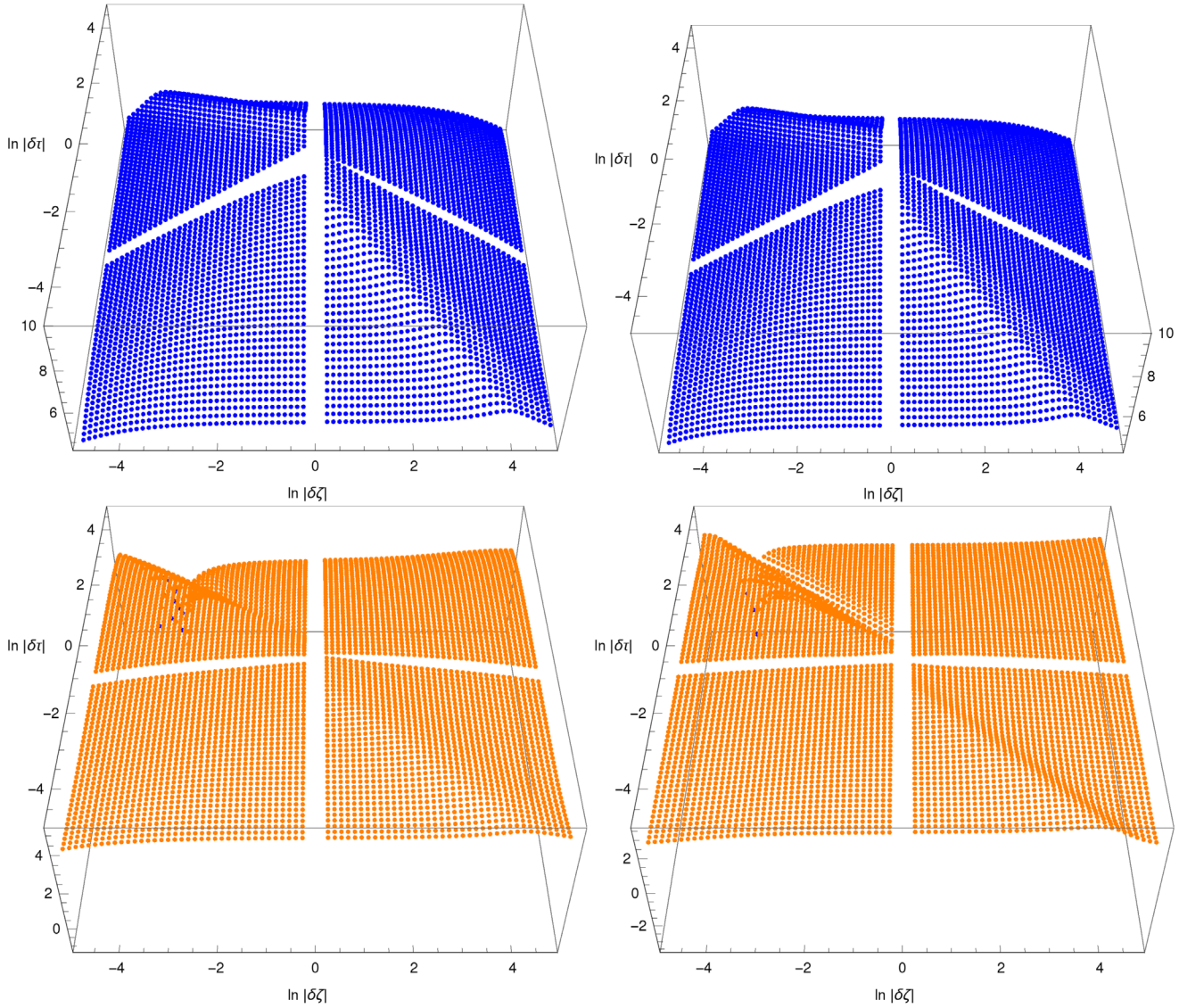

FIG. 10. The four components (t, x, y and z [left to right, top to bottom]) of $\ln|\mathcal{F}^{\alpha}_{\rm conf}|$ on a small patch of the world sheet about the cusp. Four quadrants in $\{\log\tau, \log\zeta\}$ are displayed with the smallest $|\tau|$ and $|\zeta|$ at the center of the picture, oriented in the same way as the usual linear system about $\{0, 0\}$. Orange (blue) represent positive (negative) values.

$$F^{z}_{1} \approx -\frac{1}{2\gamma}(\mathcal{F}^{t}_{\rm conf} - \mathcal{F}^{x}_{\rm conf})(\zeta + \tau) + \cdots. \tag{6.11}$$

Since γ scales as the fourth power of the distance from the cusp we infer that F^{μ}_{1} is naively four orders more singular than $\mathcal{F}^{\mu}_{\rm conf}$. However, as can be seen in Table III, it turns out that $\mathcal{F}^{t}_{\rm conf} \approx \mathcal{F}^{x}_{\rm conf}$ near the cusp so the leading-order divergence cancels and at worst F^{μ}_{1} diverges as the inverse fourth power of the distance from the cusp. At next-from-leading order the asymptotic expression for F^{μ}_{1} is anti-symmetric about the cusp. (This behavior, combined with the mixing of components, is what makes the analysis of $\mathcal{F}^{\mu}_{\rm conf}$ clearer than working directly with F^{μ}_{1}.) With the world sheet weighting we naively infer that $\sqrt{-\gamma}F^{\mu}_{1}$ diverges as the inverse quadratic power of the distance from the cusp, one power worse than $\mathcal{F}^{\mu}_{\rm conf}$. Now we must consider the role of F^{μ}_{2}.

To understand the behavior of F^{μ}_{2} near the cusp we begin with the perturbed metric projected along the world sheet vectors $\partial_{\tau}z^{\alpha}$ and $\partial_{\zeta}z^{\alpha}$ according to

$$H_{\tau\tau} = \partial_{\tau}z^{\alpha}h_{\alpha\beta}\partial_{\tau}z^{\beta} \tag{6.12}$$

$$H_{\tau\zeta} = \partial_{\tau}z^{\alpha}h_{\alpha\beta}\partial_{\zeta}z^{\beta} \tag{6.13}$$

$$H_{\zeta\zeta} = \partial_{\zeta}z^{\alpha}h_{\alpha\beta}\partial_{\tau}z^{\beta}. \tag{6.14}$$

Evaluating the simple expression Eq. (3.7) for the relationship between F^{μ}_{2} and the world sheet projections of the metric perturbation, we find

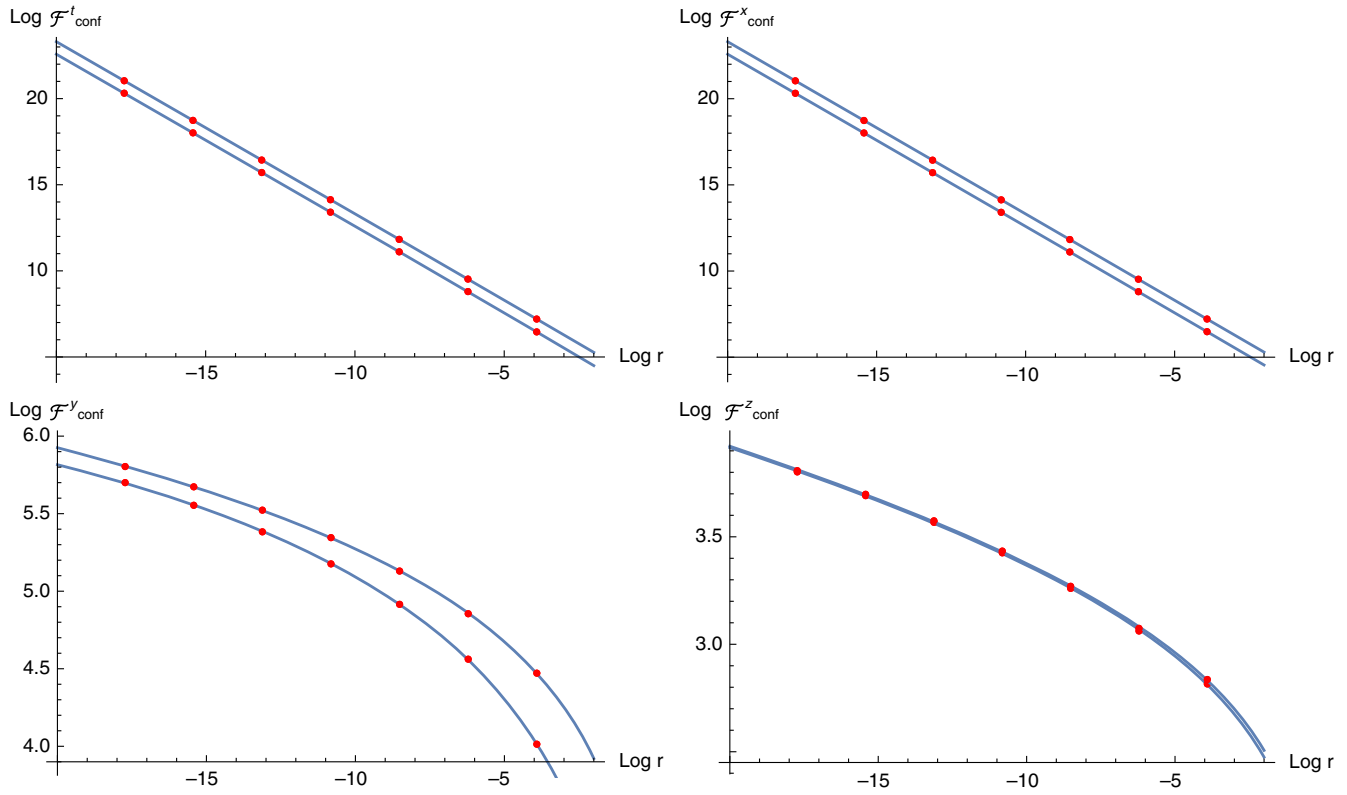

FIG. 11. The components of the smooth integral contribution to $\mathcal{F}^\mu_{\rm conf}$ along two rays at angles $\theta = 0$ and $\pi/2$ are shown. Red dots are numerical results and blue lines are fits of the form $\log|\mathcal{F}^\mu| = a\log|\log r| + b\log r + c$. For $\mu = t$, $(a, b, c) = (0.098, -0.99, 2.45)$ for $\theta = 0$ and $(0.046, -1, 3.24)$ for $\theta = \pi/2$; likewise, for $\mu = x$, $(a, b, c) = (0.044, -1, 2.52)$ and $(0.018, -1, 3.28)$. These fits show that the dominant behavior in the direction of motion of the cusp as $r \to 0$ is $1/r$. In the other directions, the behavior is consistent with a logarithmic divergence at leading order: $\mu = y$, $(a, b, c) = (0.79, -0.011, 3.35)$ and (1.23,0.013,2.39); $\mu = z$, $(a, b, c) = (0.43, -0.025, 2.13)$ and (0.41, −0.026, 2.17).

$$F_2^t \approx F_2^x \approx \frac{1}{2(-\gamma)^{3/2}}[2(5H_{\tau\zeta} - H_{\tau\tau} - H_{\zeta\zeta})\zeta + (4H_{\tau\zeta} - H_{\tau\tau} - H_{\zeta\zeta})\tau + \cdots], \tag{6.15}$$

$$F_2^y \approx \frac{2(6H_{\tau\zeta} - H_{\tau\tau} - H_{\zeta\zeta})(\zeta^2 + 3\tau\zeta + \tau^2) + \cdots}{2(-\gamma)^{3/2}}, \tag{6.16}$$

$$F_2^z \approx \frac{2(2H_{\tau\zeta} - H_{\tau\tau} - H_{\zeta\zeta})(\zeta^2 + 3\tau\zeta + \tau^2) + \cdots}{2(-\gamma)^{3/2}}. \tag{6.17}$$

With the finite behavior of the world sheet projections of the metric perturbation, it is straightforward to deduce the corresponding scaling of the divergence in F_2^μ. We find that at worst F_2^t and F_2^x diverge as the inverse fifth power of distance from the cusp. With the world sheet weighting $\sqrt{-\gamma}F_2^\mu$ diverges as the inverse cubic power of the distance from the cusp. However, as this leading-order divergence is antisymmetric about the cusp its integral over a patch around the cusp cancels the leading-order divergence to leave only subleading pieces.

We are now left with asymptotic forms for $\sqrt{-\gamma}F_1^\mu$ and $\sqrt{-\gamma}F_2^\mu$, each scaling as the square of the inverse distance from the cusp. These are individually nonintegrable. However, once the asymptotic forms given in Table III for the quantities in Eqs. (6.9)–(6.11) and (6.15)–(6.17) are taken into account, we find that the leading-order divergent behavior exactly cancels (see Table IV) to the level of accuracy of the numerically fitted coefficients in the combination $\sqrt{-\gamma}(F_1^\mu + F_2^\mu)$ yielding the full force $\sqrt{-\gamma}F^\mu$ which at worst diverges as the inverse distance from the cusp, and hence is integrable. This divergence is no worse than $\mathcal{F}^\mu_{\rm conf}$ itself.

A detailed understanding of the behavior of these divergences near cusps allows us to solve either the general covariant equation of motion (3.5) or the corresponding Eq. (3.14) in which specific conformal gauge choices have been adopted.

D. Garfinkle and Vachaspati string with kinks

The third case we will explore is from a class of strings found by Garfinkle and Vachaspati (GV) [59]. These strings contain two kinks that travel in the same direction on an oscillating and twisting string loop. We choose a particular representation from the general class with the following right- and left-moving modes:

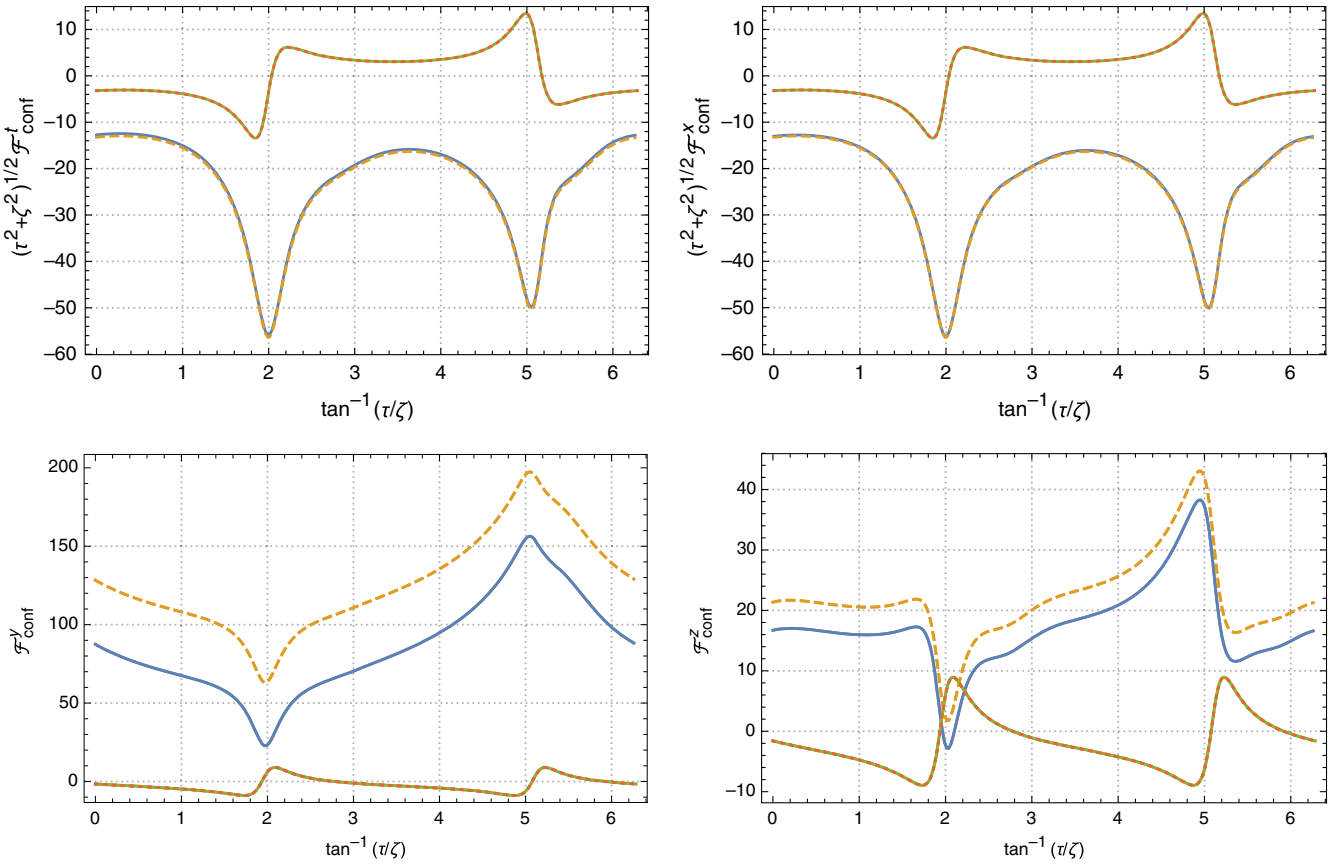

FIG. 12. $\mathcal{F}^{\mu}_{\rm conf}$ for the nonintersecting KT string ($\alpha = 1/2$ and $\phi = 0$) in the neighborhood of the cusp at $\tau = 0 = \zeta$. The t and x components have been scaled by the radial (Euclidean) distance from the cusp, and the y and z components have not been scaled at all. Each panel displays two separate contributions to the total force. For t and x components the upper (green solid and red dotted) lines give the field point contribution. It is antisymmetric in angle and integrates over the angle to give zero (in fact, when taken over the whole world sheet the integral also vanishes exactly). The lower (blue solid and orange dashed) lines give the smooth integral contribution. It is single signed and large where $\sqrt{-\gamma}$ is small. We plot scaled results for $r = 0.02$ (solid lines) and $r = 0.002$ (dashed/dotted lines) for each contribution to the total. These overlap and show in a qualitative fashion the dominant $1/r$ scaling near the cusp for both contributions to the t and x components. In the lower panels we display the y and z components. As before, the contribution from the field point is given by the green solid and red dotted curves. In this case it is independent of r to lowest order (and integrates over the angle to give 4π at this order). The solid blue and dashed orange lines show that the integral contributions increase slowly as r decreases, consistent with the $\log r$ type behavior.

TABLE III. First-order fits for force combinations near the cusp with form $a + b\tau + c\zeta + (d\tau^2 + e\tau\zeta + f\zeta^2)/r$ with $r = \sqrt{\tau^2 + \zeta^2}$ and second-order fits for the world sheet projected metric perturbations with form $a + b\tau + c\zeta + d\tau^2 + e\tau\zeta + f\zeta^2$ over the radial range $2 \times 10^{-8} \le r \le 2 \times 10^{-4}$. The table provides the two force combinations and three world sheet projected metric perturbations that appear in the asymptotic forms for F^{μ}_1 and F^{μ}_2. The last two columns give the common log of ϵ (the root mean square error between the data and the fit) and Q (the ratio of the variation in the data divided by ϵ).

Quantity	a	b	c	d	e	f	$\log_{10}\epsilon$	$\log_{10} Q$
$F^t - F^x$	14.68	276.43	117.42	−41.51	12.47	−25.45	−3.08	1.06
$F^z(\tau+\zeta) + F^y(3\tau+\zeta)$	0	521.81	175.92	−126.45	38.64	16.21	−2.67	0.91
$H_{\tau\tau}$	11.49	−6.53	−15.33	18.76	84.03	101.7	−7.22	3.9
$H_{\zeta\zeta}$	0	0	0.01	64.4	196	237.13	−7.03	1.32
$H_{\tau\zeta}$	0	−7.66	−17.94	22.71	69.29	56.75	−7.05	3.8

TABLE IV. The numerical results for the expansion of $\sqrt{-\gamma}F^\mu$ in r (averaged over the angle) for the fit given in Table III. For $\sqrt{-\gamma}(F_1+F_2)\sim\sum_n c_n r^n$ the columns are the leading powers of the expansion ($n=-4$ to 0), the rows are the spacetime components and the table values are the common log of the expansion coefficients ($d_n=\log_{10}|c_n|$). The symbol $<$ means a numerical result $|c_n|<10^{-12}$. When the fitting range is narrowed about the cusp the $1/r^2$ contribution decreases $\propto r$ and the other pieces are fixed. From this we infer that the leading nonzero piece of F^μ varies as $1/r$.

Order Component	−4	−3	−2	−1	0
t	$<$	$<$	−2.01	1.28	1.25
x	$<$	$<$	−2.01	1.28	1.25
y	$<$	$<$	$<$	$<$	2.75
z	$<$	$<$	$<$	$<$	2.03

$$a^\mu(\zeta^+)=[\zeta^+,0,a^2(\zeta^+),a^3(\zeta^+)] \tag{6.18}$$

$$b^\mu(\zeta^-)=\left[\zeta^-,\frac{L}{2\pi}\cos\frac{2\pi\zeta^-}{L},0,\frac{L}{2\pi}\sin\frac{2\pi\zeta^-}{L}\right] \tag{6.19}$$

where

$$\begin{aligned}a^2(x)&=\frac{L}{\pi}\sum_j\delta_{j,\lfloor\frac{2x}{L}\rfloor}(-1)^{\lfloor\frac{j+1}{2}\rfloor}\cos\left(\frac{\pi}{4}+(-1)^j\frac{\pi x}{L}\right)\\ a^3(x)&=\frac{L}{\pi}\sum_j\delta_{j,\lfloor\frac{2x}{L}\rfloor}(-1)^{\lfloor\frac{j}{2}\rfloor}\left[\sin\left(\frac{\pi}{4}+j(-1)^j\frac{\pi^2}{L}\right)\right.\\ &\quad\left.-\sin\left(\frac{\pi}{4}+(-1)^j\frac{\pi x}{L}\right)\right],\end{aligned} \tag{6.20}$$

and where the sums are over all integers j, L is the invariant length, $\lfloor x\rfloor$ is the floor function and $\delta_{j,k}$ is the Kronecker delta.

Figure 13 illustrates the configuration in spacetime at equally spaced moments in the oscillation cycle. The kink discontinuities are visible in all four snapshots. In the tangent sphere representation (shown in Fig. 14), $\mathbf{b}'$ traverses a complete great circle through the North and South poles at a steady rate; $\mathbf{a}'$ follows two disjoint segments of a great circle (longitude offset by $\pi/2$ from the one traced by $\mathbf{b}'$) between latitudes $\theta=\pm\pi/4$, also at a steady rate. The vector $\mathbf{a}'$ traces one segment and then abruptly jumps from the point $(0,y,z)$ to $(0,-y,z)$ and traces out the mirrored arc at a steady rate (and repeats). Each jump from one segment to the other yields a kink discontinuity in the spacetime representation.

While the ACO string provided a useful analytic test case with kinks against which we could compare our numerical results, it turns out that the simplicity of the ACO string (in particular, that many quantities are a constant along the string) means that many important terms that appear in the general expression for the self-force are identically zero for the ACO string. Fortunately, the GV string is sufficiently general that this is not the case. Unfortunately, however, there is no known analytic solution for the self-force for the GV string. Instead, in order to use the GV string as a test of our method, we chose a particular point on the string ($\tau=0.3L$, $\zeta=0.4L$) and computed the self-force at that point using an extensive set of different and independent methods:

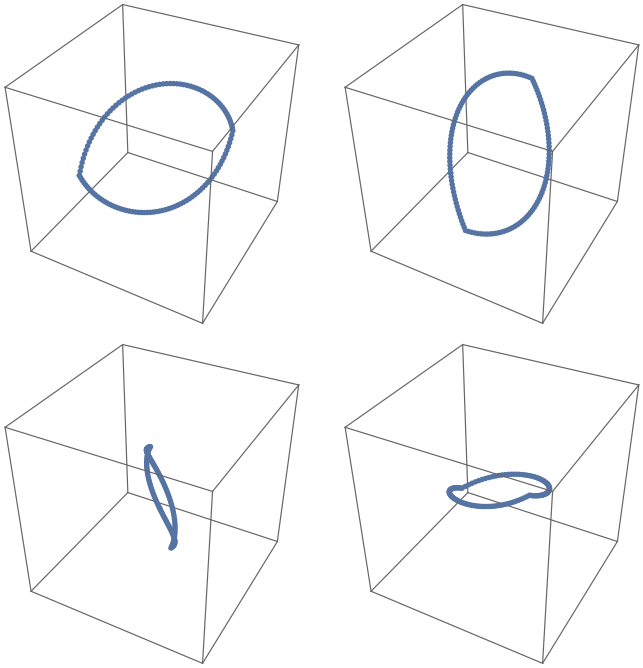

FIG. 13. The GV string loop configuration in spacetime at four equally spaced moments in the basic loop oscillation cycle $\tau=0$, $L/8$, $L/4$ and $3L/8$. Each box is the same size with fixed axes -1 to 1 and fixed orientation.

(1) We used our exact 1D method including a field point contribution and contributions from the two kinks (this is method [1D] discussed in Sec. V D).
(2) We repeated our 1D calculation (again, method [1D]) using multiple choices of integration variable (ζ^+, ζ^- and ζ). In each case, the various contributions (from the integral, field point, and two kinks) were different. Indeed, in some cases there was no contribution picked up from the kinks.
(3) We again repeated our 1D calculation using method [1D], but using a mixed coordinate choice; we used ζ^+ on one side of the field point and ζ^- on the other side. We then included a contribution at the point where these two segments meet up again, to account for the change in integration variable at that point. This contribution is exactly the one discussed in Sec. IV B, and an explicit expression is the same as the one obtained when breaking the integration at a kink, as discussed in Sec. IV A.
(4) We repeated the previously mentioned 1D calculations again, but instead of including the exact field

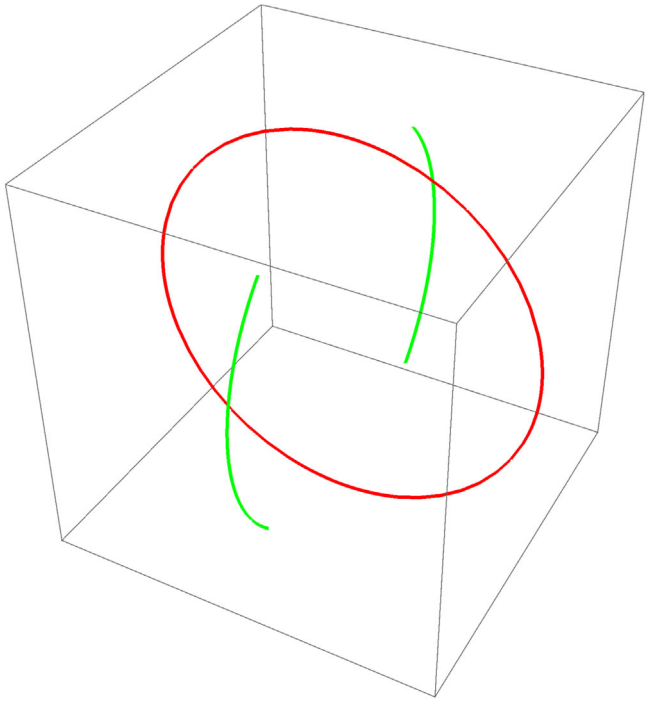

FIG. 14. The arcs on the tangent sphere traced by $\mathbf{b}'(x)$ (red line, a complete great circle passing through poles) and $\mathbf{a}'(x)$ (two green segments symmetrically cut from a great circle) for the GV string. The line is made by a series of points, equally spaced in argument x for the left- and right-moving modes. A blowup of the line in the figure would show equal intervals between the points. When the kink is "rounded off" (nonzero Δ as described in the text) a few of these points will sit between the pictured green arcs and the green line is formally continuous. The $\mathbf{a}'(x)$ tangent vector moves very rapidly from one side to the other.

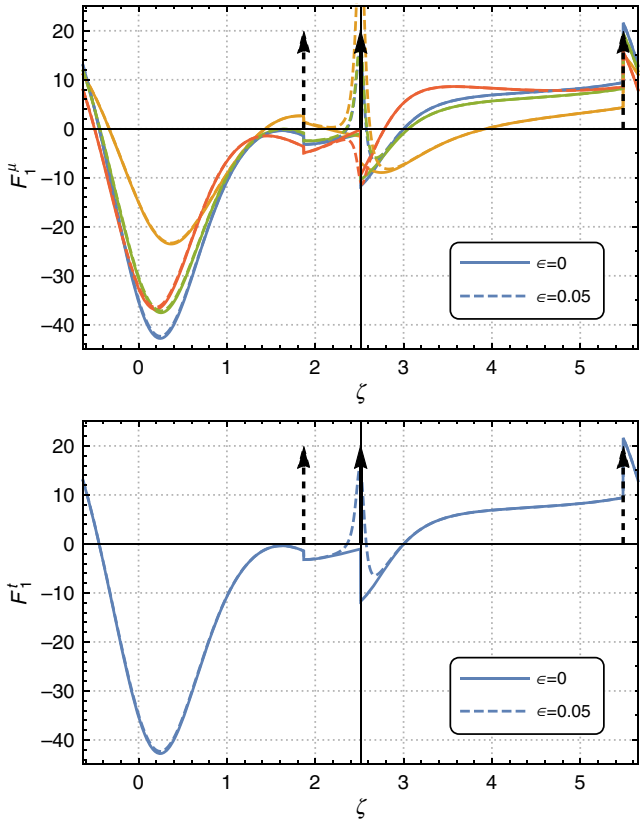

FIG. 15. Integrand used to compute the self-force for the Garfinkle-Vachaspati string. These correspond to the values in the ζ column of Table V. Distributional contributions from the kinks and field point are denoted by dashed and solid arrows, respectively. The top panel shows all four components of the force vector, while the bottom panel only shows the t-component.

point term, we considered an over-retarded image of the string (method [1DO]). In that case, we find that the over-retarded integrand picks up a δ-function type feature nearby the field point (see Fig. 15). For finite over-retardation this manifests itself as a narrow Gaussian, and the Gaussian gets narrower and sharper as the over-retardation parameter is shrunk towards zero. Reassuringly, in the limit of the Gaussian shrinking down to zero size we recover a result which agrees with the previous calculations and can identify the δ-function with the field point contribution.

(5) Finally, we repeated the calculation in a completely independent way, directly evaluating the self-force from the 2D integral (method [2D]) without the reduction to a 1D integral. This was significantly less efficient, but provided an important check as there is no need to consider any split into field-point-plus-integral-plus-kink contributions. Instead, we smeared out the δ function in the Green function and also introduced a slight smoothing of the kinks, as discussed in detail in Appendix E. Yet again, reassuringly, in the limit of our smearing and smoothing parameters going to zero we recovered a result which was in perfect agreement with all of the other methods.

The results of this extensive set of tests are given in Table V. We see that all methods produce results which are consistent within their respective error bars. The [2D] method is least accurate, due to the need for a 2D rather than a 1D numerical integral. The [1DO] method also poses challenges for numerical accuracy due to the presence of sharp features (i.e., the Gaussian approximation to the delta function for the field point contribution), as does the [1DOS] method for portions of the integral nearby kinks.

The three exact [1D] methods all work reasonably well; however even in this case not all methods are equally computationally efficient. In particular, calculations based on a single null coordinate encounter a strong divergence in the integrand as the field point is approached from one side (the particular side is dependent on whether one uses ζ^+ or ζ^- as the integration variable). This diverging integral

TABLE V. Comparison of methods for computing the self-force at a generic point ($\tau = 0.3L$, $\zeta = 0.4L$) on the GV string.

	Contribution	ζ^-	ζ^+	ζ^-/ζ^+	ζ	2D	ζ^-_ϵ	ζ^+_ϵ	ζ_ϵ
F^t_1	$\int$	-330.558	$-12.73(1)$	6.89229	-25.6962	$-12.76(2)$	$-330.60(4)$	$-12.7488(1)$	$-22.4707(2)$
	δ			$\cdots$	3.22536	$\cdots$	$\cdots$	$\cdots$	$\cdots$
	Kink 1	358.819	$\cdots$	$\cdots$	16.7989	$\cdots$	358.819	$\cdots$	16.7989
	Kink 2	-41.0096	$\cdots$	$\cdots$	-7.07683	$\cdots$	-41.0096	$\cdots$	-7.07683
	$\zeta^- \leftrightarrow \zeta^+$	$\cdots$	$\cdots$	-19.6411	$\cdots$	$\cdots$	$\cdots$	$\cdots$	$\cdots$
	Total	$-12.7488(1)$	$-12.73(1)$	-12.7488	-12.7488	$-12.76(2)$	$-12.8(1)$	$-12.7488(1)$	$-12.7487(2)$
F^x_1	$\int$	$-300.675(1)$	$-2.64(7)$	8.62259	-21.7023	$-2.58(3)$	$-300.63(4)$	$-2.56339(6)$	$-14.8591(9)$
	δ			$\cdots$	6.84317	$\cdots$	$\cdots$	$\cdots$	$\cdots$
	Kink 1	287.628	$\cdots$	$\cdots$	14.7570	$\cdots$	287.628	$\cdots$	14.7570
	Kink 2	10.4832	$\cdots$	$\cdots$	-2.46129	$\cdots$	10.4832	$\cdots$	-2.46129
	$\zeta^- \leftrightarrow \zeta^+$	$\cdots$	$\cdots$	-11.186	$\cdots$	$\cdots$	$\cdots$	$\cdots$	$\cdots$
	Total	$-2.5637(8)$	$-2.64(7)$	-2.56342	-2.56342	$-2.58(3)$	$-2.52(8)$	$-2.56339(6)$	$-2.56333(9)$
F^y_1	$\int$	-304.564	$-10.7066(4)$	6.6211	-23.4832	$-10.72(2)$	$-304.59(3)$	$-10.7068(1)$	$-20.0615(2)$
	δ			$\cdots$	3.42159	$\cdots$	$\cdots$	$\cdots$	$\cdots$
	Kink 1	326.143	$\cdots$	$\cdots$	15.4176	$\cdots$	326.143	$\cdots$	15.4176
	Kink 2	-32.2859	$\cdots$	$\cdots$	-6.06281	$\cdots$	-32.2859	$\cdots$	-6.06281
	$\zeta^- \leftrightarrow \zeta^+$	$\cdots$	$\cdots$	-17.3279	$\cdots$	$\cdots$	$\cdots$	$\cdots$	$\cdots$
	Total	-10.7069	$-10.7066(4)$	-10.7068	-10.7068	$-10.72(2)$	$-10.7(1)$	$-10.7068(1)$	$-10.7067(2)$
F^z_1	$\int$	$-190.140(1)$	$-13.82(7)$	2.25465	-15.9946	$-13.90(1)$	$-190.22(8)$	$-13.8960(1)$	$-16.9795(2)$
	δ			$\cdots$	-0.985094	$\cdots$	$\cdots$	$\cdots$	$\cdots$
	Kink 1	234.551	$\cdots$	$\cdots$	10.0429	$\cdots$	234.551	$\cdots$	10.0429
	Kink 2	-58.3072	$\cdots$	$\cdots$	-6.95921	$\cdots$	-58.3072	$\cdots$	-6.95921
	$\zeta^- \leftrightarrow \zeta^+$	$\cdots$	$\cdots$	-16.1507	$\cdots$	$\cdots$	$\cdots$	$\cdots$	$\cdots$
	Total	$-13.8958(7)$	$-13.82(7)$	-13.896	-13.8960	$-13.90(1)$	$-13.97(9)$	$-13.8960(1)$	$-13.8958(2)$

largely cancels against the field point contribution,[20] leaving a relatively small overall contribution from the field-point-plus-integral combination. We found that the remaining two approaches (integration with respect to ζ; and half-ζ^+ half-ζ^- plus coordinate change term) were comparable in terms of computational efficiency.

Importantly, other than accuracy concerns, all methods produced results which are unambiguous in agreeing with each other.

Finally, we used the [1D] method (specifically, integrating with respect to ζ and including field point and kink contributions) to evaluate the self-force at all points on the GV string. The results are shown in Figs. 16 and 17. Figure 16 shows how each of the contributions to F^μ_1 contribute to the overall result, while Fig. 17 shows F^μ_1 and F^μ_2 themselves, as well as their sum. As in the other string test cases, we find that the self-force is finite almost everywhere on the string, with the exception of exactly on the kinks, where it diverges.

[20]In practice, we were only able to obtain finite results by evaluating the integral up to a short distance from the field point and evaluating the expression for the field point contribution at the point where the integral was cut off. We recovered a unique and consistent result as the cutoff point was pushed towards the actual field point.

We have analyzed the form of the divergence near the kink by calculating the total backreaction force to high accuracy along a set of world sheet points for a line that runs perpendicular to the kink with coordinates $(\tau, \zeta) = (\pi/2 + \zeta^+/2, -\pi/2 + \zeta^+/2)$ for $-21 < \log|\zeta^+| < -11$ for positive and negative ζ^+. Locally, the kink can be described in terms of the changes to the unit tangent vector e_t, the velocity vector e_v and $e_\perp = e_v \times e_t/|e_v \times e_t|$ which form the perpendicular coordinate system $\{e_t, e_v, e_\perp\}$. We find that e_v and e_t lie in the $y-z$ plane and $e_\perp$ along the x-direction. Letting $\Delta e = e_+ - e_-$ stand for the change in time of each unit vector,

$$\Delta e_\perp = \{2, 0, 0\} \tag{6.21}$$

$$\Delta e_t \simeq \{0, -1.85, 0\} \tag{6.22}$$

$$\delta e_v \simeq \{0, -0.77, 0\}. \tag{6.23}$$

The kink is a y-reflection of the velocity and tangent vectors in the $y-z$ plane.

On each side of the kink we fit each component of F^α with forms that include combinations of constant, linear and ln terms in $|\zeta^+|$. We select the linear or ln fit, whichever is best; it turns out that this corresponds to the term with coefficients that are of order unity. We report the inferred scaling in Table VI.

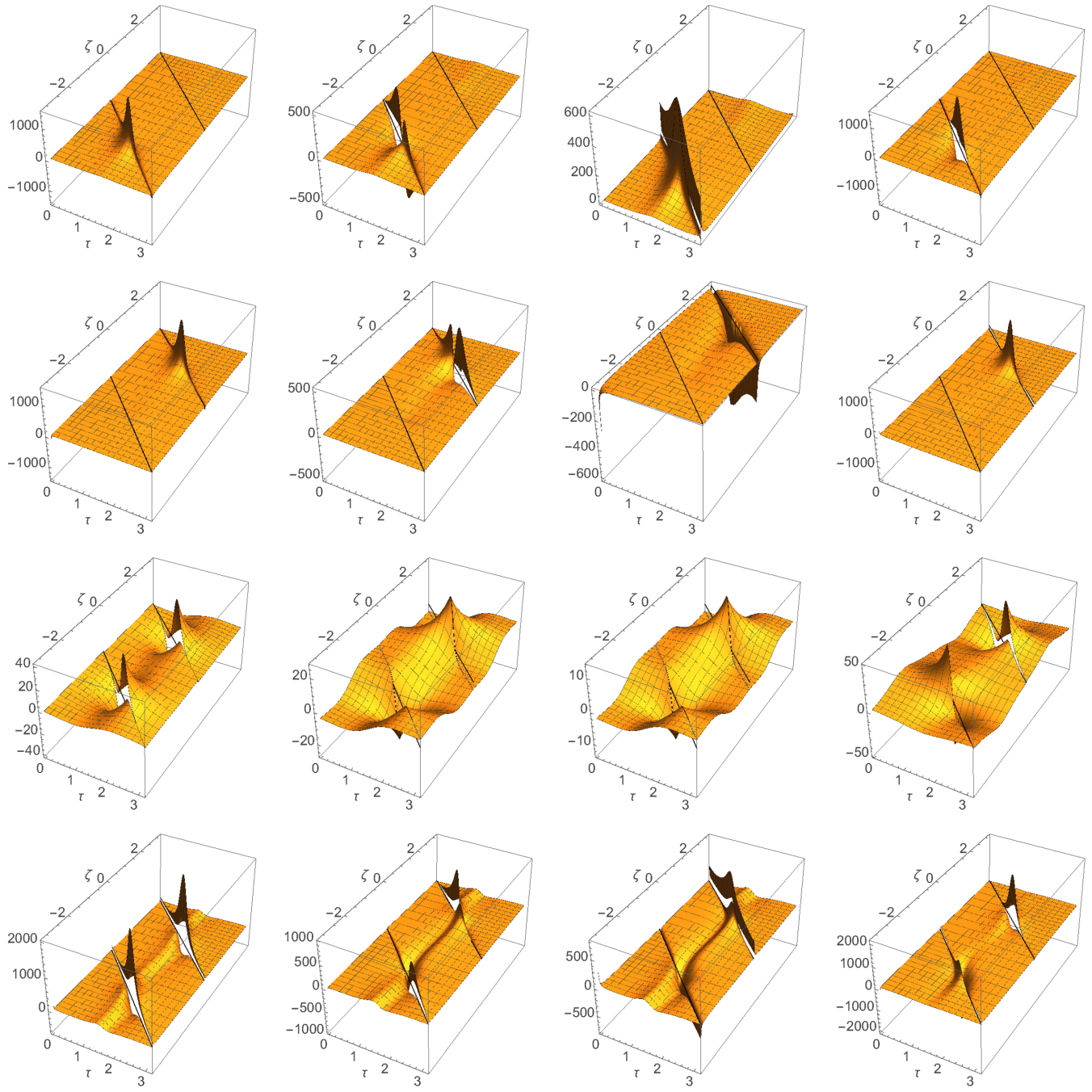

FIG. 16. Contributions to F_1^μ for the Garfinkle and Vachaspati string when computed using the 1D integration method with integration with respect to ζ. Each subfigure shows the relevant contribution to the force at all points on the string in the region $\tau \in (0, L/2)$, $\zeta \in (-L/2, L/2)$; all other points can be obtained from the standard periodic extension of the string. Each column corresponds to a different component of the force: F_1^t, F_1^x, F_1^y, and F_1^z. The rows correspond to the contributions from (i) the kink that passes through ($\tau = 0$, $\zeta = 0$); (ii) the kink that passes through ($\tau = 0$, $\zeta = \pi$); (iii) the field point; and (iv) the integral over ζ (ignoring distributional contributions at the kinks and field point). The two kinks are denoted by diagonal black lines. For the purposes of the plots, we have set the string tension, μ, and Newton's constant, G, equal to 1; other values simply introduce an overall scaling.

The results are similar to but not identical to the ACO case. First, note that there is one redundancy $F^t = -F^z$ so we have 3 GV force components to compare to ACO. The GV coordinate directions of the force are not the same as the normal and longitudinal directions in the ACO case and this complicates a direct one-for-one comparison. Nonetheless, we see analogous behavior. Most prominently the GV divergence for $\zeta^+ < 0$ of F^t and F^y scales close

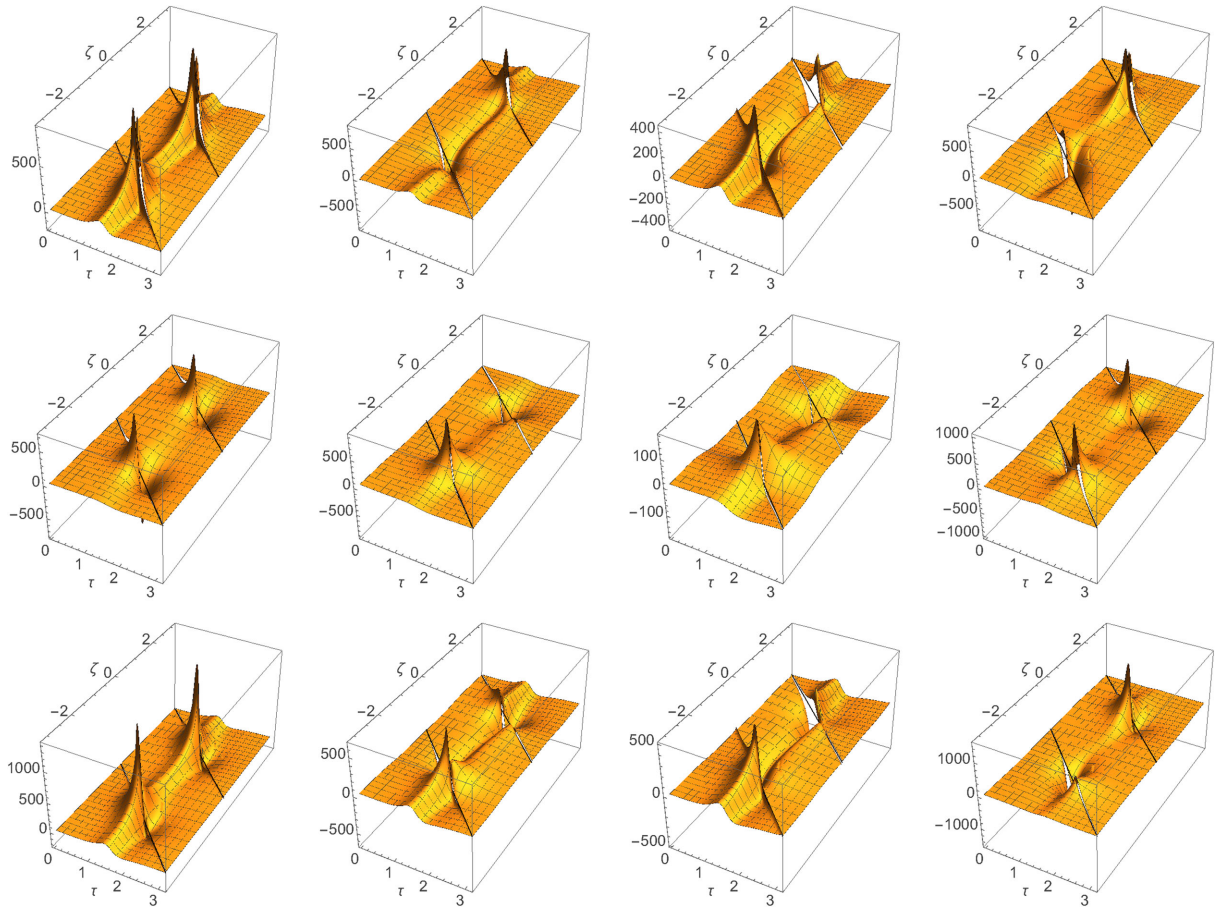

FIG. 17. The two pieces of the self-force, F_1^μ (row 1) and F_2^μ (row 2), and the total force $F^\mu = F_1^\mu + F_2^\mu$ (row 3), for the Garfinkle and Vachaspati string as a function of position on the string. The F_1^μ part can be obtained by summing the four rows in Fig. 16. For the purposes of the plots, we have set the string tension, μ, and Newton's constant, G, equal to 1; other values simply introduce an overall scaling.

to $\propto (|\zeta^+|)^{-1/3}$ like ACO's F^t and F^N. One difference is that the GV forces for all components with $\zeta^+ > 0$ approach nonzero constant values. The ACO loop has no curvature on one side of the kink, which is probably responsible for the fact that two of its components approach zero. Curiously, the ACO divergence for $F^L \propto \ln|\zeta^+|$ on both sides of the kink is absent for any components in the GV case. Likewise, the completely finite GV result for F^x on both sides of the kink is absent in the ACO case. Despite these differences the most important observation is that the GV divergent self-force $\propto (|\zeta^+|)^{-1/3}$ integrates to a finite value so we expect the physical displacement of the string to be finite.

TABLE VI. Asymptotic form for the force near the kink; 1 means a nonzero constant.

Sign	F^t	F^x	F^y	F^z
$\zeta^+ < 0$	$\lvert\zeta^+\rvert^{-0.33}$	1	$\lvert\zeta^+\rvert^{-0.33}$	$\lvert\zeta^+\rvert^{-0.33}$
$\zeta^+ > 0$	1	1	1	1

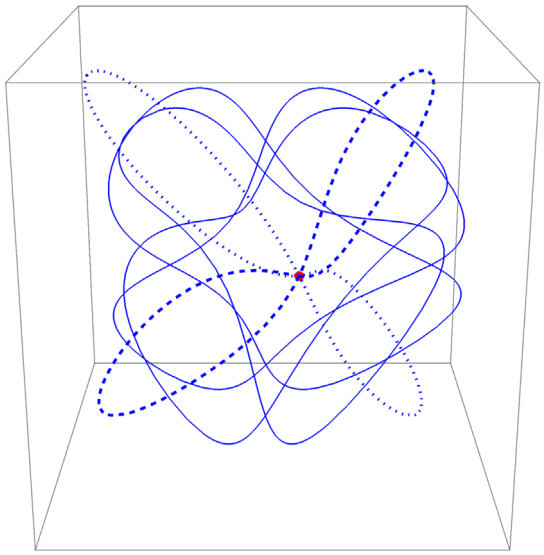

FIG. 18. The Kibble string loop configuration for $p = 1/2$ in spacetime at six equally spaced moments $\tau = j\pi/6$ for $j = 0$ to 5 (invariant length 2π) in the basic loop oscillation cycle. The blue dashed and dotted loops self-intersect at the central red dot. The solid blue lines are nonintersecting configurations.

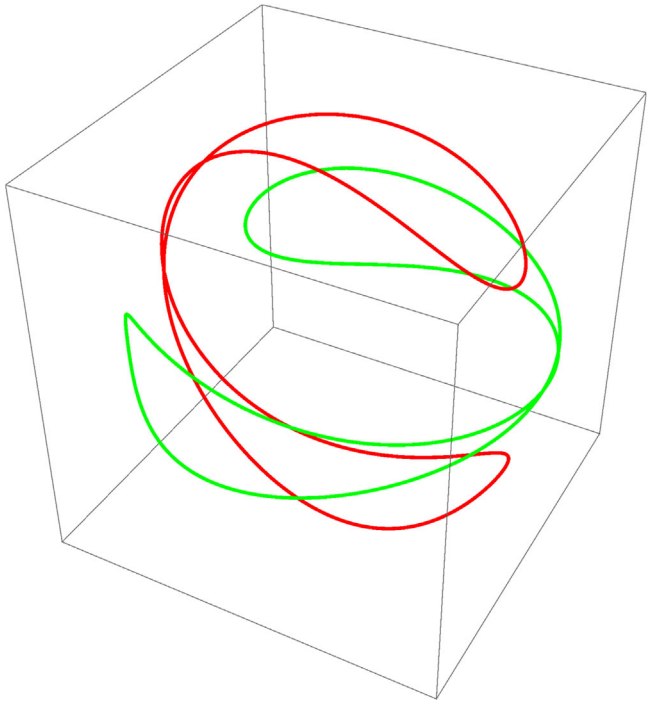

FIG. 19. The arcs on the tangent sphere traced by $\mathbf{a}'(x)$ and $-\mathbf{b}'(x)$ for the Kibble string resemble the seams on a baseball. The green and red lines are smooth and continuous and do not intersect each other. They satisfy an integral condition such that the loop has zero total momentum.

E. Kibble self-intersecting strings

The ACO and GV strings possess a pair of traveling kinks that circulate around the loop throughout the period of oscillation while the KT string forms two transient cusps each period. In the tangent sphere representation the kink discontinuities are jumps in $\mathbf{a}'$ and/or $\mathbf{b}'$ while the cusps form whenever $\mathbf{a}'$ and $\mathbf{b}'$ cross. The nature of the self-intersections of string loops is not immediately apparent from the tangent sphere representation. In the case of the KT string with $\alpha = 0$ and $\phi = \pi/6$ the string collapses to a line and the overlap is a spacelike length of string. Unless nature prefers special loop configurations the generic type of self-intersection will be weaker than in the above KT case. Here we investigate the Kibble string loop [13] which is simpler than any of the previous cases in these respects: it has no discontinuities or crossings on the tangent sphere, i.e., the loop is smooth and continuous everywhere, *and* it self-intersects at a spacetime point not along a spacelike line.

We integrate the tangent vectors [59] to give explicit forms for the right and left modes:

$$a^{\mu}(\zeta^{+}) = [\zeta^{+}, f_1(\zeta^{+}), f_2(\zeta^{+}), f_3(\zeta^{+})] \tag{6.24}$$

$$b^{\mu}(-\zeta^{-}) = [\zeta^{-}, -f_1(\zeta^{-}), -f_3(\zeta^{-}), -f_2(\zeta^{-})] \tag{6.25}$$

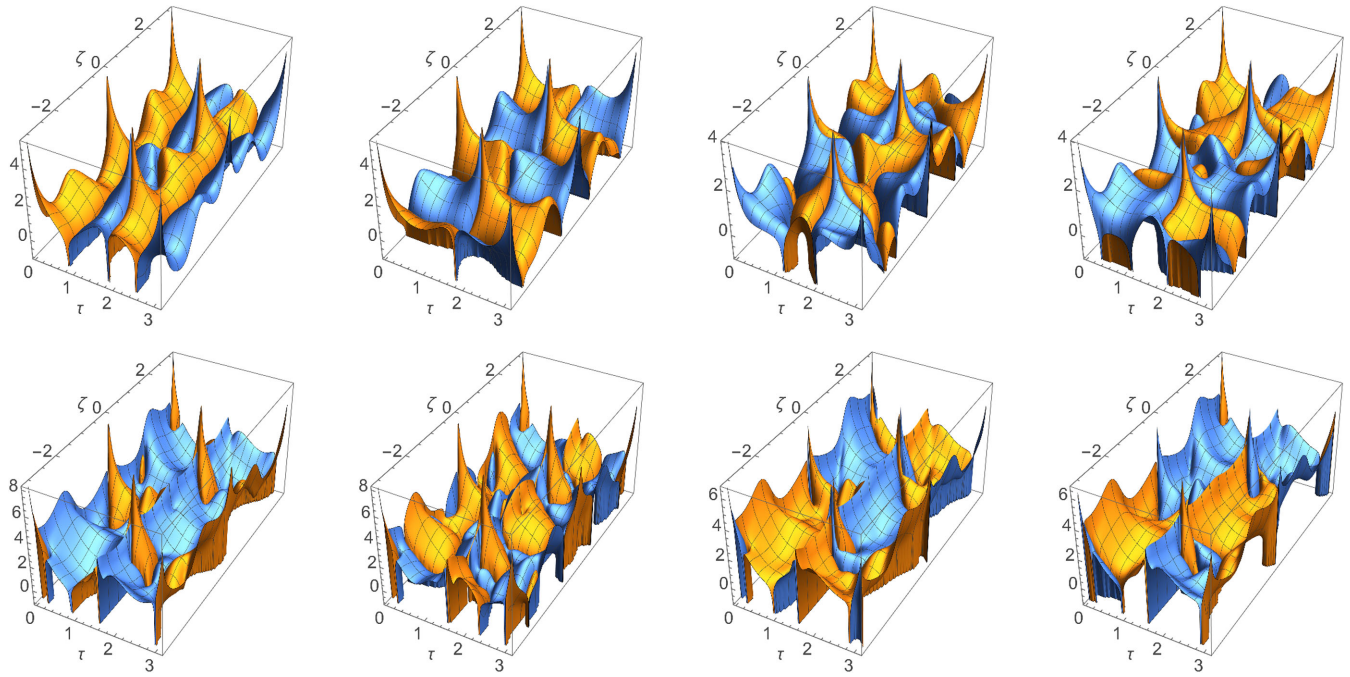

FIG. 20. Contributions to F_1^{μ} for the Kibble string when computed using the [1D] integration method with integration with respect to ζ. Each subfigure shows the relevant contribution to the force at all points on the string in the region $\tau \in (0, L/2), \zeta \in (-L/2, L/2)$; all other points can be obtained from the standard periodic extension of the string. Each column corresponds to a different component of the force: F_1^t, F_1^x, F_1^y, and F_1^z. The rows correspond to the contributions from (i) the field point and (ii) the integral over ζ (ignoring distributional contributions at the field point). For the purposes of the plots, we have set the string tension, μ, and Newton's constant, G, equal to 1; other values simply introduce an overall scaling. Note that we have used a logarithmic scale and denoted positive (negative) values by coloring the plot orange (blue).

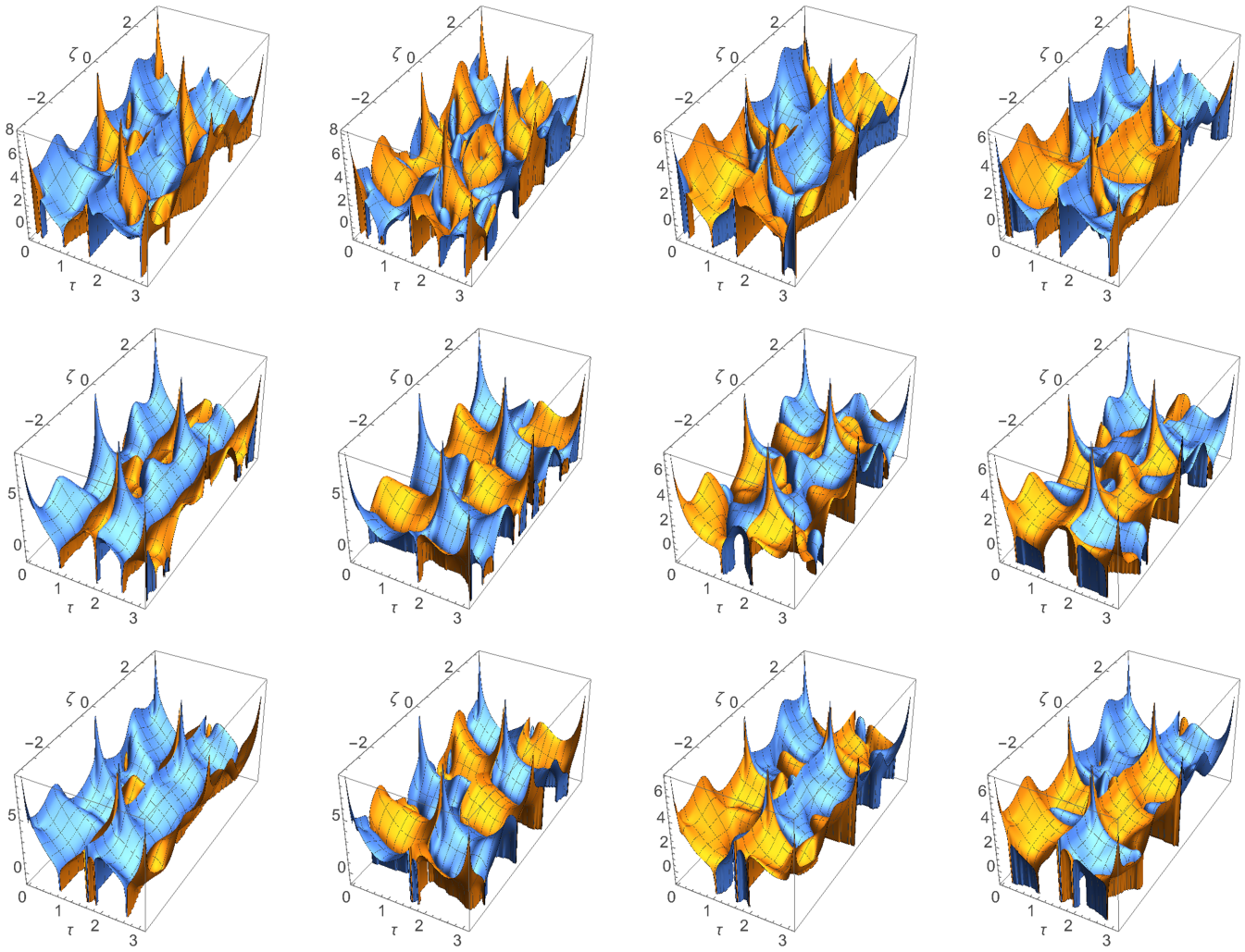

FIG. 21. The two pieces of the self-force, F_1^μ (row 1) and F_2^μ (row 2), for the Kibble string as a function of position on the string. The F_1^μ part can be obtained by summing the two rows in Fig. 20. For the purposes of the plots, we have set the string tension, μ, and Newton's constant, G, equal to 1; other values simply introduce an overall scaling. Note that we have used a logarithmic scale and denoted positive (negative) values by coloring the plot orange (blue).

where

$$f_1(x) = \frac{L}{2\pi}\left(\frac{(1+p^2)^2\sin 2y + (p^2/4)\sin 4y}{2+5p^2+2p^4}\right) \tag{6.26}$$

$$f_2(x) = \frac{L}{2\pi}\cos 2y\left(\frac{-2+4p^2+2p^4+p^2\cos 2y}{4+10p^2+4p^4}\right) \tag{6.27}$$

$$f_3(x) = \frac{L}{2\pi}2^{3/2}p\cos y\left(\frac{5+3p^2+2\cos 2y}{6+15p^2+6p^4}\right) \tag{6.28}$$

$$y = \frac{2\pi x}{L} \tag{6.29}$$

where p is a constant. We choose for the numerical example $p = 1/2$. This is a more complicated loop in terms of harmonic content than either the GV or KT loops. Figure 18 shows six equally spaced snapshots of the loop during the fundamental oscillation period. The dashed and dotted lines show the times when a self-intersection occurs at the center (red dot). Figure 19 gives the tangent sphere representation which resembles the seams of a baseball.

This loop has collisions at world sheet coordinates $\{\tau,\zeta\} = \{0,\pm\pi/2\}$ and $\{\tau,\zeta\} = \{\pi/2,0\}$ and $\{\pi/2,\pi\}$. We describe the limiting behavior near $\{\tau,\zeta\} = \{0,\pm\pi/2\}$. The velocities of the two bits of string are equal and opposite: $\dot{z}^i = \pm\{0,-0.26,-0.26\}$. The tangent vectors are $dz^i/d\zeta = \{-0.85,\pm 0.26,\mp 0.26\}$ (an angle of $\sim$0.94rad). The acceleration vectors are $\ddot{z}^i = \{0,-0.41,0.41\}$. The

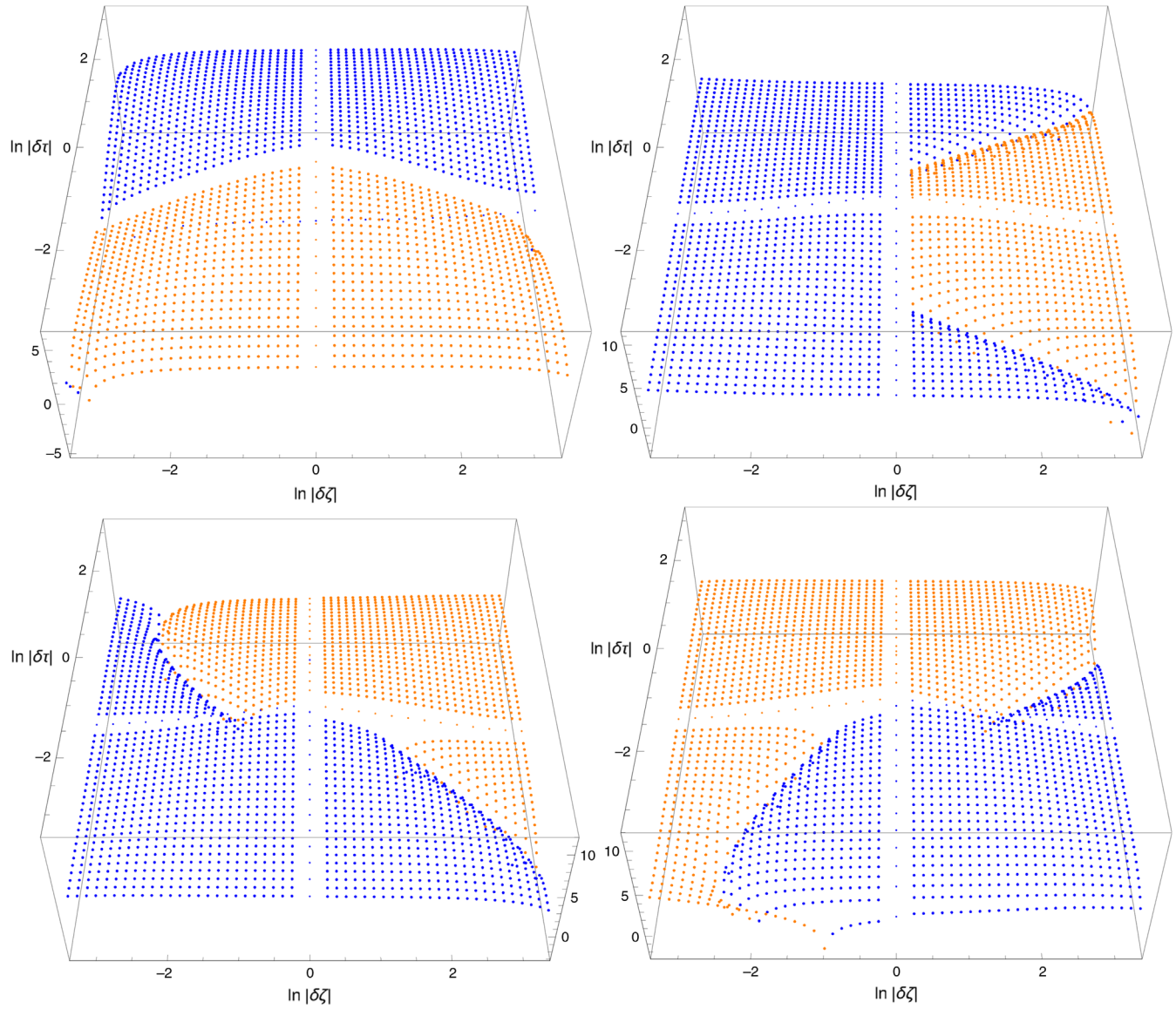

FIG. 22. The four components (t, x, y, and z [left to right, top to bottom]) of $\ln|\mathcal{F}^t_{\rm conf}|$ for a small patch of the world sheet about the crossing point. Four quadrants in $\{\delta\tau, \delta\zeta\}$ are displayed in log absolute value coordinates (oriented to match the usual linear system about $\{\tau, \zeta\} = \{0, \pi/2\}$). Blue (orange) represents negative (positive) values. The small dots have been added for $\delta\tau = 0$ and $\delta\zeta = 0$.

gravitational radiation emitted by each piece of string should be similar.

The net effect of the crossing is small. The bumps at the collision points on the full scale world sheet representations in Figs. 20 and 21 are difficult to distinguish at all. Here we look in more detail near those crossings.

Component F^t is displayed in a small two-dimensional patch about the crossing point in the top left plot of Fig. 22. As $\tau \to 0$ at fixed $\zeta = \pi/2$ (the vertical line of small dots in the picture) F^t diverges $\propto \tau^{-1}$ with a change of sign as τ passes through zero. The results at $\pm\tau$ are nearly equal and opposite. We find that the sum of the two components at $\pm\tau$ is nearly constant as $|\tau| \to 0$, numerically approximately $\propto |\tau|^{0.05}$. As ζ varies near $\pi/2$ (fixed $\tau = 0$, the horizontal line of small dots) the results on each side of the crossing point are finite and the zero value is not exactly at $\delta\zeta = 0$. These results are quite sensitive to the size of $\delta\tau$ since the surface changes sign (from plus to minus infinity) near $\delta\tau = 0$.

We have formally fit the power law variation for $\delta\tau$ near $\tau = 0$ and for $\delta\zeta$ near $\zeta = \pi/2$. Table VII summarizes the slopes extracted for F^α along fixed τ and fixed ζ coordinates passing exactly through the crossing point. Some components vary such that an integral over just one side would yield a divergent quantity; however, the symmetric sum is always integrable.

The plot of F^t shows it to be approximately a product of individual functions of τ and ζ. The other force

TABLE VII. Kibble loop divergent behavior at the crossing point $\tau = 0$ and $\zeta = \pi/2$. The columns labeled $\tau = 0$ give ν for the scaling of the force component along the string near the crossing point $\propto |\zeta - \pi/2|^{\nu}$. Likewise, the ones labeled $\zeta = \pi/2$ describe the scaling $\propto |\tau|^{\nu}$ for times before and after the appearance of the crossing. "One side" means the scaling of the absolute value (approximately the same on each side); "Net" means the scaling of the symmetric sum of points on opposite sides of the crossing point. Small ν results are numerically close to finite limits but in any case are integrable. The "$\cdots$" indicates values that are not well defined because of a zero-crossing at $\tau = 0$.

	ζ varies; $\tau = 0$		τ varies; $\zeta = \pi/2$	
Component	One side	Net	One side	Net
F^t	$\cdots$	$\cdots$	-1.0	0.04
F^x	-1.1	-0.04	-0.04	-0.03
F^y	-1.1	-0.06	-1.0	-0.05
F^z	-1.1	-0.05	-0.96	-0.04

components are more complicated. Components F^x, F^y and F^z are shown in small two-dimensional patches in the other plots of Fig. 22. The small dots show the variation along the coordinate axes.

In summary, we find the effect of the string crossing leads to integrable forces for all components in this example.

F. Comparisons to radiated quantities evaluated in the far field

As an additional consistency check on our results, we compute the radiated energy and compare it to the energy dissipated through the local self-force. The latter can be computed using the change in the 4-momentum of the string,

$$\Delta P^{\mu} = \mu \int \mathcal{F}^{\mu}_{\rm conf} d\zeta d\tau, \tag{6.30}$$

where the conformal-gauge force $\mathcal{F}^{\mu}_{\rm conf}$ is given by Eq. (3.9) and where the region of integration is given by the fundamental period of the world sheet: $-L/2 \le \zeta < L/2$ and $0 \le \tau < L/2$. In practice, we evaluate the integrand at $N \sim 10^4$ equally spaced points on a two-dimensional surface and approximate the integral as the sum of the function values at the points times the world sheet area per point. This is a low accuracy method that is suited to the occurrence of steep spikes at various points on the world sheet; we estimate the accuracy of the results to be within 1%–5%.

The work done on the string by the self-force lowers its energy, $\Delta P^0 < 0$, and should be exactly balanced by the flux carried to infinity, which must be $-\Delta P^0 > 0$.

TABLE VIII. The total energy loss integrated over one fundamental period of the loop oscillation in the center of mass frame of the loop. The far field is calculated with the formalism of Allen and Ottewill [96]. The analytic result for the ACO loop in the far field is from Ref. [61]. The numerical results for the direct energy loss integrate $\mathcal{F}^{\mu}_{\rm conf}$ over the world sheet according to the description in this section. The analytic results for the direct energy loss for the ACO loop are from Ref. [81].

Case	Far field (numerical)	Far field (analytic)	Direct (numerical)	Direct (analytic)
ACO	122.537	122.53	125.515	122.53
KT $\alpha = 0$, $\phi = \pi/6$	349.677	$\cdots$	355.643	$\cdots$
KT $\alpha = 1/2$, $\phi = 0$	241.321	$\cdots$	238.259	$\cdots$
GV	131.304	$\cdots$	132.486	$\cdots$
Kibble	137.6	$\cdots$	135.428	$\cdots$

We separately compute this flux to infinity using the formalism of Allen and Ottewill [96], in which the stress-energy tensor is a sum of individual Fourier components of the undamped string. For each overtone n we numerically integrate $dP^{(n)}/d\Omega$ over the sphere. We compute N overtones and then fit and sum a power law extrapolation for $N \to \infty$. This yields a result which is approximately 1% accurate.

Table VIII compares the results of the two calculations. We find good numerical agreement within the expected accuracy of the result.

VII. DISCUSSION

We have developed a general method for calculating the self-force due to gravitational perturbations of a lightly damped string loop. Our approach breaks up the calculation into smooth integrals over the retarded image of the loop plus boundary terms. The latter are used to take account of the special contributions when the source and field point coincide and when discontinuities are visible on the past image of the loop. These may be from kinks or cusps or crossings (spacetime points where intercommutation events might occur). Our methodology is quite general and can be used for arbitrary choices of spacetime and world sheet gauges.

There are some existing calculations of the gravitational self-force for cosmic strings [76,81,84]; however these results have all relied on simplifications or approximations that do not hold in general. For example, although Quashnock and Spergel [76] used a numerical approach not too different from ours, they did not discuss any of the various distributional type contributions that

we have studied in detail here. Our results[21] suggest that their use of a pair of null coordinates sidesteps the issue of a contribution from the field point. The issue of contributions from kinks, however, remains unaddressed. Additionally, given the limited computational resources available at the time, their numerical calculations were restricted to a low-resolution study in a restricted set of cases. In the case of Refs. [81,84], approximations based on simple string configurations were made which, while reasonable in some cases, do not fully capture the behavior for generic string configurations.

Our numerical calculations have passed a number of validation checks including comparisons with existing analytical results, comparisons of the integrated power radiated over a fundamental period against the flux of gravitational energy measured at large distances, and cross-comparisons of several semi-independent methods for computing the self-force. From the perspective of computational efficiency it is clear that the [1D] methods based on either integration with respect to ζ or a Quashnock-Spergel type mixed integration with respect to ζ_+ and ζ_- are the best choice. The other [1D] methods (using a single null coordinate or over-retardation) inevitably encounter large numerical cancellations nearby the field point, making them significantly more computationally demanding. The [2D] method is even worse and is orders of magnitude more demanding than any of the [1D] methods.

While the preferred [1D] methods work well in general, there are certain cases where they also run into numerical challenges. Since the self-force diverges as one approaches kinks and cusps (in such a way that the displacement of the world sheet is finite) it is unavoidable that one would encounter numerically divergent quantities at one point or another. In this work, we handled the issue of divergences in a brute force manner by simply evaluating quantities to a sufficiently high accuracy that they can be canceled to leave a residual which is still accurately determined. While this approach works reasonably well, the calculation could be made significantly more efficient by developing an alternative approach to the problem. One promising possibility is to borrow from results in the point particle case [100–102], where it was found that the separation of the full metric perturbation into a so-called "puncture field" that captures the singular behavior plus a "residual field" that is more numerically well behaved. In the point particle case, by basing the puncture field on an approximation to the singular field proposed by Detweiler and Whiting [103], one can work directly with the residual field as it is entirely responsible for driving the motion. In the case of a cosmic string we do not yet have an analogous Detweiler-Whiting type singular field. One could attempt to derive one following the matched expansion methods of Ref. [104]. Alternatively, even without such a derivation a local analysis of the type done in Sec. IV D may yield an approximation to the singular behavior of the metric perturbation which leaves a numerically well-behaved residual field, and which is sufficiently simple that its integrated contribution to the motion can be determined analytically. Indeed, a preliminary analysis for the ACO string (where the self-force is known analytically) suggests that exactly this approach will work well and has been found to significantly improve the accuracy with which the integrated motion can be determined, even in the presence of a divergent self-force at the kinks.

The ultimate goal of our program is to evolve cosmic strings under the influence of the self-force and to study the consequences of backreaction on cusp formation, smoothing of kinks, and other astrophysically relevant features of cosmic strings. This paper represents the first step in such an endeavor. We can now compute the self-force for an arbitrary cosmic string with a reasonable level of accuracy and with the freedom to arbitrarily choose coordinates and gauges which are most suitable for evolution. The next step is to implement this into a numerical evolution scheme. This will be presented in a future work.

ACKNOWLEDGMENTS

We thank J. J. Blanco-Pillado, David Nichols, Ken Olum, Adrian Ottewill, Joe Polchinski, Leo Stein, Peter Taylor, Henry Tye, Jeremy Wachter and Yang Zhang for helpful conversations. B. W. and D. C. gratefully acknowledge support from the John Templeton Foundation New Frontiers Program under Grant No. 37426 (University of Chicago)—FP050136-B (Cornell University). D. C. acknowledges that this material is based upon work supported by the National Science Foundation under Grant No. 1417132. E. F. acknowledges the support of the National Science Foundation under Grants No. 1404105 and No. 1707800.

Note Added.—Concurrent to our own work Blanco-Pillado, Olum and Wachter did related work on cosmic string backreaction; that paper and this one were submitted at the same time. As far as we know, the results are in agreement where they overlap.

APPENDIX A: ADAPTED TETRADS ON THE WORLD SHEET

1. Definition of adapted tetrad

Suppose that we have a set of four linearly independent basis vectors $\vec{e}_{\hat{0}}$, $\vec{e}_{\hat{1}}$, $\vec{e}_{\hat{2}}$, $\vec{e}_{\hat{3}}$, defined on the world sheet, where $\vec{e}_{\hat{0}}$ is timelike and the other vectors are spacelike. If $\vec{e}_{\hat{0}}$ and $\vec{e}_{\hat{1}}$ are tangent to the world sheet, and if the other two vectors are orthogonal, we will say that the tetrad is adapted to the world sheet. Such tetrads are convenient since the four vectors can be used as a basis for spacetime tensors, while the first two vectors can be used as a basis for world

[21]For example see the third column in Table V for the GV case, but we also performed the same check for the other configurations discussed in this paper.

sheet tensors. We will not require in the following that the basis be orthogonal or orthonormal.

We now introduce the following index notations. Hatted lowercase Greek indices will run over $\hat{0}$, $\hat{1}$, $\hat{2}$, $\hat{3}$, so for example an expansion of a vector $\vec{v}$ on the orthonormal basis will be written as

$$\vec{v} = v^{\hat{\alpha}}\vec{e}_{\hat{\alpha}}. \tag{A1}$$

We will use hatted capital roman indices $\hat{A}, \hat{B}, \ldots$ to run over $\hat{0}$, $\hat{1}$, the directions along the world sheet, and hatted capital greek indices $\hat{\Gamma}, \hat{\Sigma}, \ldots$ to run over $\hat{2}$, $\hat{3}$, the directions orthogonal to the world sheet. So the decomposition (A1) of a general vector can be rewritten as

$$\vec{v} = v^{\hat{A}}\vec{e}_{\hat{A}} + v^{\hat{\Sigma}}\vec{e}_{\hat{\Sigma}}. \tag{A2}$$

We define the dual basis of one-forms ${w^{\hat{\alpha}}}_{\alpha}$ by

$${w^{\hat{\alpha}}}_{\alpha}{e_{\hat{\beta}}}^{\alpha} = \delta^{\hat{\alpha}}_{\hat{\beta}}. \tag{A3}$$

The basis vectors and dual basis vectors can be used to express tetrad basis components of tensors in terms of coordinate basis components and vice versa in the usual way:

$$v^{\hat{\alpha}} = {w^{\hat{\alpha}}}_{\alpha}v^{\alpha}, \qquad v_{\hat{\alpha}} = {e_{\hat{\alpha}}}^{\alpha}v_{\alpha}, \tag{A4}$$

etc.

2. Examples of adapted tetrads

Let us adopt the conventional parametrization of the background world sheet [14]:

$$\vec{X}(\tau,\zeta) = \left(\tau, \frac{1}{2}\mathbf{a}(\zeta-\tau) + \frac{1}{2}\mathbf{b}(\zeta+\tau)\right), \tag{A5}$$

where $\mathbf{a}'^2 = \mathbf{b}'^2 = 1$. (Here the notation is that boldface quantities are three-vectors, and quantities with arrows are four-vectors.) We can then define an orthonormal tetrad of basis vectors

$$\vec{e}_{\hat{0}} = f_0(2, -\mathbf{a}' + \mathbf{b}'), \tag{A6a}$$

$$\vec{e}_{\hat{1}} = f_1(0, \mathbf{a}' + \mathbf{b}'), \tag{A6b}$$

$$\vec{e}_{\hat{2}} = f_2(1 - \mathbf{a}'\cdot\mathbf{b}', -\mathbf{a}' + \mathbf{b}'), \tag{A6c}$$

$$\vec{e}_{\hat{3}} = f_3(0, \mathbf{a}' \times \mathbf{b}'), \tag{A6d}$$

where $f_0 = f_1 = [2(1+\mathbf{a}'\cdot\mathbf{b}')]^{-1/2}$, $f_2 = [1-(\mathbf{a}'\cdot\mathbf{b}')^2]^{-1/2}$ and $f_3 = 1/|\mathbf{a}'\times\mathbf{b}'|$. This is an adapted tetrad since the vectors $\vec{e}_{\hat{0}}$ and $\vec{e}_{\hat{1}}$ point along the world sheet (they are proportional to ∂_τ and ∂_ζ), while $\vec{e}_{\hat{2}}$ and $\vec{e}_{\hat{3}}$ are orthogonal to it. Another choice of adapted tetrad is given in Eqs. (A6) but with the coefficients $f_{\hat{\alpha}}$ set to unity. This is an orthogonal tetrad, but not an orthonormal tetrad, and might be more convenient to use in computations.

3. Geometric quantities in terms of the tetrad basis

The spacetime metric on the tetrad basis is

$$g_{\hat{\alpha}\hat{\beta}} = \vec{e}_{\hat{\alpha}}\cdot\vec{e}_{\hat{\beta}}. \tag{A7}$$

It follows from the definition of the adapted tetrad that this has a block diagonal form with two 2×2 sub-blocks, i.e., that $g_{\hat{A}\hat{\Gamma}} = 0$. Also the induced metric on the tetrad basis is just one of the 2×2 sub-blocks:

$$\gamma_{\hat{A}\hat{B}} = \vec{e}_{\hat{A}}\cdot\vec{e}_{\hat{B}} = g_{\hat{A}\hat{B}}. \tag{A8}$$

It also follows that

$$\gamma^{\hat{A}\hat{B}} = g^{\hat{A}\hat{B}}. \tag{A9}$$

Hatted indices are raised and lowered with $g_{\hat{\alpha}\hat{\beta}}$. For vectors $v^{\hat{\alpha}}$ parallel to the world sheet we have $v^{\hat{\Gamma}} = 0$ and $v_{\hat{\Gamma}} = 0$, so indices can equivalently be raised and lowered just with $\gamma_{\hat{A}\hat{B}}$.

The projection tensor (2.2) can be expressed in terms of the tetrad vectors and dual vectors as

$${P^{\beta}}_{\gamma} = {e_{\hat{A}}}^{\beta}{w^{\hat{A}}}_{\gamma}, \tag{A10}$$

and the orthogonal projection tensor is

$${\perp^{\beta}}_{\gamma} = {e_{\hat{\Gamma}}}^{\beta}{w^{\hat{\Gamma}}}_{\gamma}. \tag{A11}$$

Inserting these expressions into the definition (2.5) of the extrinsic curvature tensor gives

$$\begin{aligned} K_{\mu\nu\rho} &= -{P_{\mu}}^{\alpha}P_{\nu\beta}\nabla_{\alpha}{\perp^{\beta}}_{\rho} \\ &= -{e_{\hat{A}}}^{\alpha}{w^{\hat{A}}}_{\mu}g_{\nu\lambda}{e_{\hat{B}}}^{\lambda}{w^{\hat{B}}}_{\beta}\nabla_{\alpha}({e_{\hat{\Gamma}}}^{\beta}{w^{\hat{\Gamma}}}_{\rho}) \\ &= -{e_{\hat{A}}}^{\alpha}{w^{\hat{A}}}_{\mu}g_{\nu\lambda}{e_{\hat{B}}}^{\lambda}{w^{\hat{B}}}_{\beta}\nabla_{\alpha}({e_{\hat{\Gamma}}}^{\beta}){w^{\hat{\Gamma}}}_{\rho}. \end{aligned} \tag{A12}$$

It follows that the nonzero components of the extrinsic curvature tensor on the tetrad basis are

$$K_{\hat{A}}{}^{\hat{B}}{}_{\hat{\Gamma}} = -{e_{\hat{A}}}^{\alpha}{w^{\hat{B}}}_{\beta}\nabla_{\alpha}{e_{\hat{\Gamma}}}^{\beta}. \tag{A13}$$

Note that this formula is valid for an arbitrary adapted tetrad, not just an orthonormal one.

4. Explicit form of equation of motion in orthogonal gauge using adapted tetrad

a. Orthogonal gauge

An alternative world sheet gauge choice is to impose that the displacement vector be orthogonal to the world sheet everywhere:

$$P^{\alpha}{}_{\beta} z^{\beta}_{(1)} = 0 \tag{A14}$$

or

$$\perp^{\alpha}{}_{\beta} z^{\beta}_{(1)} = z^{\alpha}_{(1)}. \tag{A15}$$

From the general form (3.10) of linearized gauge transformations we see that it is always possible to achieve this gauge.

b. Form of equation of motion

In the orthogonal gauge, the displacement vector is orthogonal to the world sheet, so we can express it as an expansion in terms of two components on an adapted tetrad:

$$\vec{z}_{(1)} = z^{\hat{\Gamma}}_{(1)} \vec{e}_{\hat{\Gamma}}. \tag{A16}$$

We now write the general equation of motion (3.5) in the schematic form:

$$L[\vec{z}_{(1)}]^{\alpha} = \mathcal{F}^{\alpha}, \tag{A17}$$

where L is the differential operator that appears on the left-hand side, and $\mathcal{F}$ is the forcing term linear in $h_{\alpha\beta}$ on the right-hand side. Writing this equation on the orthonormal basis gives

$$L[\vec{z}_{(1)}]^{\hat{\alpha}} = \mathcal{F}^{\hat{\alpha}}. \tag{A18}$$

Now the $\hat{\alpha} = \hat{0}$ and $\hat{\alpha} = \hat{1}$ components of this equation vanish identically, since both sides are perpendicular to the world sheet. So, we end up with an equation with only two components:

$$L[\vec{z}_{(1)}]^{\hat{\Gamma}} = \mathcal{F}^{\hat{\Gamma}}. \tag{A19}$$

This will give two coupled equations for the two components $z^{\hat{2}}_{(1)}$ and $z^{\hat{3}}_{(1)}$ of the displacement vector.

We now derive the following explicit form of the differential operator on the orthonormal basis:

$$L[\vec{z}_{(1)}]^{\hat{\Gamma}} = \Delta z^{\hat{\Gamma}}_{(1)} + \mathcal{K}^{A\hat{\Gamma}}{}_{\hat{\Sigma}} \partial_A z^{\hat{\Sigma}}_{(1)} + \mathcal{M}^{\hat{\Gamma}}{}_{\hat{\Sigma}} z^{\hat{\Sigma}}_{(1)}. \tag{A20}$$

Here ∂_a denotes a derivative with respect to the world sheet coordinates ζ^a, and $\triangle$ is the scalar differential operator

$$\Delta = \frac{1}{\sqrt{\gamma}} \eta^{ab} \partial_a \partial_b. \tag{A21}$$

The mass matrix $\mathcal{M}$ is given by

$$\mathcal{M}^{\hat{\Gamma}}{}_{\hat{\Sigma}} = w^{\hat{\Gamma}}{}_{\alpha} \Delta e_{\hat{\Sigma}}{}^{\alpha} + \lambda_{\hat{\Sigma}\hat{A}\hat{B}} K^{\hat{A}\hat{B}\hat{\Gamma}}. \tag{A22}$$

Also

$$\lambda_{\hat{\Sigma}\hat{A}\hat{B}} = -\gamma_{\hat{B}\hat{C}} w^{\hat{C}}{}_{\alpha} e_{\hat{A}}{}^{\mu} \nabla_{\mu} e_{\hat{\Sigma}}{}^{\alpha} - \gamma_{\hat{A}\hat{C}} w^{\hat{C}}{}_{\alpha} e_{\hat{B}}{}^{\mu} \nabla_{\mu} e_{\hat{\Sigma}}{}^{\alpha}. \tag{A23}$$

Note that all the derivatives in this expression are along the world sheet, so the expression is well defined (the basis vectors are not defined off the world sheet, so orthogonal derivatives are not well defined). Finally the quantity $\mathcal{K}$ is given by

$$\mathcal{K}^{a\hat{\Gamma}}{}_{\hat{\Sigma}} = \frac{2}{\sqrt{\gamma}} w^{\hat{\Gamma}}{}_{\alpha} \eta^{ab} \partial_b e_{\hat{\Sigma}}{}^{\alpha}. \tag{A24}$$

c. Derivation

From Eq. (3.5), dropping the Riemann term since we are working in flat spacetime, and replacing all indices with hatted indices, we get

$$L[\vec{z}_{(1)}]^{\hat{\Gamma}} = \perp^{\hat{\Gamma}}{}_{\hat{\chi}} \bar{\nabla}_{\hat{\mu}} \bar{\nabla}^{\hat{\mu}} z^{\hat{\chi}}_{(1)} - 2\bar{\nabla}_{\hat{\mu}} z^{\hat{\alpha}}_{(1)} K^{\hat{\mu}}{}_{\hat{\alpha}}{}^{\hat{\Gamma}}. \tag{A25}$$

Consider first the second term in Eq. (A25). Since the extrinsic curvature tensor is parallel to the world sheet on its first two indices, we can drop the bar on the derivative operator. Also we can replace the indices $\hat{\mu}$ and $\hat{\alpha}$ by world sheet indices $\hat{A}$ and $\hat{B}$, giving

$$-2K^{\hat{A}}{}_{\hat{B}}{}^{\hat{\Gamma}} \nabla_{\hat{A}} z^{\hat{B}}_{(1)} = -2K^{\hat{A}}{}_{\hat{B}}{}^{\hat{\Gamma}} e_{\hat{A}}{}^{\alpha} w^{\hat{B}}{}_{\beta} \nabla_{\alpha} z^{\beta}_{(1)}. \tag{A26}$$

Now inserting the expansion (A16) of the displacement vector gives

$$-2K^{\hat{A}}{}_{\hat{B}}{}^{\hat{\Gamma}} e_{\hat{A}}{}^{\alpha} w^{\hat{B}}{}_{\beta} \nabla_{\alpha} (z^{\hat{\Gamma}}_{(1)} e_{\hat{\Gamma}}{}^{\beta}) = -2K^{\hat{A}}{}_{\hat{B}}{}^{\hat{\Gamma}} e_{\hat{A}}{}^{\alpha} w^{\hat{B}}{}_{\beta} z^{\hat{\Gamma}}_{(1)} \nabla_{\alpha} e_{\hat{\Gamma}}{}^{\beta}, \tag{A27}$$

where we have used the orthonormality of $\hat{A}$ and $\hat{\Gamma}$ directions. This gives the second term in the mass matrix (A22).

To evaluate the first term in Eq. (A25), we temporarily return to the coordinate form of this term, the first term on the left-hand side of Eq. (3.5). Then we use the general result (valid in arbitrary gauges) for this term that

$$\perp^{\rho}{}_{\chi} \bar{\nabla}_{\mu} \bar{\nabla}^{\mu} z^{\chi}_{(1)} = \perp^{\rho}{}_{\chi} \frac{1}{\sqrt{\gamma}} \partial_a (\sqrt{\gamma} \gamma^{ab} \partial_b z^{\chi}_{(1)}). \tag{A28}$$

We now use the fact that we have chosen conformal gauge to zeroth order, so that $\sqrt{\gamma}\gamma^{ab} = \eta^{ab}$. This gives

$$\perp^{\rho}{}_{\chi} \bar{\nabla}_{\mu} \bar{\nabla}^{\mu} z^{\chi}_{(1)} = \perp^{\rho}{}_{\chi} \frac{1}{\sqrt{\gamma}} \eta^{ab} \partial_a \partial_b z^{\chi}_{(1)}. \tag{A29}$$

We now convert the ρ and χ indices in this equation to orthonormal indices, by multiplying by appropriate factors of e and w, and also by inserting the expansion (A16) of the displacement vector. We use the formula

$$\Delta(z^{\hat{\Gamma}}_{(1)} e_{\hat{\Gamma}}{}^{\chi}) = \Delta(z^{\hat{\Gamma}}_{(1)}) e_{\hat{\Gamma}}{}^{\chi} + z^{\hat{\Gamma}}_{(1)} \Delta e_{\hat{\Gamma}}{}^{\chi} + \frac{2}{\sqrt{\gamma}} \eta^{ab} \partial_a z^{\hat{\Gamma}}_{(1)} \partial_b e_{\hat{\Gamma}}{}^{\chi}. \tag{A30}$$

The three terms in this expression generate, respectively, the first term in Eq. (A20), the first term in the mass matrix (A22), and the second term in Eq. (A20).

APPENDIX B: COORDINATE SYSTEMS WITHIN THE CLASS OF CONFORMAL GAUGES

Within the conformal gauge, there is freedom in the particular choice of world sheet coordinates $\{\zeta^1, \zeta^2\}$. For example, they may be chosen to be space-time ($\zeta^a = [\tau, \zeta]$); null ($\zeta^a = [\zeta^-, \zeta^+] \equiv [\tau - \zeta, \tau + \zeta] = [2\tau - \zeta^+, \zeta^+]$); or seminull ($\zeta^a = [\tau, \zeta^+] \equiv [\tau, \tau + \zeta]$). The relation between derivatives in the various coordinates is given by

$$\left(\frac{\partial}{\partial \zeta^+}\right)_\tau = \left(\frac{\partial}{\partial \zeta}\right)_\tau = \left(\frac{\partial}{\partial \zeta^+}\right)_{\zeta^-} - \left(\frac{\partial}{\partial \zeta^-}\right)_{\zeta^+}, \tag{B1}$$

$$\left(\frac{\partial}{\partial \tau}\right)_{\zeta^+} = \left(\frac{\partial}{\partial \tau}\right)_\zeta - \left(\frac{\partial}{\partial \zeta}\right)_\tau = 2\left(\frac{\partial}{\partial \zeta^-}\right)_{\zeta^+}. \tag{B2}$$

As mentioned in Sec. IV D, the conformal gauge condition imposes that derivatives of the world sheet be related. In space-time coordinates the τ and ζ derivatives are related by

$$\partial_\tau z^\alpha \partial_\tau z_\alpha + \partial_\zeta z^\alpha \partial_\zeta z_\alpha = 0, \qquad \partial_\tau z^\alpha \partial_\zeta z_\alpha = 0. \tag{B3}$$

Equivalently, the null derivatives are related by

$$\partial_{\zeta^+} z^\alpha \partial_{\zeta^+} z_\alpha = 0, \qquad \partial_{\zeta^-} z^\alpha \partial_{\zeta^-} z_\alpha = 0, \tag{B4}$$

and the seminull derivatives are related by

$$\partial_\tau z^\alpha \partial_\tau z_\alpha = 0, \qquad \partial_\tau z^\alpha \partial_{\zeta^+} z_\alpha + \partial_{\zeta^+} z^\alpha \partial_{\zeta^+} z_\alpha = 0. \tag{B5}$$

Additionally, the equation of motion (3.4) reduces to

$$\phi^{-1}[\partial_{\zeta\zeta} z^\alpha - \partial_{\tau\tau} z^\alpha] = 0 \tag{B6}$$

in space-time coordinates, to

$$-4\phi^{-1} \partial_{\zeta^+\zeta^-} z^\alpha = 0 \tag{B7}$$

in null coordinates, and to

$$-\phi^{-1}[\partial_{\tau\tau} z^\alpha + 2\partial_{\zeta^+\tau} z^\alpha] = 0 \tag{B8}$$

in seminull coordinates. The solutions can be written in terms of left-moving and right-moving waves, i.e., in terms of two functions $a^\alpha(\zeta^+)$ and $b^\alpha(\zeta^-)$ that satisfy the tangent sphere condition $g_{\alpha\beta}\partial_{\zeta^+} a^\alpha \partial_{\zeta^+} a^\beta = 0 = g_{\alpha\beta}\partial_{\zeta^-} b^\alpha \partial_{\zeta^-} b^\beta$.

APPENDIX C: ENERGY-MOMENTUM LOSS FORMULAS

We review the QS [76] result for energy-momentum loss by self-forces in light-cone coordinates and conformal gauge. We note that these results can be generalized to arbitrary gauge choice. Finally, we rewrite the energy-momentum loss formulas directly in terms of the conformal-gauge force using Eq. (3.14). We utilize the result to evaluate the dissipative effects on the string.

QS analyzed a string with mass per length μ, spacetime position of the world sheet $x^\mu = z^\mu(\zeta^1, \zeta^2)$ where the two coordinates covering the world sheet are $\zeta^a = \{\zeta^1, \zeta^2\}$; $g_{\mu\nu} = \{-, +, +, +\}$; and $\zeta^a = \{\zeta^1, \zeta^2\} = \{\tau, \zeta\}$. The Nambu-Goto action is

$$S = -\mu \int d^2\zeta \sqrt{-\gamma} \tag{C1}$$

$$\gamma_{ab} = g_{\mu\nu} \frac{\partial z^\mu}{\partial \zeta^a} \frac{\partial z^\nu}{\partial \zeta^b} \tag{C2}$$

$$\gamma = \det \gamma_{ab} \tag{C3}$$

and $\gamma < 0$. We have the stress-energy tensor [Eq. (12.2.2) of [105]]

$$T^{\mu\nu}(x) = \frac{2}{\sqrt{-g(x)}} \left(\frac{\delta S}{\delta g_{\mu\nu}(x)}\right) \tag{C4}$$

$$g = \det g_{\mu\nu}. \tag{C5}$$

Now using $\dot{z}^\mu = z^\mu_{,\tau}$, $z'^\mu = z^\mu_{,\zeta}$, $\dot{z}^2 = g_{\mu\nu}\dot{z}^\mu \dot{z}^\nu$, $z'^2 = g_{\mu\nu} z'^\mu z'^\nu$, $z' \cdot \dot{z} = g_{\mu\nu} z'^\mu \dot{z}^\nu$ and $\delta g_{\alpha\beta}(x)/\delta g_{\mu\nu}(x') = \delta^4(x - x')(\delta^\mu_\alpha \delta^\nu_\beta + \delta^\nu_\alpha \delta^\mu_\beta)/2$ we can write

$$T^{\mu\nu} = \frac{\mu}{\sqrt{-g}} \int \frac{d^2\zeta}{\sqrt{-\gamma}} \delta^4(x - z(\zeta)) C^{\mu\nu} \tag{C6}$$

$$C^{\mu\nu} = D^{\mu\nu} + E^{\mu\nu} \tag{C7}$$

$$D^{\mu\nu} = \dot{z}^\mu \dot{z}^\nu (z')^2 + z'^\mu z'^\nu (\dot{z})^2 \tag{C8}$$

$$E^{\mu\nu} = (z' \cdot \dot{z})(z'^\mu \dot{z}^\nu + \dot{z}^\mu z'^\nu). \tag{C9}$$

This differs from QS Eq. (3.2) in two details: the power of the determinant of the induced metric is $-1/2$ not $1/2$ and there is an explicit occurrence of the determinant of the spacetime metric.

The Lagrangian $L = -\mu\sqrt{-\gamma}$ leads to the equations of motion [QS Eq. (3.3)]. With the gauge choices $\dot{x}\cdot x' = 0$ and $(\dot{x})^2 + (x'^2) = 0$ we have

$$\sqrt{-\gamma} = -(\dot{x})^2 = (x')^2 \tag{C10}$$

and QS Eq. (3.6)

$$\ddot{x}^\nu - x''^\nu = -\Gamma^\nu_{\alpha\beta}(\dot{x}^\alpha\dot{x}^\beta - x'^\alpha x'^\beta). \tag{C11}$$

In light-cone coordinates $u \equiv \tau + \zeta$ and $v \equiv \tau - \zeta$ these are

$$\partial_u\partial_v x^\mu = -\Gamma^\mu_{\alpha\beta}\partial_u x^\alpha \partial_v x^\beta \tag{C12}$$

$$g_{\alpha\beta}\partial_u x^\alpha \partial_u x^\beta = 0 \tag{C13}$$

$$g_{\alpha\beta}\partial_v x^\alpha \partial_v x^\beta = 0. \tag{C14}$$

In flat background these reduce to

$$x^\mu_{(0),uv} = 0 \tag{C15}$$

with gauge conditions

$$\eta_{\mu\nu}x^\mu_{(0),u}x^\nu_{(0),u} = \eta_{\mu\nu}x^\mu_{(0),v}x^\nu_{(0),v} = 0. \tag{C16}$$

The subscripts here and below label powers of μ. Our $\phi = -\gamma_{(0)} > 0$.

For general background the stress-energy tensor is $T^{\mu\nu} \equiv \mu I^{\mu\nu}$ where

$$I^{\mu\nu} = \frac{1}{\sqrt{-g}}\int dudv G^{\mu\nu}\delta^{(4)}(x-z) \tag{C17}$$

and

$$G^{\mu\nu} = z^\mu_{,u}z^\nu_{,v} + z^\mu_{,v}z^\nu_{,u}. \tag{C18}$$

The form is exact and does not explicitly involve γ. This is QS Eq. (3.12) supplemented with an explicit determinant of the spacetime metric. We can regard G (and γ) as functions of u and v via $x = z(u, v)$.

Integrating the covariant derivative of the stress-energy tensor $\nabla_\nu T^{\mu\nu}$ over a large cylinder with spatial extent beyond the source and asymptotically flat and between two time slices over weight $\sqrt{-g}d^4x$ gives the covariant conservation law

$$\int d^4x\sqrt{-g}\nabla_\nu T^{\mu\nu} = \int d^4x(\sqrt{-g}T^{\mu\nu})_{,\nu} + \int d^4x\sqrt{-g}\Gamma^\mu_{\alpha\beta}T^{\alpha\beta}. \tag{C19}$$

The first term on the left is rewritten

$$\int d^4x(\sqrt{-g}T^{\mu\nu})_{,\nu} = \int d^4x(\sqrt{-g}T^{\mu 0})_{,0} + \int d^4x(\sqrt{-g}T^{\mu i})_{,i}. \tag{C20}$$

Defining

$$P^\mu \equiv \int d^3x\sqrt{-g}T^{\mu 0} \tag{C21}$$

$$\Delta P^\mu \equiv \int dt P^\mu_{,0} \tag{C22}$$

and applying Gauss's law to the integral at spatial infinity

$$\int d^3x(\sqrt{-g}T^{\mu i})_{,i} = 0 \tag{C23}$$

we find the change in the source momentum

$$\int d^4x(\sqrt{-g}T^{\mu\nu})_{,\nu} = \Delta P^\mu. \tag{C24}$$

Inserting this result into Eq. (C19) and rearranging, we get

$$\Delta P^\mu = \int d^4x\sqrt{-g}(\nabla_\nu T^{\mu\nu} - \Gamma^\mu_{\alpha\beta}T^{\alpha\beta}) = \int d^4x(\sqrt{-g}T^{\mu\nu})_{,\nu}. \tag{C25}$$

It is not too surprising that the form is identical to Eq. (C24).

Next, use the explicit form for the stress-energy tensor on the right-hand side. How well do we need to know the terms? Since $P \sim \mu$, if we wish $\Delta P \sim \mu^2$ then we need $\sqrt{-g}T \sim \mu\sqrt{-g}I$ accurate to order μ^2. Since there is one factor of μ which is explicit one needs $I = I_{(0+1)}$, but, as mentioned earlier, I is exact.[22]

Integrate over a fundamental period in time and a large volume containing the string source:

$$\int(\sqrt{-g}T^{\mu\nu})_{,\nu}d^4x = \mu\int d^4x\partial_\nu\int dudv G^{\mu\nu}\delta^4(x-z) \tag{C26}$$

$$= \mu\int d^4x\int dudv G^{\mu\nu}\partial_\nu(\delta^4(x-z)). \tag{C27}$$

[22]In our formalism, this is not the case; we start with Eq. (3.16) with $g_{\mu\nu} \to \eta_{\mu\nu}$ and all other quantities evaluated for the background (see footnote 1). This expression is $I_{(0)}$.

To handle the derivative of the delta function we introduce two additional independent variables for spanning the space perpendicular to the world sheet:

$$y^a = \{\zeta, \sigma_\perp\} \tag{C28}$$

$$\zeta = \{u, v\} \tag{C29}$$

$$\sigma_\perp = \{\sigma_1, \sigma_2\}. \tag{C30}$$

Define Z which extends z off the world sheet by adding a perpendicular component h for $\sigma_\perp \neq 0$:

$$Z^\mu(y) = z^\mu(\zeta) + h^\mu(\zeta, \sigma_\perp) \tag{C31}$$

$$h^\mu|_{\sigma_\perp=0} = 0 \tag{C32}$$

$$g_{\mu\nu}(\partial_\zeta z^\mu)(\partial_{\sigma_\perp} h^\nu)|_{\sigma_\perp=0} = 0. \tag{C33}$$

The third condition is the requirement that the extension lie off the world sheet. This extension is meant to be exact to all orders in μ.

Now we can formally extend the integration

$$\int du dv \delta^4(x - z) \to \int d^4y \delta^2(\sigma_\perp)\delta^4(x - Z), \tag{C34}$$

rewrite the derivative of the delta function (this is possible because the extra variables allow one-to-one coordinate transformations)

$$\frac{\partial}{\partial x^\nu}\delta^4(x - Z) = -\frac{\partial}{\partial Z^\nu}\delta^4(x - Z) \tag{C35}$$

$$= -\frac{\partial y^a}{\partial Z^\nu}\frac{\partial}{\partial y^a}\delta^4(x - Z) \tag{C36}$$

$$= -(\partial_\nu y^a)\frac{\partial}{\partial y^a}\delta^4(x - Z), \tag{C37}$$

and insert and integrate by parts:

$$\int (\sqrt{-g}T^{\mu\nu})_\nu d^4x = -\mu \int d^4x d^4y \delta^2(\sigma_\perp) G^{\mu\nu} \times (\partial_\nu y^a)(\partial_a \delta^4(x - Z)) \tag{C38}$$

$$= \mu \int d^4y \partial_a(\delta^2(\sigma_\perp) G^{\mu\nu}\, \partial_\nu y^a). \tag{C39}$$

Finally, note that $\frac{\partial Z^\mu}{\partial y^a}\frac{\partial y^b}{\partial Z^\mu} = \delta^b_a$ so that we end up with

$$\Delta P^\mu = 2\mu \int du dv \frac{\partial^2 z^\mu}{\partial u \partial v}. \tag{C40}$$

This is exact and identical to what QS derive in Eq. (4.6). Second-order results in μ follow by writing $z^\mu = z^\mu_{(0)} + z^\mu_{(1)}$, noting that the unperturbed equations of motion are $z^\mu_{(0),uv} = 0$, and finding

$$\Delta P^\mu_{(0+1)} = 0 \tag{C41}$$

$$\Delta P^\mu_{(2)} = 2\mu \int du dv \frac{\partial^2 z^\mu_{(1)}}{\partial u \partial v}. \tag{C42}$$

One needs to know the perturbed string position to apply this formula directly to calculate energy-momentum loss in the sense that $\Delta P_{(n+1)}$ requires $z_{(n)}$.

QS rewrite this using their first-order equations of motion $z^\mu_{(1),uv} = -\Gamma^\mu_{\alpha\beta(1)} z^\alpha_{(0),u} z^\beta_{(0),v}$, giving the final result for energy-momentum change to second order in μ:

$$\Delta P^\mu_{(2)} = -2\mu \int du dv \Gamma^\mu_{\alpha\beta(1)} z^\alpha_{(0),u} z^\beta_{(0),v}. \tag{C43}$$

In this form the numerical evaluation of the energy-momentum change requires the first-order metric perturbations instead of the first-order string perturbations. The linearized equations for the metric are

$$\Box g_{\mu\nu(1)} = -16\pi G(T_{\mu\nu(1)} - (1/2) g_{\mu\nu(0)} T^\rho{}_{\rho(1)}) \tag{C44}$$

where $T_{(1)} = \mu I_{(0)}$ [i.e., $\sqrt{-g}_{(0)} = 1$ and unperturbed world sheet $z = z_{(0)}$].

We can generalize this procedure by following the identical logic without make the choice of the conformal gauge. In summary,

$$S = -\mu \int d^2\zeta \sqrt{-\gamma} \tag{C45}$$

$$T^{\mu\nu}(x) = \frac{2}{\sqrt{-g}}\frac{\delta S}{\delta g_{\mu\nu}(x)} \tag{C46}$$

$$= \frac{\mu}{\sqrt{-g}} \int d^2\zeta \sqrt{-\gamma}\gamma^{ab} z^\mu_{,a} z^\nu_{,b} \delta^4(x - z) \tag{C47}$$

$$\Delta P^\mu = \mu \int d^2\zeta \frac{\partial}{\partial \zeta^b}(\sqrt{-\gamma}\gamma^{ab} z^\mu_{,a}). \tag{C48}$$

If we count orders then we need $\gamma_{(0+1)}$ and $z_{(0+1)}$ to give $\Delta P_{(2)}$. In the previous case there was no explicit appearance of the induced metric; only z was present so it was sufficient to give $z_{(0+1)}$ to find $\Delta P_{(2)}$. Now there is the possibility that $z_{(0)}$ couples to $\gamma_{(1)}$ in addition to $z_{(1)}$ coupling to $\gamma_{(0)}$.

Finally, the equation of motion, $K^\mu = 0$ [our Eq. (2.7)], is explicitly

$$K^\mu = \frac{1}{\sqrt{h}}\frac{\partial}{\partial\zeta^b}(\sqrt{h}h^{ab}z^\mu_{,a}) + P^{\alpha\beta}\Gamma^\mu_{\alpha\beta} = 0 \quad \text{(C49)}$$

and so we can also write the energy-momentum change as

$$\Delta P^\mu = -\mu\int d^2\zeta\sqrt{h}P^{\alpha\beta}\Gamma^\mu_{\alpha\beta}. \quad \text{(C50)}$$

The above pair of equations is analogous to QS's Eqs. (3.14) and (4.6). They are valid for any coordinate and gauge choice and do not presume a flat background.

To calculate energy-momentum loss we start from Eq. (C42) above, and we rewrite u and v in terms of ζ and τ to give

$$dudv = 2d\zeta d\tau \quad \text{(C51)}$$

$$\partial_u\partial_v = (1/4)(\partial_\tau^2 - \partial_\zeta^2) \quad \text{(C52)}$$

$$= -(1/4)\eta^{ab}\partial_a\partial_b \quad \text{(C53)}$$

for our definitions

$$\eta = \begin{pmatrix} -1 & 0 \\ 0 & 1 \end{pmatrix} \quad \text{(C54)}$$

$$\gamma_{ab} = \phi\eta_{ab}. \quad \text{(C55)}$$

Now Eq. (3.14) (conformal gauge at zeroth and first order) is

$$\eta^{ab}\partial_a\partial_b z^\mu_{(1)} = -\mathcal{F}^\mu_{\rm conf} \quad \text{(C56)}$$

so (C42) implies that the change in the 4-momentum of the string is

$$\Delta P^\mu_{(2)} = \mu\int \mathcal{F}^\mu_{\rm conf}d\zeta d\tau \quad \text{(C57)}$$

with the region of integration given by the fundamental period of the world sheet: $-L/2 \le \zeta < L/2$ and $0 \le \tau < L/2$. For $\mathcal{F}^0_{\rm conf} < 0$ the work done on the string lowers its energy, $\Delta P^0 < 0$, and the flux carried to infinity is $-\Delta P^0 > 0$. This form is analogous to QS Eq. (C43).

APPENDIX D: EXPANSION OF THE RETARDED TIME IN NULL COORDINATES

In Sec. IV D we derived an expansion which is useful in the case where spacelike and timelike world sheet coordinates are used. It is also useful to consider the case where null coordinates are used (and, in particular, where the variable of integration is a null world sheet coordinate). We will denote these null coordinates by ζ^+ and ζ^- and assume they can be related to spacelike and timelike coordinates in the standard way, $\zeta^+ = \tau + \zeta$ and $\zeta^- = \tau - \zeta$. Just like with the spacelike and timelike coordinates, we can write down conformal gauge orthogonality relations for these null coordinates,[23]

$$g_{\alpha\beta}\partial_{\zeta^+}z^\alpha\partial_{\zeta^+}z^\beta = 0, \quad \text{(D1)}$$

$$g_{\alpha\beta}\partial_{\zeta^-}z^\alpha\partial_{\zeta^-}z^\beta = 0, \quad \text{(D2)}$$

$$g_{\alpha\beta}\partial_{\zeta^+}z^\alpha\partial_{\zeta^-}z^\beta = -\phi. \quad \text{(D3)}$$

We also have the null coordinate version of the conformal gauge equation of motion:

$$\partial_{\zeta^-\zeta^+}z^\alpha = 0. \quad \text{(D4)}$$

Now, proceeding exactly as we did with spacelike and timelike coordinates, we can seek a local expansion of $\Delta\zeta^-(\Delta\zeta^+)$ [or, equivalently, $\Delta\zeta^+(\Delta\zeta^-)$]. As before, we will achieve this using the fact that source and field points are null separated, $\sigma(z,z') = 0$. Unlike before, however, we can no longer make the assumption that $\Delta\zeta^-$ has an expansion in *integer* powers of our order-counting parameter ϵ, where $\Delta\zeta^+ = \mathcal{O}(\epsilon)$. We can see this by starting from our expansion of $\Delta\tau(\Delta\zeta)$, rewriting it in terms of $\Delta\zeta^-$ and $\Delta\zeta^+$, and rearranging to get the expansion of $\Delta\zeta^-(\Delta\zeta^+)$.

Whether taking the direct approach or going via the spacelike and timelike expansion, we obtain the same result upon gathering terms, namely that the expansion takes a distinct form depending on the sign of $\Delta\zeta^+$:

(1) For $\Delta\zeta^+ > 0$ we get a standard integer power series;
(2) For $\Delta\zeta^+ < 0$ we find that the $\mathcal{O}(\epsilon)$ pieces cancel and we are left starting with (at least) a cubic term. The result is that our expansion now has the form

$$\Delta\zeta^- = \Delta\zeta^-_1\epsilon^{1/3} + \Delta\zeta^-_2\epsilon^{2/3} + \cdots. \quad \text{(D5)}$$

This is generically true, provided $\Delta\tau_3$ in Eq. (4.40) is nonzero, which is equivalent to the question of how the retarded image deviates from being a straight line.

As before, the expressions for the coefficients $\Delta\zeta^-_1, \Delta\zeta^-_2, \ldots$ are somewhat cumbersome. The important point this time is that they depend on σ [which is $\mathcal{O}(\epsilon^2)$]; on $\partial_\tau\sigma$, $\partial_\zeta\sigma$, and $\Delta\zeta$ [all of which are $\mathcal{O}(\epsilon)$]; and on $\bar{\phi}$ and $\bar{z}^\alpha$ and their world sheet derivatives. Two different expansions are needed based upon the sign of $\Delta\zeta^+$.

APPENDIX E: 2D CALCULATION OF THE SELF-FORCE

As an independent check on the numerical results of our 1D method, we also performed a direct 2D integration to

[23] In the coordinates $\{\zeta^+,\zeta^-\}$, the conformal factor ϕ is half of its value in the $\{\tau,\zeta\}$ system at the same world sheet point.

determine the self-force. The results of the 2D calculation are given in Sec. VI and are found to be consistent with those of the 1D method. In this Appendix we give the explicit details of the calculation.

1. Regularization

In order to devise a numerical scheme for evaluating the self-force as a 2D integral, we will allow two modifications of the delta function that enforces the exact null condition between source and field points. First, we replace the delta function itself with a nonsingular, smooth function of the spacetime interval. Second, we modify the null condition to select source points marginally timelike separated from the field point. There are two parameters, one for the characteristic width of the delta function replacement and one for the amount of over-retardation. When both jointly approach zero then the smooth function tends to the singular delta function and the source-field separation tends to the exact null separation. Our prescription is that any physical answer is the limit of a sequence of calculations with (jointly) vanishing parameters, assuming, of course, that a unique limit exists.

We integrate over the 2D surface of the source distribution using a Gaussian approximation to the delta function. The Gaussian form picks up small source contributions away from exact null separations (off shell). This 2D method of integration avoids potential pitfalls associated with the elimination of one world sheet coordinate in terms of another coordinate when solving $\sigma(x, z(\zeta^1, \zeta^2)) = 0$. Subtleties can easily arise (and be missed) in the 1D reduction. The 2D integration method therefore provides a valuable (if computationally costly) independent check on other methods.

The 2D integration produces manifestly coordinate invariant results. It is potentially susceptible to the effect of any world sheet singularity that lies off the exact null image. For example, if a kink or cusp exists anywhere on the world sheet then the associated divergence must be integrable for the method to give a well-defined limit for the force. As a practical matter, all finite integrable off shell singularities are multiplied by Gaussian wings and strongly suppressed. We believe but have not proven that contributions of singularities lying off of the image do not survive the limiting process.

2. Mathematical forms

As summarized in the main text, in Minkowski spacetime we write the modified Synge world function for two spacetime coordinates as

$$\sigma(x, z) = \frac{1}{2}(x - z)^\alpha g_{\alpha\beta}(x - z)^\beta + \sigma_0 \tag{E1}$$

where σ_0 is the over-retardation parameter (and $\sigma_0 = 0$ gives the usual world function). The retarded Green function for a source at x_s and field at x_f is

$$\mathcal{G}(x_f, x_s) = \Theta(x_s, x_f)\delta(\sigma) \tag{E2}$$

where the $\Theta = 1$ when the time of the source t_s precedes the time of the field point t_f and 0 otherwise. We replace the delta function with the Gaussian

$$\delta(q) \to \delta_G(q) \equiv \frac{e^{-q^2/(2w^2)}}{\sqrt{2\pi}w} \tag{E3}$$

which is finite for any source and field point choices. We allow two possible representations for the causality condition. In the "exact" representation we use the discontinuous Θ function. For the parts of the integrand that are directly proportional to $\mathcal{G} = \Theta\delta$ we expect that using the exact Θ representation suffices for all field-source combinations (i.e., we take the limit $w \to 0$ of an integrand with $\mathcal{G} \sim \Theta\delta_G$). However, parts of the integrand include derivatives with respect to x_f of $\mathcal{G}$. Then the situation is more complicated. We can justify ignoring the functional dependence of Θ on x_f *if* we use the exact delta function $\delta(\sigma)$. The only point where both Θ and $\delta(\sigma)$ are nonvanishing is $x_f = x_s$ and things are undefined there anyway. But it is dubious to ignore x_f dependence if we are replacing the delta function with the Gaussian δ_G because there are contributions from points x_s (away from x_f) such that the derivative of Θ with respect to x_f multiplies a nonzero off-shell δ_G. It is not obvious that it is safe to drop Θ's functional dependence on x_f *before* taking the limit of $\delta_G \to \delta$. To study the situation we replace the cutoff with a smoothed discontinuity i.e., $\Theta \to \Theta_{\tanh} \equiv (1 - \tanh((t_s - t_f)/w))/2$ and take full derivatives of $\Theta_{\tanh}\delta_G$. As a practical matter we use the same small parameter in the Gaussian and in the tanh, and we will seek convergent results in the joint limit $w \to 0$ and $\sigma_0 \to 0$.

Let f_1 and f_2 be the self-force integrands

$$f_1^\rho(x, z) = -\perp^{\rho\lambda}(x)\eta^{\mu\nu}(x)\Delta H_{\mu\nu\lambda} \tag{E4}$$

$$f_2^\rho(x, z) = K^{\mu\nu\rho}(x)\Delta h_{\mu\nu}. \tag{E5}$$

These are integrated with a uniform weight on the world sheet to give [Eq. (3.6)]

$$F_1^\rho(x) = \iint f_1^\rho(x, z)d\zeta^1 d\zeta^2 \tag{E6}$$

$$F_2^\rho(x) = \iint f_2^\rho(x, z)d\zeta^1 d\zeta^2. \tag{E7}$$

The tangential and perpendicular projection operators and the extrinsic curvature are evaluated at the field point, x. The metric perturbation quantities, ΔH and Δh, depend upon both source and field points. Replacing covariant

derivatives with partial derivatives (recall that we are working in Minkowski spacetime, in which case the two derivatives are equal), the integrands for the trace-reversed metric perturbation and metric perturbation derivative are

$$\Delta\bar{h}_{\alpha\beta} = -4G\mu\sqrt{-\gamma(z)}\eta_{\alpha\beta}(z)\mathcal{G}(x,z) \tag{E8}$$

$$\Delta\bar{h}_{\alpha\beta,\gamma} = -4G\mu\sqrt{-\gamma(z)}\eta_{\alpha\beta}(z)\,\frac{\partial\mathcal{G}(x,z)}{\partial x_f^\gamma}, \tag{E9}$$

where source and field point dependence is explicitly indicated.

We now proceed with the calculation for a given choice of w and σ_0 for the smoothed Green function. We repeat the calculation for a sequence with $w \to 0$ and $\sigma_0 \to 0$. The area of the world sheet includes all nonzero contributions to the integral but as a practical matter we limit it to regions where the magnitude of the integrand exceeds some minimum threshold.

We have used several different techniques for estimating the integrals of interest. The first approach is a simple quadrature along lines in which we evaluate f_1^ρ at a lattice of points z and estimate

$$F_1^\rho(x) \sim \frac{A_{WS}}{N}\sum_{i=1}^{N} f_1^\rho(x_{,i}) \tag{E10}$$

where $A_{WS} = \int d\zeta^1 d\zeta^2$ is the world sheet area (and likewise for F_2). This approach makes essentially no assumptions about the integrand's support but the achievable accuracy is limited in practice by the inefficiencies of working with a low-order scheme and a global grid.

Only a small part of the world sheet is important in the limiting results. The second approach is cubature, an adaptive algorithm for numerical integration based on the algorithm of Genz and implemented in routine Cuhre in the Cuba package [106]. The basic integration rule for the two-dimensional application is degree 13. We begin by identifying a part of the world sheet in which the integrand is above some threshold (say $> 10^{-12}$), apply an integration rule, repeatedly subdivide the region to estimate the global integral and errors and stop when errors are sufficiently small. This method, being higher order and more selective about the choice of points, achieves higher accuracy for a given computational cost but sometimes terminates too early if errors are misestimated.

3. KT cases I and II

The main text compares the case I and II results for 1D to those found by direct integration over the 2D world sheet. We used the rectangular area centered on the field point and of size $\pm L/2$ in both ζ^1 and ζ^2 which encompasses the entire string loop image. We parametrized the Gaussian width and the Θ function with n and m:

$$d_{\rm char} = \frac{L}{2^n} \tag{E11}$$

$$w = d_{\rm char}^4 \tag{E12}$$

$$\sigma_0 = (m d_{\rm char})^2 \tag{E13}$$

and let n range from 4 to 7 and set $m \geq 0$.[24] We accumulated the contributions to the integrals only for points with $\mathcal{G} > 10^{-4}$ for each choice of n and m. This cutoff effectively removed any effect of cusps lying off the string image. We checked sensitivity to the cutoff by recalculating with $\mathcal{G} > 10^{-3}$ and $\mathcal{G} > 10^{-2}$, finding no differences, and will drop further mentions of this parameter.

Case I is intrinsically the simplest calculation since the image of the string loop is smooth, without cusps or kinks. Several series of integrations using 2D uniform grids were performed. We studied the convergence for the following sequences:

(i) $m = 0$ (no over-retardation), Θ (exactly causal), $n = 4$–6.25
(ii) $m = 0$ (no over-retardation), $\Theta_{\rm tanh}$ (smoothed causality), $n = 4$–5.5
(iii) $m = 0.1$ (over-retardation), Θ (exactly causal), $n = 4$–5.75.

For the integration for a specific m and n we estimated the quadrature errors by halving the grid spacing and looking at successive differences in the answers (hereafter, Cauchy errors). We repeated the process until the Cauchy errors were small. We then generated sequences for varying n. In these we observed smooth, steady convergence to the [1D] results.

We extrapolated numerical results to $n = \infty$ by fitting each component F with the form $F(n) = F(\infty) + ae^{-bn}$. $F(\infty)$, a and b are found from numerical results at three specific values of n. Table II summarizes the results for one sequence with fixed $m = 0$ and an exact Θ function. The second column gives the extrapolated force solution for each component, the third is an estimate of the size of the systematic errors in extrapolation (by fitting different grid based calculations) and the fourth is the difference of $F(\infty)$ and the [1D] results. The [1D] results include the hidden delta function at the field point and the line integral with no over-retardation and exact causality. Note that the error with respect to the [1D] results is $\lesssim 4 \times 10^{-3}$ for the

[24] Note $\delta(\sigma) \sim e^{-\sigma^2/2\chi^2}/(\sqrt{2\pi}\chi)$ and $\sigma \sim ds^2 \propto L^2$ implies that $\chi \propto d_{\rm char}^2 \propto \sigma_0$. However, we use Gaussian width $w \propto \chi^2 \propto d_{\rm char}^4$ and $\sigma_0 \propto d_{\rm char}^2$. Of course, both the width and the over-retardation parameter decrease as $w \to 0$ or $n \to \infty$.

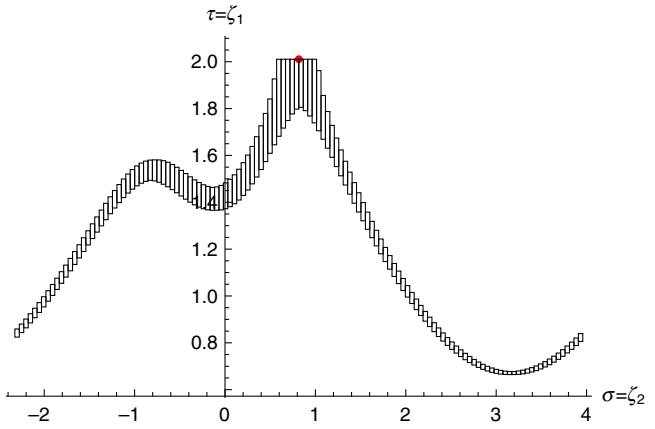

FIG. 23. The red dot shows the field point for case I for the KT string loop. The boxes enclose the regions with rms integrands $> 10^{-8}$ for $m = 0$ and $n = 5$.

individual components of F_1^ρ and $\lesssim 3 \times 10^{-5}$ for F_2^ρ. The size of the 1D-2D differences are comparable, component by component, to the Cauchy errors for the quadrature itself. These are much smaller than the contribution of the delta function at the field point.

We found case I sequences with or without over-retardation, with or without a smooth causal condition all smoothly converged to the [1D] answer. It is perhaps important to emphasize that this consistency is strong evidence that a single, well-defined limit exists and is correctly recovered with the 1D analysis for smooth loops.

We next repeated the case I sequence for $m = 0$ (no over-retardation), exactly causal Green function, for $n = 4$–7 using the cubature method. Cubature will be used for most of the remaining force evaluations because it is more efficient and has a higher accuracy. We began by selecting rectangular subregions of the world sheet that can plausibly contribute to the quadratures of interest. These closely trace the retarded string image. For example, Fig. 23 illustrates the field point (red dot) and outlines 128 subregions of interest for $m = 0$ and $n = 5$. The union of all the subregions encloses the area containing nontrivial integrands in the sense $\sqrt{\sum_\rho ((f_1^\rho)^2 + (f_2^\rho)^2)} > 10^{-8}$. The subregion bounds are found numerically. The string loop image lies within the subregions as n grows large.

The function is integrated by cubature over each separate subregion and the full answer is the sum over the set. In the cubature method the subregion is divided repeatedly until an estimated error tolerance (absolute or relative errors $\lesssim 10^{-6}$) is reached. Sometimes the error estimate is inaccurate so we also systematically increased the number of rectangles from 128 up to 2048, yielding finer and finer starting conditions. This allows a check that the error estimates are robust. Once all the subregions are accurately accounted for the total is calculated.

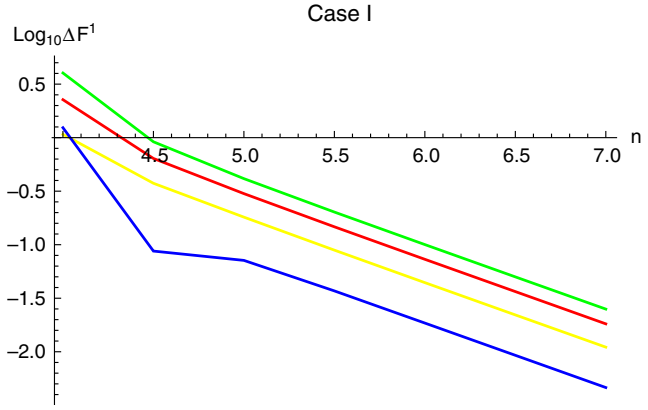

FIG. 24. The difference between smoothed Green function based 2D grid evaluation of F_1^ρ and the exact delta function [1D] evaluation as a function of n for loop I. The [2D] results should approach the [1D] results as $n \to \infty$ when the Gaussian tends to the delta function. These results have no over-retardation ($m = 0$) and use the exact Θ function for causality. The colors label results for the four spacetime components of F_1; red, yellow, green and blue correspond to components 0, 1, 2 and 3, respectively. The ordinate, $\log_{10}|F_{1,2D}^\rho - F_{1,1D}^\rho|$, quantifies the difference, component by component, as a function of n. The delta function contribution at the field point is of order unity and far larger than the 1D-2D differences. Table II gives detailed information on individual contributions.

Figures 24 and 25 plot the $\log_{10}$ absolute differences between the [2D] and [1D] calculations as a function of n. The solid lines are for [1D] calculations with the delta function contribution at the field point. The scale for the y-axis on the figures is quite different and, as expected, the error is much larger for F_1 than for F_2. The errors cease to decrease exponentially with n in Fig. 25 for 1D-2D differences of size 3×10^{-5}, likely a consequence of the intrinsic accuracy of the cubature integrations.

In summary, the case I [2D] cubature calculations agree with the [1D] calculations with a delta function contribution at the field point.

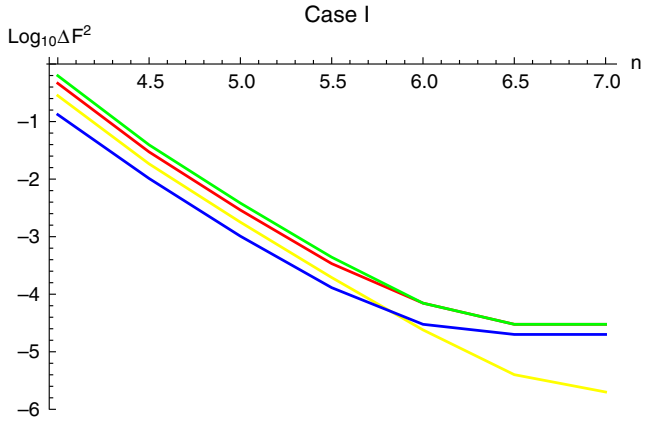

FIG. 25. Same as Fig. 24 except for F_2^ρ.

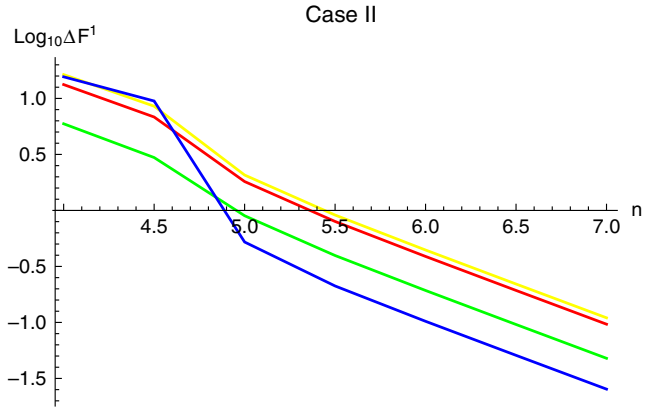

FIG. 26. Same as Fig. 24 except for loop II.

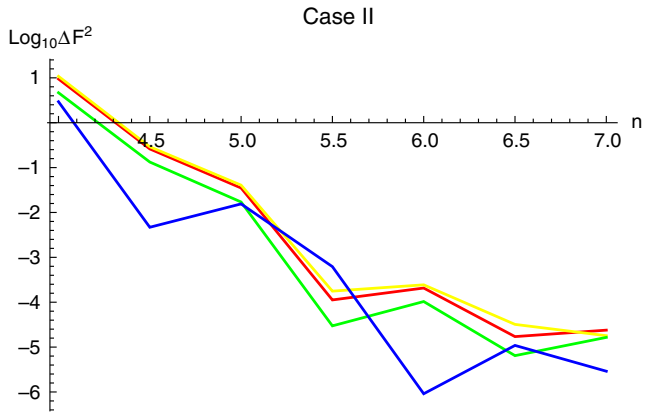

FIG. 27. Same as Fig. 24 except for F_2^ρ and loop II.

Case II is similar to case I except that a cusp occurs on the image of the string loop. We proceeded in the same manner, breaking the world sheet up into small subregions with nontrivial integrands. The main difference from case I is that there is a significant loss in precision for source points near the cusp. We had to perform those calculations with quadruple precision arithmetic. We avoided evaluating quantities at the cusp itself but sampled points as closely as needed to estimate the integrated quantities. The integrands are extremely complicated and we did not perform an analytic expansion in the vicinity of the cusp. We found (i) no numerical evidence for singular behavior and (ii) well-behaved quadratures. Figures 26 and 27 show the convergence as n increases. The basic conclusion is the same as for case I: the [2D] numerical results tend to the [1D] results when the latter include the delta function contribution at the field point.

4. Garfinkle and Vachaspati string

The assumed field point is $(\zeta^1,\zeta^2)=(\tau,\zeta)=(0.3,0.4)L$. The kinks are located at ζ^2 approximately -0.79 and 1.87. The [1D] results are given in Table V. These are calculated from the line integrals, boundary terms at each kink and the delta function at the field point as described in the main text.

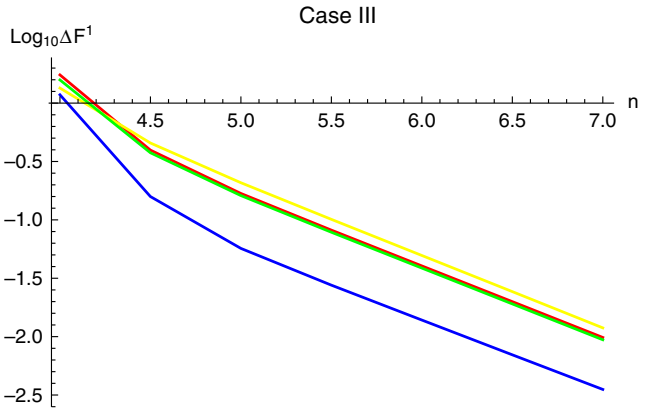

FIG. 28. Same as Fig. 24 except for loop III.

We introduce a small parameter to "round off" the kinks as follows.[25] We replace $\delta_{j,\lfloor\frac{2x}{L}\rfloor}$ with a smoothly varying function of characteristic width Δ:

$$\delta_j(x)=\frac{1}{2}\left(\tanh\left(\frac{x-x_{lo}}{\Delta}\right)-\tanh\left(\frac{x_{hi}-x}{\Delta}\right)\right) \tag{E14}$$

$$x_{lo}=\frac{jL}{2} \tag{E15}$$

$$x_{hi}=x_{lo}+\frac{L}{2}. \tag{E16}$$

For $L=2\pi$ and $\Delta=10^{-2}$ changes in the spacetime configuration of the loop are largely confined to the vicinity of the kink. They remain invisible at the resolution of Fig. 13. In the tangent sphere representation, nonzero Δ connects the green arcs. The linking curves do not lie on the unit sphere and the position $\vec{b}'$ along the curve changes very rapidly with its argument; i.e., the tangent vector quickly passes through the gap.

We have integrated the forces using the cubature method as was done for the KT string using a sequence of parameters for the $m=0$ (no over-retardation) exactly causal Green function. For $n=4$–7 we set $\Delta=e^{-1.15129n}$ (so $\Delta=10^{-2}$ at $n=4$ and 10^{-3} at $n=6$) so that the limit is the idealized kink solution. The results are shown in Figs. 28 and 29. Note that the errors in the [2D] results are far smaller than the size of the individual components that make up the [1D] calculation (the line integral, the delta function and the kink contributions).

[25]To recap, in the various 1D methods we took care to accommodate the string discontinuities, the case where the field point coincides with a source point and the process of patching different coordinate systems together. The [2D] calculations are not immune to the first of these issues.

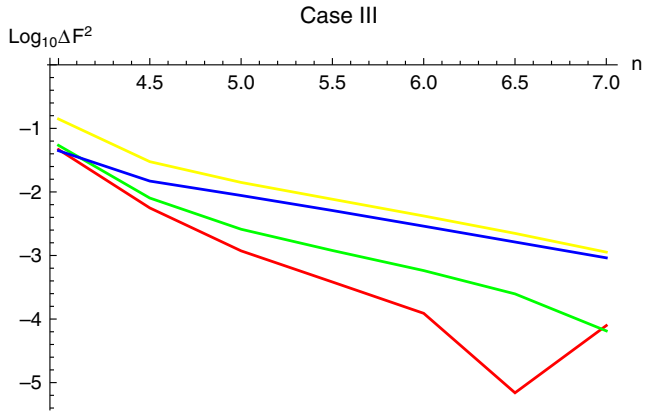

FIG. 29. Same as Fig. 24 except for F_2^o and loop III.

APPENDIX F: PARAMETRIZED FITS NEAR THE CUSP FOR THE NONINTERSECTING KT STRING

In this Appendix we give quantitative numerical fits to the behavior of the self-force in the vicinity of the cusp for the nonintersecting KT string ($\alpha = 1/2$, $\phi = 0$) described in Sec. VI C. We investigated several approaches to fitting the forces in the vicinity of the cusp.

Here, we begin with fitting the integral part of $\mathcal{F}^\mu_{\rm conf}$ since the delta function part is known in analytic form. We sampled world sheet points about the cusp extending from 2×10^{-2} to 2×10^{-8} in radius and at fixed angle θ and found that

$$\log|F^\mu| = A_1^\mu(\theta)\log x + A_2^\mu(\theta)x + A_3^\mu(\theta) \tag{F1}$$

$$x = \log r \tag{F2}$$

$$r = \sqrt{\delta\tau^2 + \delta\zeta^2} \tag{F3}$$

fits each ray very well. The ratio of the magnitude of $\log|F^\mu|$ to the root mean square error for one fitted ray is typically $\sim10^3$. We observed that angle-dependent coefficients $A_i^\mu(\theta)$ varied systematically and we selected simple parametrized forms. For F^t and F^x the form

$$A_i^\mu = a_i^\mu \chi(\theta)^{b_i^\mu} \tag{F4}$$

$$\chi(\theta) = \lim_{r\to0}\frac{\sqrt{-\gamma}}{r^2} \tag{F5}$$

gave reasonable fits. There are six scalars needed to fit each of the 2D functions F^t and F^x. For F^y we found that simple angle-dependent coefficients $A_i^\mu(\theta)$ worked well:

$$A_i = a_i + b_i T\left(\frac{\theta - c}{2\pi}\right) \tag{F6}$$

where $T(x)$ is the triangle wave with amplitude 1, period 1, $T(0) = 0$ and $T'(0) = 4$. There are seven scalars to fit (note that c is the same fitted parameter for the three A_i). For F^z the form is tolerably well fit by

$$A_i = a_i + b_i U\left(\theta - \frac{\pi}{2}\right) S\left(\frac{\theta - c}{3\pi/2}\right) - d_i U\left(\frac{\pi}{2} - \theta\right) \tag{F7}$$

where $U(x)$ is the step function (0 for $x < 0$ and 1 for $x \geq 0$), $S(x)$ is the sawtooth wave that varies from 0 to 1 with period 1, $S(0+) = 0$, and $S(1-) = 1$. There are nine scalars to fit (here $c = 0.5$ is fixed and not varied). Results are summarized in the Table IX below. The fits for F^t and F^x are close to $1/r$ because $A_2^t \sim A_2^x \sim -1$ is the dominant term (and $a_2^t \sim a_2^x \sim -1$ and $b_2^t \sim b_2^x \sim 0$). The fit for F^y is close to $\log r$ (setting $A_2^y = 0$ makes a minimal difference in Q, as shown in the table). The fit for F^z requires both A_1^z and A_2^z.

We have also fit four parameter, *ad hoc* forms. These are generally less good than the previous set and the quality varies considerably. It is best in the quadrants without the visible fold and it remains difficult to fit all quadrants together. The results (given in Table X) imply that the t- and x-components diverge as $1/r$, where $r \equiv \sqrt{\tau^2 + \zeta^2}$ is the Euclidean distance on the world sheet. A possible divergence in the y- and z-components cannot be ruled out, but is certainly not as strong as the t- and x-components.

TABLE IX. Fits based on $\log|F| = A_1\log x + A_2 x + A_3$ where $x = \log r$ and $A_i(\theta)$ are specific forms described in the text. Q is the ratio of the mean $\log|F|$ to the root mean square error of the fit.

μ	a_1	b_1	a_2	b_2	a_3	b_3	Q
t	0.0512	−0.0474	−0.996	−0.000301	2.982	−0.110	123
x	0.0207	−0.0497	−0.998	−0.000625	3.027	−0.108	123

μ	a_1	b_1	a_2	b_2	a_3	b_3	c	Q
y	0.931	0.651	0.00119	0.0349	3.096	−1.429	0.314	87
	0.942	0.335	⋯	⋯	3.084	−1.089	0.314	82

μ	a_1	b_1	d_1	a_2	b_2	d_2	a_3	b_3	d_3	c	Q
z	1.053	−0.961	0.617	0.0145	−0.0524	0.0396	0.679	2.495	−1.422	0.5	87
	0.925	−0.490	0.262	⋯	⋯	⋯	0.815	1.992	−1.041	0.5	30

TABLE X. Two-dimensional fits to $\log|\mathcal{F}^{\mu}_{\rm conf}|$ near the cusp ($0.0013 < \{\tau, |\zeta|\} < 0.0021$) using the form $a + b\log\sqrt{-\gamma} + c\cos\theta + d\sin\theta$ where $\cos\theta = \tau/r$, $\sin\theta = \zeta/r$ and $r = \sqrt{\tau^2+\zeta^2}$. The fit goodness is quantified by ϵ, the root mean square error between the fit and the actual data (both as logs), and Q, the ratio of the total variation in $\log\mathcal{F}^{\mu}_{\rm conf}$ divided by ϵ. "All" means a single fit to the whole plane; ++ means the fit restricted to $\tau \geq 0$ and $\zeta \geq 0$ and similarly for +−, −+ and −−. Asymptotically $F \propto 2b/\tau$ for $\zeta = 0$ and $2b/\zeta$ for $\tau = 0$.

μ	$\operatorname{sgn}\delta\tau\operatorname{sgn}\delta\zeta$	a	b	c	d	ϵ	Q
t	All	3.95292	−0.414102	0.151793	0.0721235	0.131773	4.77971
	++	3.01226	−0.502883	0.178088	0.212065	0.00341496	163.388
	+−	4.22776	−0.474782	−0.757188	0.686015	0.0569798	11.6713
	−+	3.24345	−0.468097	0.395402	0.427249	0.118002	4.78373
	−−	2.69632	−0.502038	−0.0722535	−0.418941	0.0189629	28.1211
x	All	3.97366	−0.412535	0.151562	0.0719106	0.131271	4.78016
	++	3.04136	−0.500672	0.176313	0.20999	0.00282476	196.672
	+−	4.24515	−0.473347	−0.755537	0.684603	0.0567632	11.6804
	−+	3.26301	−0.466743	0.395591	0.425764	0.11768	4.78189
	−−	2.72609	−0.499806	−0.0708712	−0.416556	0.0186554	28.457
y	All	4.20813	−0.0398377	−0.381031	0.144944	0.134169	2.41009
	++	3.26127	−0.0948215	−0.0164481	0.48741	0.0189321	7.52428
	+−	3.61753	−0.0744807	−0.580823	−0.340387	0.167632	1.57078
	−+	3.70482	−0.0686625	−0.518819	0.296286	0.019127	8.42306
	−−	3.92864	−0.0768625	−0.17871	0.10457	0.0088657	15.2576
z	All	2.65579	−0.0161345	−0.344105	0.0271806	0.200512	1.58037
	++	1.78559	−0.0666965	−0.072034	0.460484	0.00948379	14.77
	+−	1.91589	−0.0211916	−0.156757	−0.808392	0.27011	1.37301
	−+	3.04493	−0.0625678	0.234966	−0.80721	0.0899292	2.78705
	−−	2.76864	−0.0513231	0.0852916	0.348301	0.0157434	7.3724

In addition to the full fits, we have made simpler one-dimensional fits along the coordinate axes. Table XI gives fits to $|\log\mathcal{F}^{\mu}_{\rm conf}|$ as a power law in $|\log\tau|$ along the coordinate axis $\zeta = 0$. We have separately fit the total force and just the part of the force that comes from the integral contribution. For the t- and x-components of the total force the scaling is clear and unambiguous. There is a measurable difference in the amplitude of the force before and after the cusp formation even though the rate of divergence is identical. (The delta function contribution scales as $1/r$ for t- and x-components.) The amplitude difference or Stokes phenomenon is smaller in the integral piece than in the total. The delta function contribution is related to the choice of the retarded Green function and the dichotomy of emission and absorption near the cusp. The y- and

TABLE XI. One-dimensional fits for the variation of $\log|\mathcal{F}^{\mu}_{\rm conf}|$ (total and continuous integral contribution) with τ for $\zeta = 0$. The range of the fit is $0.0013 < |\delta\tau| < 0.0021$ and the form is $a + b\log|\tau|$. Q is the ratio of the total variation in $\log\mathcal{F}^{\mu}_{\rm conf}$ divided by the rms error between the fit and the actual data.

		a	b	Q	a	b	Q
μ	$\operatorname{sgn}\delta\tau$	Total			Integral		
t	+	3.56	−1.00	8.9×10^3	3.30	−1.00	6.8×10^3
	−	3.08	−1.00	5.6×10^3	3.39	−1.00	7.7×10^3
x	+	3.56	−1.00	2×10^4	3.31	−1.00	1.6×10^4
	−	3.08	−1.00	1×10^4	3.40	−1.00	1.5×10^4
y	+	3.27	−0.19	60	3.46	−0.18	65
	−	4.43	−0.11	1.1×10^2	4.51	−0.10	1.1×10^2
z	+	1.71	−0.14	82	2.50	−0.09	1.3×10^2
	−	2.94	−0.07	1.5×10^2	3.27	−0.05	1.9×10^2

TABLE XII. One-dimensional fits for the variation of $\log|\mathcal{F}^{\mu}_{\rm conf}|$ (total and continuous integral contribution) with ζ at $\tau = 0$. The range of the fit is $0.0013 < |\zeta| < 0.0021$ and the form is $a + c\log|\zeta|$. Q is the ratio of the total variation in $\log\mathcal{F}^{\mu}_{\rm conf}$ divided by the rms error between the fit and the actual data.

		a	c	Q	a	c	Q
μ	$\operatorname{sgn}\delta\zeta$	Total			Integral		
t	+	2.78	−1.00	4×10^3	2.56	−1.00	3.3×10^3
	−	2.70	−1.00	4×10^3	2.89	−1.00	4.8×10^3
x	+	2.79	−1.00	9×10^3	2.58	−1.00	7×10^3
	−	2.71	−1.00	8×10^3	2.90	−1.00	10^4
y	+	4.00	−0.14	84	4.02	−0.13	85
	−	3.77	−0.15	76	3.80	−0.15	77
z	+	2.36	−0.10	120	2.48	−0.09	125
	−	2.35	−0.10	110	2.47	−0.09	120

z-components grow more slowly as the time to the cusp shrinks and the asymptotics are not as well determined. Nonetheless, the similarity of total and integral quantities implies that the delta function contribution which is constant in r (for the y- and z-components) is subdominant at the scales probed. Similarly, Table XII considers the analogous situation for $|\log \mathcal{F}^{\mu}_{\rm conf}|$ as a power law in $|\log \zeta|$ along the coordinate axis $\tau = 0$. Again, the scaling with distance to the cusp is unambiguous. The t- and x-components diverge like $|\zeta|^{-1}$ and have similar amplitudes. The Stokes-like phenomenon seems to be weaker or absent in the total force than it is in the integral contribution alone (contrary to the previous example). The string segment behaves approximately symmetrically along its length. Again, the y- and z-components grow more slowly as the cusp is approached.

[1] S. H. Henry Tye, Lect. Notes Phys. **737**, 949 (2008).
[2] A. H. Guth, Phys. Rev. D **23**, 347 (1981).
[3] A. D. Linde, Phys. Lett. **108B**, 389 (1982).
[4] A. Albrecht and P. J. Steinhardt, Phys. Rev. Lett. **48**, 1220 (1982).
[5] A. Albrecht and N. Turok, Phys. Rev. Lett. **54**, 1868 (1985).
[6] D. P. Bennett and F. R. Bouchet, Phys. Rev. Lett. **60**, 257 (1988).
[7] B. Allen and E. P. S. Shellard, Phys. Rev. Lett. **64**, 119 (1990).
[8] V. Vanchurin, K. Olum, and A. Vilenkin, Phys. Rev. D **72**, 063514 (2005).
[9] C. Ringeval, M. Sakellariadou, and F. Bouchet, J. Cosmol. Astropart. Phys. 02 (2007) 023.
[10] C. J. A. P. Martins and E. P. S. Shellard, Phys. Rev. D **73**, 043515 (2006).
[11] J. J. Blanco-Pillado, K. D. Olum, and B. Shlaer, Phys. Rev. D **83**, 083514 (2011).
[12] J. J. Blanco-Pillado, K. D. Olum, and B. Shlaer, Phys. Rev. D **89**, 023512 (2014).
[13] T. W. B. Kibble, J. Phys. A **9**, 1387 (1976).
[14] A. Vilenkin and E. P. S. Shellard, *Cosmic Strings and Other Topological Defects* (Cambridge University Press, Cambridge, England, 2000).
[15] G. F. Smoot *et al.* (COBE Collaboration), Astrophys. J. **396**, L1 (1992).
[16] C. L. Bennett, A. Banday, K. M. Gorski, G. Hinshaw, P. Jackson, P. Keegstra, A. Kogut, G. F. Smoot, D. T. Wilkinson, and E. L. Wright, Astrophys. J. **464**, L1 (1996).
[17] D. N. Spergel *et al.* (WMAP Collaboration), Astrophys. J. Suppl. Ser. **170**, 377 (2007).
[18] A. Vilenkin, Phys. Rev. D **23**, 852 (1981).
[19] C. Hogan and R. Narayan, Mon. Not. R. Astron. Soc. **211**, 575 (1984).
[20] A. Vilenkin, Astrophys. J. **282**, L51 (1984).
[21] A. A. de Laix, Phys. Rev. D **56**, 6193 (1997).
[22] F. Bernardeau and J.-P. Uzan, Phys. Rev. D **63**, 023005 (2000).
[23] M. Sazhin, G. Longo, J. M. Alcala', R. Silvotti, G. Covone, O. Khovanskaya, M. Pavlov, M. Pannella, M. Radovich, and V. Testa, Mon. Not. R. Astron. Soc. **343**, 353 (2003).
[24] M. V. Sazhin, M. Capaccioli, G. Longo, M. Paolillo, and O. S. Khovanskaya, arXiv:astro-ph/0601494.
[25] J. L. Christiansen, E. Albin, K. A. James, J. Goldman, D. Maruyama, and G. F. Smoot, Phys. Rev. D **77**, 123509 (2008).
[26] L. Pogosian, S. H. H. Tye, I. Wasserman, and M. Wyman, Phys. Rev. D **68**, 023506 (2003); **73**, 089904(E) (2006).
[27] L. Pogosian, M. C. Wyman, and I. Wasserman, J. Cosmol. Astropart. Phys. 09 (2004) 008.
[28] S. H. H. Tye, I. Wasserman, and M. Wyman, Phys. Rev. D **71**, 103508 (2005); **71**, 129906(E) (2005).
[29] M. Wyman, L. Pogosian, and I. Wasserman, Phys. Rev. D **72**, 023513 (2005); **73**, 089905(E) (2006).
[30] L. Pogosian, I. Wasserman, and M. Wyman, arXiv:astro-ph/0604141.
[31] U. Seljak, A. Slosar, and P. McDonald, J. Cosmol. Astropart. Phys. 10 (2006) 014.
[32] N. Bevis, M. Hindmarsh, M. Kunz, and J. Urrestilla, Phys. Rev. D **76**, 043005 (2007).
[33] A. A. Fraisse, J. Cosmol. Astropart. Phys. 03 (2007) 008.
[34] L. Pogosian, S. H. H. Tye, I. Wasserman, and M. Wyman, J. Cosmol. Astropart. Phys. 02 (2009) 013.
[35] P. A. R. Ade *et al.* (Planck Collaboration), Astron. Astrophys. **571**, A25 (2014).
[36] T. Vachaspati and A. Vilenkin, Phys. Rev. D **31**, 3052 (1985).
[37] A. Economou, D. Harari, and M. Sakellariadou, Phys. Rev. D **45**, 433 (1992).
[38] R. A. Battye, R. R. Caldwell, and E. P. S. Shellard, in *Topological Defects in Cosmology* (1997), pp. 11–31.
[39] T. Damour and A. Vilenkin, Phys. Rev. Lett. **85**, 3761 (2000).
[40] T. Damour and A. Vilenkin, Phys. Rev. D **64**, 064008 (2001).
[41] T. Damour and A. Vilenkin, Phys. Rev. D **71**, 063510 (2005).
[42] X. Siemens, J. Creighton, I. Maor, S. Ray Majumder, K. Cannon, and J. Read, Phys. Rev. D **73**, 105001 (2006).
[43] C. J. Hogan, Phys. Rev. D **74**, 043526 (2006).
[44] X. Siemens, V. Mandic, and J. Creighton, Phys. Rev. Lett. **98**, 111101 (2007).
[45] B. Abbott *et al.* (LIGO Scientific Collaboration), Phys. Rev. D **76**, 082001 (2007).
[46] B. P. Abbott *et al.* (LIGO Scientific Collaboration), Phys. Rev. D **80**, 062002 (2009).
[47] B. P. Abbott *et al.* (VIRGO and LIGO Scientific Collaboration), Nature (London) **460**, 990 (2009).

[48] J. Aasi *et al.* (VIRGO and LIGO Scientific Collaboration), Phys. Rev. Lett. **112**, 131101 (2014).
[49] B. P. Abbott *et al.* (Virgo and LIGO Scientific Collaboration), Phys. Rev. Lett. **118**, 121101 (2017); **119**, 029901(E) (2017).
[50] F. R. Bouchet and D. P. Bennett, Phys. Rev. D **41**, 720 (1990).
[51] R. R. Caldwell and B. Allen, Phys. Rev. D **45**, 3447 (1992).
[52] V. M. Kaspi, J. H. Taylor, and M. F. Ryba, Astrophys. J. **428**, 713 (1994).
[53] F. A. Jenet, G. B. Hobbs, W. van Straten, R. N. Manchester, M. Bailes, J. P. W. Verbiest, R. T. Edwards, A. W. Hotan, J. M. Sarkissian, and S. M. Ord, Astrophys. J. **653**, 1571 (2006).
[54] M. R. DePies and C. J. Hogan, Phys. Rev. D **75**, 125006 (2007).
[55] J. J. Blanco-Pillado and K. D. Olum, Phys. Rev. D **96**, 104046 (2017).
[56] J. J. Blanco-Pillado, K. D. Olum, and X. Siemens, Phys. Lett. B **778**, 392 (2018).
[57] D. F. Chernoff and S. H. H. Tye, Int. J. Mod. Phys. D **24**, 1530010 (2015).
[58] C. J. Burden, Phys. Lett. **164B**, 277 (1985).
[59] D. Garfinkle and T. Vachaspati, Phys. Rev. D **36**, 2229 (1987).
[60] R. Durrer, Nucl. Phys. **B328**, 238 (1989).
[61] B. Allen, P. Casper, and A. Ottewill, Phys. Rev. D **50**, 3703 (1994).
[62] B. Allen and P. Casper, Phys. Rev. D **50**, 2496 (1994).
[63] B. Allen, P. Casper, and A. Ottewill, Phys. Rev. D **51**, 1546 (1995).
[64] P. Casper and B. Allen, Phys. Rev. D **52**, 4337 (1995).
[65] J. Polchinski, Int. J. Mod. Phys. A **20**, 3413 (2005); AIP Conf. Proc. **743**, 331 (2005).
[66] J. Polchinski and J. V. Rocha, Phys. Rev. D **74**, 083504 (2006).
[67] J. Polchinski, in *Recent Developments in Theoretical and Experimental General Relativity, Gravitation and Relativistic Field Theories. Proceedings, 11th Marcel Grossmann Meeting, MG11, Berlin, Germany, 2006. Pt. A-C* (World Scientific, Singapore, 2007), pp. 105–125.
[68] J. Polchinski and J. V. Rocha, Phys. Rev. D **75**, 123503 (2007).
[69] F. Dubath, J. Polchinski, and J. V. Rocha, Phys. Rev. D **77**, 123528 (2008).
[70] J. Polchinski, Phil. Trans. R. Soc. A **366**, 2859 (2008).
[71] D. F. Chernoff, arXiv:0908.4077.
[72] D. F. Chernoff and S. H. H. Tye, J. Cosmol. Astropart. Phys. 05 (2018) 002.
[73] C. J. Hogan and M. J. Rees, Nature (London) **311**, 109 (1984).
[74] C. J. Hogan, Nature (London) **326**, 853 (1987).
[75] A. Bohe, Phys. Rev. D **84**, 065016 (2011).
[76] J. M. Quashnock and D. N. Spergel, Phys. Rev. D **42**, 2505 (1990).
[77] R. J. Scherrer, J. M. Quashnock, D. N. Spergel, and W. H. Press, Phys. Rev. D **42**, 1908 (1990).
[78] P. A. M. Dirac, Proc. R. Soc. A **167**, 148 (1938).
[79] B. Carter and R. A. Battye, Phys. Lett. B **430**, 49 (1998).
[80] A. Buonanno and T. Damour, Phys. Rev. D **60**, 023517 (1999).
[81] M. R. Anderson, Classical Quantum Gravity **22**, 2539 (2005).
[82] A. Buonanno and T. Damour, Phys. Lett. B **432**, 51 (1998).
[83] J. M. Wachter and K. D. Olum, Phys. Rev. Lett. **118**, 051301 (2017).
[84] J. M. Wachter and K. D. Olum, Phys. Rev. D **95**, 023519 (2017).
[85] R. A. Battye and B. Carter, Phys. Lett. B **357**, 29 (1995).
[86] B. Carter, Phys. Rev. D **48**, 4835 (1993).
[87] R. A. Battye and B. Carter, Classical Quantum Gravity **17**, 3325 (2000).
[88] B. Carter, in *Recent Developments in Gravitation and Mathematical Physics. Proceedings, 2nd Mexican School, Tlaxcala, Mexico, 1996* (Science Network Publ., Konstanz, Germany, 1997).
[89] C. W. Misner, K. S. Thorne, and J. A. Wheeler, *Gravitation* (W.H. Freeman and Co., San Francisco, 1973).
[90] R. A. Battye and B. Carter, Phys. Lett. B **357**, 29 (1995).
[91] B. Carter and R. A. Battye, Phys. Lett. B **430**, 49 (1998).
[92] J. V. Bladel, IEEE Antennas Propag. Mag. **33**, 69 (1991).
[93] E. Poisson, A. Pound, and I. Vega, Living Rev. Relativity **14**, 7 (2011).
[94] A. Pound, Phys. Rev. D **81**, 124009 (2010).
[95] T. Damour, Nuovo Cimento B **26**, 157 (1975).
[96] B. Allen and A. C. Ottewill, Phys. Rev. D **63**, 063507 (2001).
[97] M. Anderson, Classical Quantum Gravity **26**, 025006 (2009).
[98] T. W. B. Kibble and N. Turok, Phys. Lett. **116B**, 141 (1982).
[99] N. Turok, Nucl. Phys. **B242**, 520 (1984).
[100] I. Vega and S. Detweiler, Phys. Rev. D **77**, 084008 (2008).
[101] L. Barack and D. A. Golbourn, Phys. Rev. D **76**, 044020 (2007).
[102] B. Wardell and N. Warburton, Phys. Rev. D **92**, 084019 (2015).
[103] S. Detweiler and B. F. Whiting, Phys. Rev. D **67**, 024025 (2003).
[104] A. Pound, Phys. Rev. D **81**, 024023 (2010).
[105] S. Weinberg, *Gravitation and Cosmology: Principles and Applications of the General Theory of Relativity, by Steven Weinberg* (Wiley-VCH, New York, 1972), p. 688.
[106] T. Hahn, Comput. Phys. Commun. **168**, 78 (2005).